QUANTUM-CHEMICAL STUDY OF GEOMETRICAL AND ELECTRONIC STRUCTURES OF AROMATIC FIVE-MEMBERED HETEROCYCLIC OLIGOMERS IN THE GROUND AND LOWEST SINGLET EXCITED STATES

A THESIS SUBMITTED TO
THE GRADUATE SCHOOL OF NATURAL AND APPLIED SCIENCES
OF
MIDDLE EAST TECHNICAL UNIVERSITY

BY

NEVİN ÖKSÜZ

IN PARTIAL FULFILLMENT OF THE REQUIREMENTS
FOR
THE DEGREE OF MASTER OF SCIENCE

IN

DEPARTMENT OF CHEMISTRY

SEPTEMBER 2004

Approval of the Graduate School of Natural and Applied Sciences

Prof. Dr. Canan ÖZGEN
Director

I certify that this thesis satisfies all the requirements as a thesis for the degree of Master of Science.

Prof. Dr. Hüseyin İŞÇİ

Head of Department

This is to certify that we have read this thesis and that in our opinion it is fully adequate, in scope and quality, as a thesis for the degree of Master of Science.

Prof. Dr. Levent Toppare
Co-Supervisor

Prof. Dr. İlker ÖZKAN
Supervisor

Examining Committee Members

Prof. Dr. Ahmet ÖNAL (METU, CHEM)

Prof. Dr. İlker ÖZKAN (METU, CHEM)

Prof. Dr. Levent TOPPARE (METU, CHEM)

Prof. Dr. Jale HACALOĞLU (METU, CHEM)

Prof. Dr. Levent AKSU (GAZİ U., CHED)

I hereby declare that all information in this document has been obtained and presented in accordance with academic rules and ethical conduct. I also declare that, as required by these rules and conduct, I have fully cited and referenced all material and results that are not original to this work.

Name, Last name : Nevin ÖKSÜZ

Signature :

ABSTRACT

QUANTUM CHEMICAL STUDY OF GEOMETRIES AND ELECTRONIC STRUCTURES OF AROMATIC FIVE-MEMBERED HETEROCYCLIC OLIGOMERS IN THE GROUND AND LOWEST SINGLET EXCITED STATES

Öksüz, Nevin
M. S., Department of Chemistry
Supervisor : Prof. Dr. İlker Özkan
Co-Advisor: Prof. Dr. Levent Toppare

September 2004, 149 pages

The nature of the ground state and the first (lowest) singlet excited state geometrical conformations and electronic transitions in the aromatic five-membered heterocyclic oligomers –oligothiophenes (**nT**), oligofurans (**nF**), and oligopyrroles (**nP**)- containing up to six monomer units (total of 18 molecules) were explored using several computational methodologies. Geometry optimizations were carried out at Austin Model 1 (AM1), Restricted Hartree-Fock (RHF/6-31G*), and Density Functional Theory (DFT, B3LYP/6-31G*) levels for the ground-state conformations of these structurally well-defined heterocyclic oligomers. The Configuration Interaction Singles (CIS) method with the 6-31G* basis set was

chosen in computation of the optimal geometry of the lowest singlet excited state. Lowest singlet excitation $S_1 \leftarrow S_0$ energies were calculated using the Zerner's Intermediate Neglect of Differential Overlap for Spectroscopy (ZINDO/S), CIS (CIS/6-31G*), and Time-Dependent DFT (TDDFT/6-31G* and TDDFT/6-31+G*) methods. In computation of the emission $S_1 \rightarrow S_0$ energies, we have employed all methods above except ZINDO/S.

In investigation of geometries of the ground and lowest singlet excited state, we compared the bond length alternation (BLA) parameters, Δr_i in the conjugated backbone of the oligomers. Saturation of the geometrical parameters at the center of oligomers was observed after a certain chain length.

Among all methodologies used in computation of excitation ($S_1 \leftarrow S_0$) and emission ($S_1 \rightarrow S_0$) energies, TDDFT results showed the best agreement with experimental data. Fits of computed and experimental excitation energies to an exponential function using the least squares method enabled us to predict Effective Conjugation Length (ECL) values. We obtained the ECLs of 17 (17), 16 (15), and 14 (13) monomer units for polythiophene (PTh), polyfuran (PFu), and polypyrrole (PPr), which have very good agreement with the results obtained from the fits of experimental data (the values in parentheses).

Keywords: Oligothiophene, Oligofuran, Oligopyrrole, Excited state geometry optimization, Configuration interaction singles (CIS), Time-dependent density functional theory (TDDFT)

ÖZ

AROMATİK BEŞ ÜYELİ HETEROHALKALI OLİGOMERLERİN TEMEL VE EN DÜŞÜK TEKLİ UYARILMIŞ HALLERDEKİ GEOMETRİLERİNİN VE ELEKTRONİK YAPILARININ KUVANTUM KİMYASAL ÇALIŞMASI

Öksüz, Nevin
Yüksek Lisans, Kimya Bölümü
Tez Yöneticisi : Prof. Dr. İlker Özkan
Ortak Tez Yöneticisi: Prof. Dr. Levent Toppare

Eylül 2004, 149 sayfa

Altı taneye kadar monomer birimi içeren aromatik beş üyeli heterohalkalı oligomerlerin (toplam 18 molekül) –oligotiyofenler (**nT**), oligofuranlar (**nF**), ve oligopiroller (**nP**)- temel hal ve ilk (en düşük) tekli uyarılmış hallerdeki geometrik konformasyonlarının ve elektronik geçişlerinin doğası birkaç farklı hesapsal yöntemle araştırıldı. Yapıları kesin olarak tanımlanmış bu heterohalkalı oligomerin temel hal konformasyonlari için geometri optimizasyonları Austin Modeli 1 (AM1), Sınırlı Hartree-Fock (RHF/6-31G*) ve Yoğunluk Fonksiyoneli Teorisi (DFT, B3LYP/6-31G*) seviyelerinde gerçekleştirildi. En düşük tekli uyarılmış haldeki optimal geometrinin hesaplanmasında 6-31G* temel seti ile birlikte Tekli Konfigurasyon Etkileşimi (CIS) metodu seçildi. En düşük tekli uyarılma $S_1 \leftarrow S_0$

enerjileri ZINDO/S, CIS (CIS/6-31G*), ve Zamana Bağlı DFT (TDDFT/6-31G* ve TDDFT/6-31+G*) metodları kullanılarak hesaplandı. Emisyon enerjilerinin $S_1 \rightarrow S_0$ hesaplanmasında ZINDO/S dışında yukarıda bahsedilen metodların hepsi kullanıldı.

Temel ve en düşük tekli uyarılmış haldeki geometrilerin incelenmesinde oligomerlerin konjüge omurgalarındaki bağ uzunluğu değişimi (BLA) parametreleri, Δr_i karşılaştırıldı. Oligomerlerin merkezlerindeki geometrik parametrelerin belli bir zincir uzunluğundan sonra doygunluğa ulaştığı gözlendi.

Uyarılma ($S_1 \leftarrow S_0$) ve emisyon ($S_1 \rightarrow S_0$) enerjilerinin hesaplanmasında kullanılan tüm metodlar arasında TDDFT sonuçları deneysel değerlerle en iyi uyumu gösterdi. En küçük kareler metodu kullanılarak hesaplanan ve deneysel olarak elde edilen uyarılma enerjilerinin bir üstel fonksiyona uygun hale getirilmesi Etkin Konjugasyon Uzunluğu (ECL) değerlerini tahmin etmemize olanak sağladı. Deneysel verilerin fitlerinden elde edilen sonuçlarla (parentezler içindeki veriler) çok iyi uyum gösteren politiyofen (PTh), polifuran (PFu), and polipirol (PPr) için ECL değerlerini 17 (17), 16 (15), ve 14 (13) monomer birimi olarak elde ettik.

Anahtar Kelimeler: Oligotiyofen, Oligofuran, Oligopirol, Uyarılmış hal geometri optimizasyonu, Tekli konfigürasyon etkileşimi (CIS), Zamana bağlı yoğunluk fonksiyoneli teorisi (TDDFT)

To my dearest sister, Nazan

ACKNOWLEDGMENTS

I wish to express a wealth of gratitude to my thesis advisor, Prof. Dr. İlker ÖZKAN, for his guidance, advice, criticism, encouragement, and insight throughout the research.

I would like to thank to Prof. Dr. Levent TOPPARE for his suggestions and comments.

Armağan KINAL is gratefully acknowledged for the friendship and helpful discussions. I also would like to thank to the other fellow researchers in the computational chemistry group, Mehrdad GHOULAMI, Yavuz DEDE, and Uğur BOZKAYA for their support and friendship.

Finally, my family deserves the most heartfelt thanks due to their love and encouragement during my life and my research. Without their sacrifice and dedication to this undertaking I would have never succeeded.

TABLE OF CONTENTS

ABSTRACT.....iv
ÖZ vi
ACKNOWLEDGMENTS ix
TABLE OF CONTENTS x
LIST OF TABLES xiii
LIST OF FIGURES.....xv
LIST OF ABBREVIATIONS.....xix
CHAPTER
1. INTRODUCTION.....1
1.1 General Electronic Properties of Conjugated Systems..... 1
1.1.1 Bond Length Alternation (BLA) 3
1.1.2 Interring Torsion Angle Effect 4
1.1.3 Effective Conjugation Length (ECL)..... 5
1.2 Conjugated Polymers..... 7
1.3 Conjugated Oligomers 8
1.4 Aromatic Five-Membered Heterocyclic Oligomers..... 10
1.4.1 Specific Electronic Properties of Aromatic Five-Membered Heterocyclic Systems 11
1.4.1.1 Frontier Molecular Orbitals of Heterocyclic Systems..... 12
1.4.1.2 Franck-Condon Principle..... 15
1.4.1.3 Excited State Electronic Structures of Heterocyclic Systems 16
1.4.1.4 Why are Sophisticated Quantum-Chemical Calculations Needed? 18
1.4.2 Subclasses of Aromatic Five-Membered Heterocyclic Oligomers 20
1.4.2.1 Thiophene Oligomers 21
1.4.2.1.1 Polythiophene..... 21
1.4.2.1.2 Physical Properties of Thiophene Oligomers 21
1.4.2.1.3 Applications of Thiophene Oligomers 24
1.4.2.2 Furan Oligomers 25
1.4.2.2.1 Polyfuran..... 25
1.4.2.2.2 Physical Properties of Furan Oligomer 25

1.4.2.3 Pyrrole Oligomers 26
1.4.2.3.1 Polypyrrole 26
1.4.2.3.2 Physical Properties of Pyrrole Oligomers 27
1.5 Scope of the Study 27
2. THEORETICAL CALCULATION METHODS 30
2.1 Introduction 30
2.2 Background 31
2.2.1 The Hartree-Fock Theory 32
2.2.2 Restricted and Unrestricted Hartree-Fock Wave Functions 34
2.2.3 The Basis Set Approximation 35
2.3 Computational Methods 37
2.3.1 *Ab Initio* Methods 37
2.3.2 Semi-Empirical Methods 37
2.3.2.1 Austin Model 1 (AM1) 39
2.3.2.2 Zerner's Intermediate Neglect of Differential Overlap Method Parameterized for Spectroscopy (ZINDO/S) 39
2.3.4 Electron Correlation Methods 40
2.3.4.1 Configuration Interaction (CI) 40
2.3.4.2 Configuration Interaction Singles (CIS) 42
2.3.5 Density Functional Theory 43
2.3.5.1 Generalized Gradient Approximation (GGA) 45
2.3.5.2 Hybrid methods 46
2.3.5.3 Time-Dependent Density Functional Theory (TDDFT) 46
2.4 Computational Procedure 47
3. RESULTS AND DISCUSSION 49
3.1 Geometry Optimizations 49
3.1.1 Ground State Geometries 49
3.1.2 Lattice Relaxation 65
3.1.3 Excited State Geometries 67
3.2 Molecular Orbital Analysis 72
3.3 Transition Energies 77
3.3.1 Excitation Energies ($S_1 \leftarrow S_0$) 77
3.3.2 Emission Energies ($S_1 \rightarrow S_0$) 86
4. CONCLUSION 90

REFERENCES 92

APPENDICES

A. Cartesian Coordinates of Ground State Geometries of Studied Structures at AM1 Level 110

A.1 Cartesian Coordinates of Ground State Geometries of Thiophene Oligomers (**nT**) at AM1 Level 110

A.2 Cartesian Coordinates of Ground State Geometries of Furan Oligomers (**nF**) at AM1 Level 113

A.3 Cartesian Coordinates of Ground State Geometries of Pyrrole Oligomers (**nP**) at AM1 Level 116

B. Cartesian Coordinates of Ground State Geometries of Studied Structures at HF/6-31G* Level 120

B.1 Cartesian Coordinates of Ground State Geometries of Thiophene Oligomers (**nT**) at HF/6-31G* Level..... 120

B.2 Cartesian Coordinates of Ground State Geometries of Furan Oligomers (**nF**) at HF/6-31G* Level..... 123

B.3 Cartesian Coordinates of Ground State Geometries of Pyrrole Oligomers (**nP**) at HF/6-31G* Level..... 126

C. Cartesian Coordinates of Ground State Geometries of Studied Structures at B3LYP/6-31G* Level.....130

C.1 Cartesian Coordinates of Ground State Geometries of Thiophene Oligomers (**nT**) at B3LYP/6-31G* Level..... 130

C.2 Cartesian Coordinates of Ground State Geometries of Furan Oligomers (**nF**) at B3LYP/6-31G* Level..... 133

C.3 Cartesian Coordinates of Ground State Geometries of Pyrrole Oligomers (**nP**) at B3LYP/6-31G* Level..... 136

D. Cartesian Coordinates of Lowest Singlet Excited State Geometries of Studied Structures at CIS/6-31G* Level 140

D.1 Cartesian Coordinates of Lowest Singlet Excited State Geometries of Thiophene Oligomers (**nT**) at CIS/6-31G* Level..... 140

D.2 Cartesian Coordinates of Lowest Singlet Excited State Geometries of Furan Oligomers (**nF**) at CIS/6-31G* Level..... 143

D.3 Cartesian Coordinates of Lowest Singlet Excited State Geometries of Pyrrole Oligomers (**nP**) at CIS/6-31G* Level 146

LIST OF TABLES

Table 1.1 Ionization potentials (IP) and electron affinities (EA) of the heteroatoms (X=S, O, N), and energy gap (E_g) values of the corresponding polymers that includes these heteroatoms- S for polythiophene, O for polyfuran, and N for polypyrrole[a]..... 14

Table 1.2 Experimental Absorption Energies (in eV) of thiophene oligomers (**nT**). 22

Table 1.3 Experimental Fluorescence Energies (in eV) of thiophene oligomers (**nT**) 22

Table 1.4 Solid-state and low temperature absorption data (in eV) of thiophene oligomers (**nT**)..... 22

Table 1.5 Absorption and Fluorescence data (in eV) of furan oligomers (**nF**) [36].. 26

Table 1.6 Absorption data (eV) of pyrrole oligomers (**nP**) [152] 27

Table 2.1 Acronyms for some popular functionals in DFT..... 45

Table 3.1 Optimized bond lengths (Å) in the ground state (S_0) and the lowest singlet excited state (S_1) of thiophene oligomers (**nT**) 50

Table 3.2 Relative and average errors in the computed geometrical parameters of some selected thiophene oligomers (**nT**)[a]. 51

Table 3.3 Optimized bond lengths (Å) in the ground state (S_0) and the lowest singlet excited state (S_1) of furan oligomers (**nF**)..... 57

Table 3.4 Optimized bond lengths (Å) in the ground state (S_0) and the lowest singlet excited state (S_1) of pyrrole oligomers (**nP**)..... 61

Table 3.5 Absorption energies (ΔE_{abs}) and oscillator strengths (f) of thiophene oligomers (**nT**) computed at various levels of theory[a]..... 79

Table 3.6 Absorption energies (ΔE_{abs}) and oscillator strengths (f) of furan oligomers (**nF**) computed at various levels of theory[a] 80

Table 3.7 Absorption energies (ΔE_{abs}) and oscillator strengths (f) of pyrrole oligomers (**nP**) computed at various levels of theory[a]..... 81

Table 3.8 Predicted vertical emission energy (eV) in the $S_1 \rightarrow S_0$ transition of bifuran (**2F**) at various levels of theory[a] 86

Table 3.9 Emission energies (ΔE_{ems}) and oscillator strengths (f) of thiophene

oligomers (**nT**) computed at various levels of theory. [a] 87

Table 3.10 Emission energies (ΔE_{ems}) and oscillator strengths (f) of furan oligomers (**nF**) computed at various levels of theory. [a] 88

Table 3.11 Emission energies (ΔE_{ems}) and oscillator strengths (f) of pyrrole oligomers (**nP**) computed at various levels of theory. [a] 88

Table 3.12 Stokes shifts (eV) obtained as the difference between the absorption energies calculated at TDDFT/6-31G*//RHF/6-31G* and the fluorescence energies calculated at TDDFT/6-31G*//CIS/6-31G* levels for oligothiophene (**nT**), oligofuran (**nF**), and oligopyrrole (**nP**), where n=1-6. 89

LIST OF FIGURES

Figure 1.1 Examples of conjugated systems: Structures of (a) all *trans*-polyacetylene (*trans*-PA), (b) all *cis*-polyacetylene (*cis*-PA), and (c) polythiophene (PTh)..... 1

Figure 1.2 Energy gap (Eg) in extended conjugated systems..... 2

Figure 1.3 The site positions, *i*, in bithiophene (**2T**)..... 3

Figure 1.4 The Kekulé forms of thiophene (**1T**), furan (**1F**), and pyrrole (**1P**). 10

Figure 1.5 Structures of (a) *trans-cisoid*-polyacetylene, and (b) polyheterocycles (X=S, O, or NH)..... 10

Figure 1.6 Mesomeric resonance forms of polyheterocycles (X=S, O, or NH). 11

Figure 1.7 Qualitative scheme of the interaction between the hydrocarbon skeleton and the heteroatom to form the five-membered ring. 12

Figure 1.8 Orbital correlation diagrams for the π-valence orbitals of the *syn*-1,3-butadiene and aromatic heterocycles at RHF/6-31G* level. All species belong to the C_{2v} point group. Detailed quantitative data may be found elsewhere [12]..... 13

Figure 1.9 Frontier orbitals of *syn*-1,3-butadiene and aromatic heterocycles [12].... 13

Figure 1.10 Representations of Franck-Condon type vertical transition (1), resonance fluorescence (2), and relaxed fluorescence (3) 15

Figure 1. 11 The molecular structure of octatetraene (belongs to the C_{2h} point group) 19

Figure 1.12 The main electronic configurations contributing to the ground state S_0 and the lowest singlet excited states S_1 and S_2 in the case of octatetraene 20

Figure 1.13 Molecular structures of oligothiophenes (**nT**) and polythiophene (very large n)..... 21

Figure 1.14 Molecular structures of oligofurans (**nF**) and polyfuran (very large n) . 25

Figure 1.15 Molecular structure of oligopyrroles (**nP**) and polypyrrole (very large n) 26

Figure 2.1 Representation of excited Slater determinants generated from a HF reference……...41

Figure 3.1 Numbering of sites and bonds between carbon atoms in the hexamers of oligoheterocycles (X=S, O, or NH). In general, r_i reflects the bond length between carbon atoms C_i and C_{i+1}. 49

Figure 3.2 Evolution with site position, *i* (see Figure 3.1), of the bond-length alternation, $\Delta r_i = (-1)^i (r_i - r_{i-1})$ in the ground state of sexithiophene (**6T**) calculated at AM1, RHF/6-31G*, and B3LYP/6-31G* levels. 52

Figure 3.3 Evolution with site position, *i* of the bond-length alternation, $\Delta r_i = (-1)^i (r_i - r_{i-1})$ in the ground state of **1T** (a), **2T** (b), **3T** (a), **4T** (b), **5T** (a), and **6T** (b) calculated at B3LYP/6-31G* level. In order to compare oligomers of different lengths, the numbering in Figure 3.1 has been changed. The sites at 0 and 1 above refer to; in (a) intraring, in (b) interring sites at the center of the oligomers. 55

Figure 3.4 Evolution with site position, *i* (see Figure 3.1), of the bond-length alternation, $\Delta r_i = (-1)^i (r_i - r_{i-1})$ in the ground state of sexifuran (**6F**) calculated at AM1, RHF/6-31G*, and B3LYP/6-31G* levels. 58

Figure 3.5 Evolution with site position, *i* of the bond-length alternation, $\Delta r_i = (-1)^i (r_i - r_{i-1})$ in the ground state of **1F** (a), **2F** (b), **3F** (a), **4F** (b), **5F** (a), and **6F** (b) calculated at B3LYP/6-31G* level. In order to compare oligomers of different lengths, the numbering in Figure 3.1 has been changed. The sites at 0 and 1 above refer to; in (a) intraring, in (b) interring sites at the center of the oligomers. 59

Figure 3.6 Evolution with site position, *i* (see Figure 3.1), of the bond-length alternation, $\Delta r_i = (-1)^i (r_i - r_{i-1})$ in the ground state of sexithiophene (**6P**) calculated at AM1, RHF/6-31G*, and B3LYP/6-31G* levels. 62

Figure 3.7 Evolution with site position, *i* of the bond-length alternation, $\Delta r_i = (-1)^i (r_i - r_{i-1})$ in the ground state of **1P** (a), **2P** (b), **3P** (a), **4P** (b), **5P** (a), and **6P** (b) calculated at B3LYP/6-31G* level. In order to compare oligomers of different lengths, the numbering in Figure 3.1 has been changed. The sites at 0 and 1 above refer to; in (a) intraring, in (b) interring sites at the center of the oligomers. 63

Figure 3.8 Evolution with site position, *i* (see Figure 3.1), of the bond-length alternation, $\Delta r_i = (-1)^i (r_i - r_{i-1})$ in the ground state of **6T**, **6F**, and **6P** (b) calculated at B3LYP/6-31G* level 64

Figure 3.9 Evolution with site position, *i* (see Figure 3.1), of changes in single and double bond lengths (as indicated) between the ground state (B3LYP/6-31G*) and lowest singlet excited state (CIS/6-31G*) values shown for **6T**. 65

Figure 3.10 Evolution with site position, *i* (see Figure 3.1), of changes in single and double bond lengths (as indicated) between the ground state (B3LYP/6-31G*) and lowest singlet excited state (CIS/6-31G*) values shown for **6F** as indicated. 66

Figure 3.11 Evolution with site position, *i* (see Figure 3.1), of changes in single and double bond lengths (as indicated) between the ground state (B3LYP/6-31G*) and lowest singlet excited state (CIS/6-31G*) values shown for **6P**. 66

Figure 3.12 Evolution with site position, *i*, of the bond-length alternation, $\Delta r_i = (-1)^i (r_i - r_{i-1})$ in the lowest singlet excited state of **3T**, **4T**, **5T** and **6T** calculated at CIS/6-31G* level. In order to compare oligomers of different lengths, the numbering in Figure 3.1 has been changed. The sites at 0 and 1 above refer to; in (a) intraring, in (b) interring sites at the center of the oligomers. 69

Figure 3.13 Evolution with site position, *i*, of the bond-length alternation, $\Delta r_i = (-1)^i (r_i - r_{i-1})$ in the lowest singlet excited state of **3F**, **4F**, **5F** and **6F** calculated at CIS/6-31G* level. In order to compare oligomers of different lengths, the numbering in Figure 3.1 has been changed. The sites at 0 and 1 above refer to; in (a) intraring, in (b) interring sites at the center of the oligomers. 70

Figure 3.14 Evolution with site position, *i*, of the bond-length alternation, $\Delta r_i = (-1)^i (r_i - r_{i-1})$ in the lowest singlet excited state of **3P**, **4P**, **5P** and **6P** calculated at CIS/6-31G* level. In order to compare oligomers of different lengths, the numbering in Figure 3.1 has been changed. The sites at 0 and 1 above refer to; in (a) intraring, in (b) interring sites at the center of the oligomers. 70

Figure 3.15 Evolution with site position, *i* (the numbering in Figure 3.1 is changed by assigning *i*=0 to the carbon atom at the center of an oligomer), of the bond-length alternation, $\Delta r_i = (-1)^i (r_i - r_{i-1})$ in the lowest singlet excited state of **6T**, **6F** and **6P** calculated at CIS/6-31G* level. 71

Figure 3.16 Molecular structure of *trans-cisoid* acetylene hexamers, **6A**. 73

Figure 3.17 (a) Schematic representation of the HOMO for trans-cisoid acetylene hexamer, **6A**. (b) Schematic representation of the HOMO for aromatic thiophene hexamer, **6T**. (c) Schematic representation of the HOMO for aromatic furan hexamer, **6F**. (d) Schematic representation of the HOMO for aromatic pyrrole hexamer, **6P**. 73

Figure 3.18 (a) Schematic representation of the HOMO-1 for trans-cisoid acetylene hexamer, **6A**. (b) Schematic representation of the HOMO-1 for aromatic thiophene hexamer, **6T**. (c) Schematic representation of the HOMO-1 for aromatic furan hexamer, **6F**. (d) Schematic representation of the

HOMO-1 for aromatic pyrrole hexamer, **6P**. 74

Figure 3.19 (a) Schematic representation of the HOMO-2 for trans-cisoid acetylene hexamer, **6A**. (b) Schematic representation of the HOMO-2 for aromatic thiophene hexamer, **6T**. (c) Schematic representation of the HOMO-2 for aromatic furan hexamer, **6F**. (d) Schematic representation of the HOMO-2 for aromatic pyrrole hexamer, **6P**. 74

Figure 3.20 (a) Schematic representation of the LUMO for trans-cisoid acetylene hexamer, **6A**. (b) Schematic representation of the LUMO for aromatic thiophene hexamer, **6T**. (c) Schematic representation of the LUMO for aromatic furan hexamer, **6F**. (d) Schematic representation of the LUMO for aromatic pyrrole hexamer, **6P**. 75

Figure 3.21 (a) Schematic representation of the LUMO+1 for trans-cisoid acetylene hexamer, **6A**. (b) Schematic representation of the LUMO+1 for aromatic thiophene hexamer, **6T**. (c) Schematic representation of the LUMO+1 for aromatic furan hexamer, **6F**. (d) Schematic representation of the LUMO+1 for aromatic pyrrole hexamer, **6P**. 76

Figure 3.22 (a) Schematic representation of the LUMO+2 for trans-cisoid acetylene hexamer, **6A**. (b) Schematic representation of the LUMO+2 for aromatic thiophene hexamer, **6T**. (c) Schematic representation of the LUMO+2 for aromatic furan hexamer, **6F**. (d) Schematic representation of the LUMO+2 for aromatic pyrrole hexamer, **6P**. 76

Figure 3.23 Convergence of the computed (—, CIS/6-31G*//B3LYP/6-31G*) and experimental (---, in CH_2Cl_2) excitation energies ($S_1 \leftarrow S_0$) in thiophene oligomers (**nT**). Computed (●) and experimental (○) data is included. 83

Figure 3.24 Convergence of the computed (—, CIS/6-31G*//RHF/6-31G*) and experimental (---, in acetonitrile) excitation energies ($S_1 \leftarrow S_0$) in furan oligomers (**nF**). Computed (●) and experimental (○) data is included. 84

Figure 3.25 Convergence of the computed (—, CIS/6-31G*//B3LYP/6-31G*) and experimental (---, in CH_2Cl_2) excitation energies ($S_1 \leftarrow S_0$) in pyrrole oligomers (**nP**). Computed (●) and experimental (○) data is included. 85

LIST OF ABBREVIATIONS

Å	Angstrom
AO	Atomic orbital
AM1	Austin Model 1
B3LYP	Becke' s three parameter exchange hybrid functional with Lee, Yang, Parr (LYP) correlation functional
BLA	Bond Length Alternation
CC	Coupled cluster theory
CI	Configuration interaction
CIS	Configuration Interaction Singles
ΔE_{abs}	Absorption energy
ΔE_{ems}	Emission energy
Δr_i	Bond length alternation parameter
DFT	Density functional theory
ECL	Effective Conjugation Length
GTO	Gaussian type orbital
HF	Hartree-Fock theory
HOMO	Highest occupied molecular orbital
LED	Light-Emitting Diode
LUMO	Lowest unoccupied molecular orbital
MO	Molecular orbital
nF	Furan oligomers
NMR	Nuclear magnetic resonance spectroscopy
nP	Pyrrole oligomers
nT	Thiophene oligomers

PES	Potential energy surface
PA	Polyacetylene
PFu	Polyfuran
PPr	Polypyrrole
PTh	Polythiophene
ψ	Wave function (state function)
RHF	Restricted Hartree-Fock
S_0	Ground state
S_1	Lowest singlet excited state
STO	Slater type orbital
TDDFT	Time-Dependent Density Functional Theory
TFFET	Thin-Film Field-Effect Transistor

CHAPTER 1

INTRODUCTION

1.1 General Electronic Properties of Conjugated Systems

The general structure of conjugated systems is represented by a one-dimensional chain comprising alternating double- and single-bonds, which may include heteroatoms (Figure 1.1).

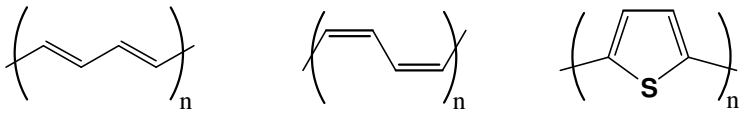

(a) (b) (c)

Figure 1.1 Examples of conjugated systems: Structures of (a) all *trans*-polyacetylene (*trans*-PA), (b) all *cis*-polyacetylene (*cis*-PA), and (c) polythiophene (PTh).

One of the main features of the conjugated systems is the highest occupied molecular orbital (HOMO)- lowest unoccupied molecular orbital (LUMO) energy gap. The energy gap (E_g) (Figure 1.2) represents the difference in energy between HOMO and LUMO. In the case of very large molecules, i.e., polymers, it is called as the band gap. The energy gap can be determined by measuring the low-energy absorption edge of the electronic absorption spectrum, or by computing the minimum electronic excitation energy.

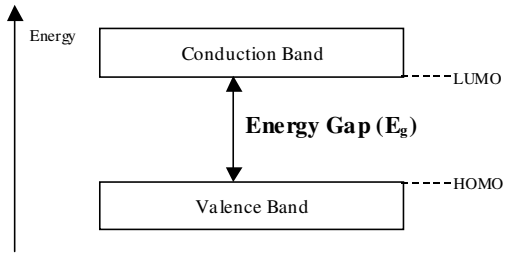

Figure 1.2 Energy gap (Eg) in extended conjugated systems.

In conjugated systems, the p_{π}-orbitals of the carbon atoms mesomerize more or less, i.e., the single and double bonds become similar. In other words, π electrons move easily from one bond to the other (they are delocalized). Hence, a system of π-electrons extending over a large number of sp^2-carbons is formed. This π-system is the origin of the unique electronic and optical properties of linearly conjugated systems.

If π-electrons were to show a full delocalization, carbon-carbon bonds lengths would be equal, E_g would be zero, and these systems would show conductivities just like a metal. However, due to some electronic effects such as electron-electron correlation (see Chapter 2), this structure is unstable. To stabilize its structure the system acts in a way to localize single and double bonds, i.e., π-electron distribution is not uniform in conjugated systems [1]. This leads to the finite E_g values for the conjugated polymers [2].

The band gap of polyacetylene (PA) is 1.50 eV. Polymers showing lower E_g values than PA can be considered as small band gap conjugated polymers. In addition to the increase in conductivity, small band gap in conjugated systems will have important consequences on the physical properties. For instance, the red shift of the absorption and emission spectra resulting from a decrease in E_g will make available conjugated polymers transparent in the visible spectral range and potentially useful for the fabrication of light-emitting diodes (LEDs) operating in the IR [3].

The magnitude of the band gap of polyaromatic-conjugated systems depends on five factors:

- The bond length alternation (BLA),

- The interring torsion angles,
- The linear and cyclic π-conjugation,
- The substitution,
- The intermolecular interactions.

First three contributions are important from the point of view of this study, and will be explained in the following parts. The other factors are not considered (see Section 1.5).

1.1.1 Bond Length Alternation (BLA)

Bond length alternation (BLA) is defined as the average of the difference in length between the neighboring longer (single) and shorter (double) bonds in the conjugated pathway. In this work, BLA values, Δr_i were determined as

$$\Delta r_i = (-1)^i \left(r_i - r_{i-1} \right), \; i = 2, 3, .., 4\,n\text{-}1 \tag{1.1}$$

where i are site positions (Figure 1.3), r_i is the bond length between (i-1)th and (i)th carbon atoms, and n is the number of rings in the oligomer of interest. The sign modulation factor in equation 1.1 ensures that Δr_i values will be represented by positive numbers in a molecule with alternating double and single bonds.

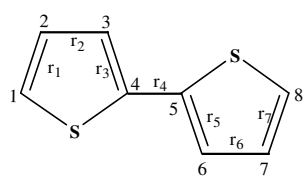

Figure 1.3 The site positions, *i*, in bithiophene (**2T**).

Few points must be mentioned about the site positions, i. Firstly, the r_i values corresponding to single and double bonds are for i = 2, 4, … and i = 1, 3, .., respectively. In addition, for intraring sites, the values of site positions are i = 2, 3, 6, 7, etc. At the interring sites the values become i = 4, 5, 8, 9, etc. For example, the first BLA parameters, Δr_i for the intraring and interring sites in bithiophene (2T)

are:

$$\Delta r_2 = (-1)^2 \left(r_2 - r_1\right) = r_2 - r_1 \text{ for the first intraring site, i = 2} \quad (1.2)$$

$$\Delta r_4 = (-1)^4 \left(r_4 - r_3\right) = r_4 - r_3 \text{ for the first interring site, i = 4}$$

where r_i are indicated in Figure 1.3.

The bond-length alternation parameter, Δr_i, reflects the uneven distribution of the π-electron density along the conjugated chain. The sign of Δr_i indicates whether the system is in a quinoid (negative) or an aromatic (positive) form (see Figure 1.6). Reduction of the magnitude of BLA means that a molecule in the bond-alternate polyene limit gets nearer to the bond-equivalent cyanine limit [4]. In the cyanine limit (or in benzoid-like geometry), contribution of two canonical resonance structures to the state of interest becomes equal, and thus, the BLA in this state is zero.

BLA in the conjugated path is critical in understanding the efficiency of delocalization, and thus, many properties of conjugated systems. It is important to reduce the bond length alternation in order to decrease the band gap of one-dimensional polymers [5]. In the case of polyacetylene, various theoretical calculations [6, 5e] support that the band gap increases as the BLA increases. However, this kind of a correlation does not hold for conjugated polymers based on aromatic rings [5d].

1.1.2 Interring Torsion Angle Effect

In linear conjugated systems containing aromatic cycles, the existence of single bonds between two rings allows the occurrence of interannular rotations. As the interring torsion angle increases, the magnitude of the overlap between the p_π orbitals on the carbon atoms connecting two rings gets smaller. This means that the system starts to depart from coplanarity reducing the extension of the linear π conjugation. Thus, any departure from coplanarity will result in an increase in E_g.

It has been proved in many other experimental and theoretical studies that interring torsion angles play an important role in determining physical properties of

π-conjugated systems containing cyclic repeating units. In this study, however, all systems considered are planar, and thus, we do not take into account this effect.

1.1.3 Effective Conjugation Length (ECL)

It is very straightforward to think continuity of the π-conjugation for an extended conjugated system with a linear backbone. This "conjugation and no end" concept was initially thought to be a characteristic property of linearly π-conjugated systems. However, it was soon realized that an *effective conjugation length (ECL)* [7] exists even in very long, fully conjugated chains that have no structural deficiencies. The ECL [7, 8] defines the number of repeat or monomer units in a π-conjugated polymer that are required to furnish size-independent optical, redox, or other properties. Being a numerical quantity, it has no generally valid theoretical basis. It is very difficult to use physical properties of polymers in determination of effective conjugation length. However, oligomers are used as prime candidates in studies aimed at determination of the ECL [9]. The ECL of a π-conjugated polymer has been proved to be of great value in theoretical and experimental understanding of many properties of these systems [10]. In addition, knowledge of the ECL enables one to substitute high-molecular-weight polymers by shorter oligomers that have reached convergence of their physical properties and display better processability in specific applications.

There may be different reasons for a π-conjugated polymer to exhibit a convergent limit for certain physical properties such as the longest wavelength electronic absorption (λ_{abs}) and fluorescence (λ_{fluo}) maxima. For instance, distortions from planarity of the conjugated backbone by rotations around single bonds reduce π overlap, and thus the conjugation exhibits a limited extension. Cyclic π-conjugation within the component rings renders the mobility of π electrons as in the case of conjugated polyaromatic systems. Indeed, this aromaticity results in a competition between π-electron confinement within the rings and delocalization along the chain [11]. Others [12] have proved the presence of a strong cyclic π-conjugation in extended systems of thiophene, furan, and pyrrole,

which may be related to the limited linear conjugation length in corresponding polymers of these systems.

A simple and commonly used way to evaluate the ECL includes plotting a relevant physical property (such as the longest-wavelength absorption energy, E_{max}) against the inverse number of repeating units, *n*. Extrapolation to infinite chain length yields c_0 which is the E_{max} value of the oligomer with length equal to the ECL [7].

$$E_{max} = c_0 + \frac{1}{n} c_1 , \ \lim_{n \to \infty} E_{max} = c_0 \tag{1.3}$$

where c_1 is the E_{max} value of the oligomer with length *n*.

This empirical equation leads satisfying regression of physical properties of short-length oligomers since both the number of electrons and the length of the π system increase simultaneously as additional monomer units are added [13]. However, deviations occur from this inverse relationship for very long oligomers (higher *n* values) and the infinite polymer because the actual curve is expected to have asymptotic behavior. The value of *n* that the deviation starts is very difficult to recognize because of the limited physical data on longer oligomers. Nevertheless, the effect of the deviations can be easily seen in the polymer data, i.e., in the c_0 value. Therefore, it has been concluded that this equation results in wrong ECL values and should be replaced by another expression [7]. There are several proposed algorithms for calculation of the ECL and their applications to conjugated systems in the literature [14]. A simple and reliable algorithm has been presented by Meier *et. al.* [7]:

$$\begin{aligned} E(n) &= E_\infty + (E_1 - E_\infty) e^{-a(n-1)} \\ \lambda(n) &= \lambda_\infty + (\lambda_1 - \lambda_\infty) e^{-b(n-1)} \end{aligned} \tag{1.4}$$

where E_1 and λ_1 belong to the parent compound ($n = 1$), E_∞ and λ_∞ are the limiting values for $n \rightarrow \infty$, *a* and *b* are the numerical parameters that indicate how fast the limit of convergence is approached.

Contrary to other algorithms, the growth functions (equation 1.4) have been proved to give accurate dependence of electronic absorption and emission data on the number of repeating units. In addition, this approach allows the direct characterization of the overall effect of conjugation and the velocity of oligomeric

growth, which serves as a measure of how fast the limit of convergence is actually attained. Thus, we used these last functions to predict the ECL and the convergent values of the energies of the maximum-wavelength absorption and the fluorescence in our systems.

1.2 Conjugated Polymers

Delocalized π-system makes conjugated polymers to be -in their pristine, neutral state- one-dimensional semiconductors [15]. Like other semiconductors, they can be doped (oxidized or reduced), to increase their conductivity extremely. For the discovery and development of such conductive polymers, Shirakawa, Heeger, and MacDiarmid [16-18] received the Nobel Prize in chemistry 2000 [19]. More precisely, they have shown that polyacetylene undergoes an increase in conductivity of 12 orders of magnitude by oxidative doping. Furthermore, this discovery has prompted intense research interest in the field of conjugated polymers. The interest is, firstly, because the organic conjugated polymers have many excellent physical properties including electrical conductivity, photoconductivity, electroluminescence, photoluminescence [20], nonlinear optical activity [21], and lasing [22]. Second, and more important, reason for the tremendous work in this area is that organic conjugated polymers form a promising class of materials for scientific and technological applications because of the inherent synthetic flexibility, the ease of processing, and the possibility of tailoring characteristic properties to accomplish a desired function [23]. Applications of conjugated polymers now exist in many areas: light-emitting diodes (LED)s [24], conducting fabrics [25], thin-film field-effect transistors (TFFET) [26], solid state lasers [27], photovoltaic devices [28], photonics [29], polar cells [30], electrochromic materials [31], etc.…

The target of all these studies was (and continues to be) to design new materials with improved properties. From this respect, the challenge is to understand the basic mechanisms involved in conduction and optical processes of conjugated polymers, and use this understanding to predict the properties and to direct the design of completely new materials. Conjugated polymers, however, are

not very good candidates for physical studies. Their physical properties depend frequently on the preparation conditions [32]. They are very difficult to dissolve in any solvent because of their delocalized π electronic and cross-linked structures [33]. The morphology problems such as statistical chain length distribution, interruption of conjugation and conducting pathways by mislinkages, and other chemical and structural defects make this class of polymers, like all polymers, devoid of a rigidly defined structural principle. Thus, a deeper understanding the origin of a given property from the experimental data is very arduous. In addition, results of the theoretical calculations on polymers are very difficult to interpret because there is almost no opportunity to compare them with the experimental data.

1.3 Conjugated Oligomers

Oligomers constitute the lower homologues of polymers, since they will contain only a few monomer units [32]. The number of repeating units increases in the order:

Monomer (one unit) → Oligomer → Polymer

Although it is very difficult to draw a borderline between oligomers and polymers in terms of their molecular weights, increasing the chain length of an oligomer changes its physical properties until the ECL is reached. Thus, chemically well-defined monodisperse (unique chain length) oligomers have initially been used as finite model systems to attain structure-property relationships, and properties of their corresponding polydisperse (not unique chain length) high molecular weight analogues by extrapolation [2, 32, 34]. This study of polymer properties from properties of corresponding oligomers is called "oligomer approach". The oligomer approach was first employed by Cornil *et al*., [35], and enjoyed a lot of popularity lately [36-40]. This approach is now well established and provides invaluable information on the properties polymers [41]. However, not all physical or chemical properties of high molecular weight polymers can be modeled with the corresponding smaller oligomers because of bulk effects and size-inconsistency problems.

While π-conjugated oligomers were being studied to predict the polymer properties, they have emerged as an interesting field of their own right, because of the promising physical properties of these compounds [32]. Some physical properties of oligomers even surpass those of the polymers. Oligomers are usually more soluble than polymers depending on the size and substitution pattern. In addition, oligomers can form pure crystals. They are stable in various redox states. The precise characterization of the electronic and geometric structure succeeds both in solution and in the solid state. Their properties are intrinsically associated with those of isolated chain and affected only slightly by the environment. Processability of the oligomers is generally better than that of the polymers. The extended π-system of conjugated oligomers qualifies them as chromophores with broad range of optical properties. They are easily accessible to theoretical computation because consideration of only a small number of electrons is required. In fact, oligomers represent ideal systems for theoretical studies based on quantum-chemical methods [32]. Furthermore, monodisperse π-conjugated oligomers are today seen as prospective materials in science and technology, especially as molecular wires in future molecular scale electronic devices and nanotechnological devices [41, 42]. Deeper understanding of basic electronic structure of the oligomers is required to acquire desired properties that can be employed in making technologically useful materials. Thus, there has been a considerable interest in the field of π-conjugated oligomers, especially for understanding of the basic properties and processes. Even so, strong debates concerning the localization lengths of excitations, the optical oscillator strengths, etc. continue [43].

Consequently, the research centered on the π-conjugated oligomers as the medium links between two extremes, monomers, and polymers, strongly suggest a unified view and will push ahead with further explosive growth. Therefore, we have chosen to pay a particular attention on the oligomeric systems in this theoretical study.

1.4 Aromatic Five-Membered Heterocyclic Oligomers

There are three classes of the conjugated oligomers depending on the type of the building blocks: olefinic oligomers (e.g. butadiene), "hybrids" of aromatic and olefinic oligomers (e.g. stilbene oligomers), and aromatic oligomers (e.g. aromatic five-membered heterocyclic oligomers).

The cyclic compounds in molecules of which there is an element other than carbon are called heterocyclic compounds. The most common heterocyclic compounds are the ones that contain sulfur, oxygen, and nitrogen. The Kekulé forms of the aromatic five-membered heterocyclic compounds are given in Figure 1.4.

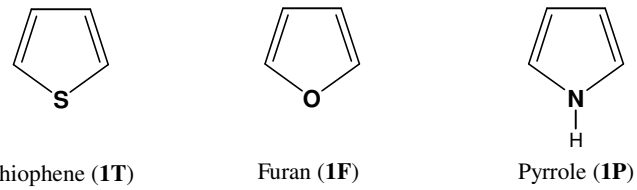

Figure 1.4 The Kekulé forms of thiophene (**1T**), furan (**1F**), and pyrrole (**1P**).

Polymers and oligomers of thiophene, furan, and pyrrole units are examples of a specific class of conjugated systems, called polyheterocycles. Polyheterocycles can be considered as conjugated chains consisting of sp^2-carbon atoms, which have an analogous structure to *cis*-PA (especially to imaginary *trans-cisoid*-polyacetylene) and are stabilized by the bridging heteroatom, *X* (Figure 1.5) [44].

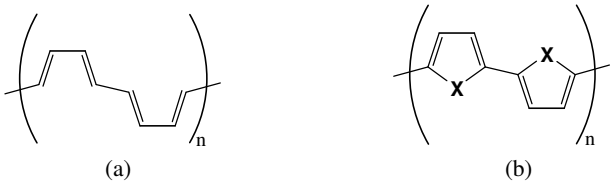

Figure 1.5 Structures of (a) *trans-cisoid*-polyacetylene, and (b) polyheterocycles (X=S, O, or NH).

In comparison to PA, this provides several interesting features such as

- A nondegenerate ground state,
- Structural versatility, which allows the modulation of their electronic and

electrochemical properties by manipulation of the monomer structure,

- Higher environmental stability.

The heteroatom in each ring of heterocyclic systems breaks the symmetry present in *trans*-polyacetylene and, thereby, removes the twofold degeneracy of the ground state. Indeed, polyheterocycles are based on a *cis*-PA backbone, which is nondegenerate in the ground state, two limiting mesomeric forms (Figure 1.6), aromatic and quinoid, contribute to the ground state [1, 5d , 45, 46].

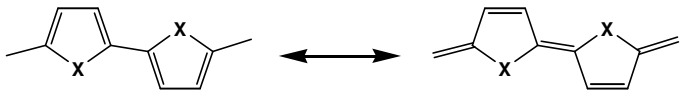

Aromatic Quinoid

Figure 1.6 Mesomeric resonance forms of polyheterocycles (X=S, O, or NH).

The aromatic and quinoid forms are not energetically equivalent [5e]. However, because of the higher stability of aromatic form, major contribution to the ground state comes from this form. Mintmire *et al.* [46, 47] claimed that the heteroatoms are responsible for the higher stability of the aromatic forms relative to the quinoid forms.

It has been concluded that the heteroatoms also play an important role in determining the band gaps of the five-membered heterocyclic systems [47-52]. This is sensible since the weaker mesomerization in polyheterocycles than that in polyacetylene is a result of the large electronic effect of the heteroatoms. Because of the weaker delocalization of the π systems, the band-gaps of polyheterocycles are large relative to that of PA. As seen, heteroatom effect is an implicit effect- the conjugation over carbon atoms will dominate the spectroscopic properties of the polyheterocycles.

1.4.1 Specific Electronic Properties of Aromatic Five-Membered Heterocyclic Systems

1.4.1.1 Frontier Molecular Orbitals of Heterocyclic Systems

Since many optical properties of the five-membered heterocyclic π-conjugated systems are related to the frontier orbitals, it is appropriate to have a closer look at the highest occupied molecular orbital (HOMO) and the lowest unoccupied molecular orbital (LUMO). Indeed, it is known that the nodal pattern of the HOMO in heteroaromatic oligomers is characteristic of the aromatic form while that of the LUMO is characteristic of the quinoid form [46, 53].

The frontier molecular orbitals of the five-membered heterocyclic systems can be considered as forming from the interaction between heteroatoms and the polyacetylene backbone. As the simplest example, a qualitative scheme for the interaction of frontier orbitals of the *syn*-1, 3-butadiene and the heteroatom to form the monomers was given (Figure 1.7) [54].

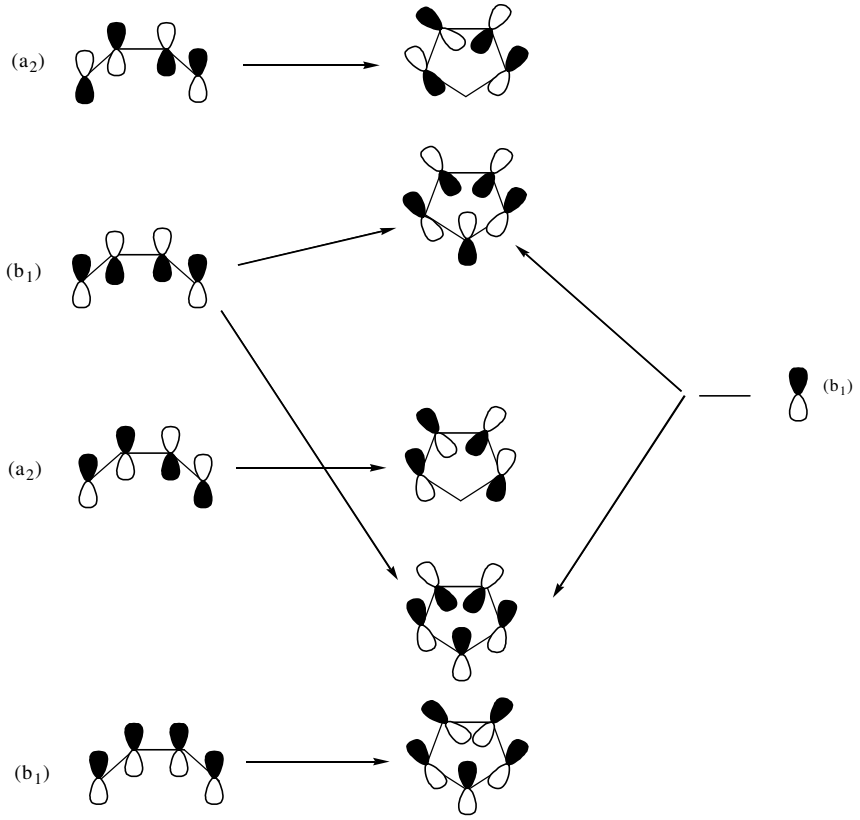

Figure 1.7 Qualitative scheme of the interaction between the hydrocarbon skeleton and the heteroatom to form the five-membered ring.

The monoelectronic energies (Figure 1.8) and the shapes (Figure 1.9) of the frontier orbitals of five-membered aromatic heterocycles (thiophene (**1T**), furan (**1F**), and pyrrole (**1P**)) and that of *syn*-1,3-butadiene (**Bu**) are shown.

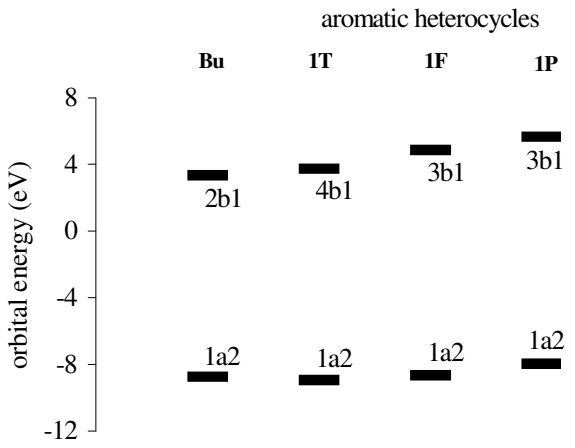

Figure 1.8 Orbital correlation diagrams for the π-valence orbitals of the *syn*-1,3-butadiene and aromatic heterocycles at RHF/6-31G* level. All species belong to the C_{2v} point group. Detailed quantitative data may be found elsewhere [12].

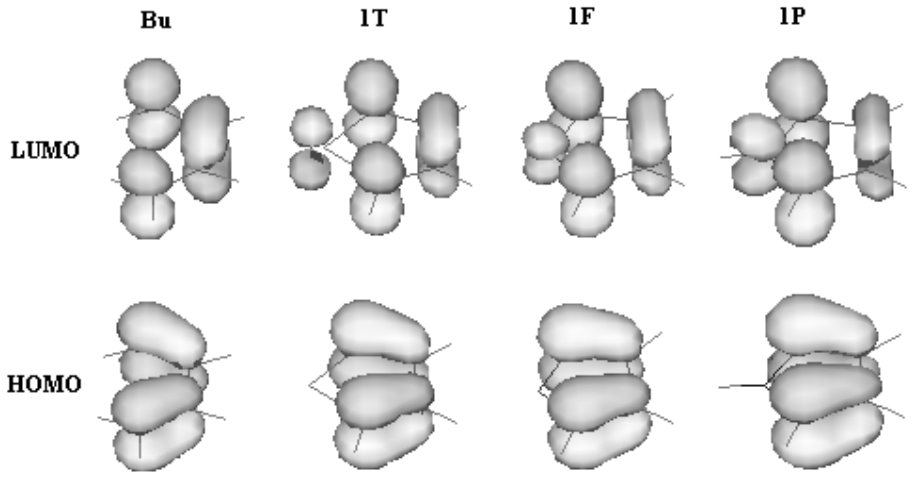

Figure 1.9 Frontier orbitals of *syn*-1,3-butadiene and aromatic heterocycles [12].

The monoelectronic energies and the shapes of the HOMO (a_2) of these systems resemble to those of *syn*-1,3-butadiene since the eigenvector associated

with the HOMO has a node passing through the heteroatom, which makes the contribution of the heteroatom to this orbital exactly zero due to symmetry. Hence, the HOMO remains approximately unchanged. Therefore, the changes in energy difference between the frontier orbitals are mainly determined by the position of the LUMO (b_1).

As shown in Figure 1.7, the LUMO of the heterocycle results from the interaction between the LUMO of the 1,3-butadiene and the out-of-plane b_1 orbital of the heteroatom, since the latter can interact only with π^* (b_1) orbital due to its symmetry. The strength of this interaction increases in the order, thiophene (3.80 eV), furan (5.00 eV), and pyrrole (7.04 eV) (the values in parentheses were for the case of trimers [12]). Thus, the degree of overlap of heteroatom p_x orbital with the butadiene π-valence orbitals is highest for sulfur, then oxygen, and nitrogen. Furthermore, the LUMO of the heterocycle is seen to have more stabilization with respect that of the hydrocarbon skeleton. Since the carbon moiety does not change for all five-membered heterocyclic systems, the magnitude of this stabilization depends on the energy of the HUMO of the heteroatom. Thus, the energy of the LUMO of the heterocycles depends upon the ionization potential of the heteroatom.

Table 1.1 Ionization potentials (IP) and electron affinities (EA) of the heteroatoms (X=S, O, N), and energy gap (E_g) values of the corresponding polymers that includes these heteroatoms- S for polythiophene, O for polyfuran, and N for polypyrrole[a].

Heteroatom/property	S	O	N
IP	43.3	57.0	60.8
EA	8.7	6.1	0.2
E_g	2.00	2.35	2.85

[a]All values are in eV.

From Table 1.1, we see that the E_g of the polymers have the same ordering as IP, but the reverse order of EA of the heteroatom. Others [55] have presented a detailed study on the correlation between EA of the heteroatom and optical and electronic properties of polyheterocycles. They have exemplified the effect of heteroatoms on physical properties of extended conjugated systems in addition to that of monomers.

1.4.1.2 Franck-Condon Principle

In the ground state of a molecule, the most probable location of the nuclei is at their equilibrium separation, R_e. When a stable ground state molecule absorbs ultraviolet/visible light, it may undergo excitation from its HOMO to an excited state such as the LUMO. Since electronic motion is much faster than nuclear motion, electronic transitions occur more favorably when the nuclear structure of the initial and final states are most similar. This statement is called *Frank-Condon Principle*. In a Franck-Condon type transition, the most intense vibronic transition is a vertical transition that occurs from the ground (S_0) to the excited state (for example, S_1), or in emission $S_1 \rightarrow S_0$ (Figure 1.10). In terms of quantum mechanics, transitions are most intense when the wave function of the upper vibrational state most closely resembles the ground state vibrational wave function.

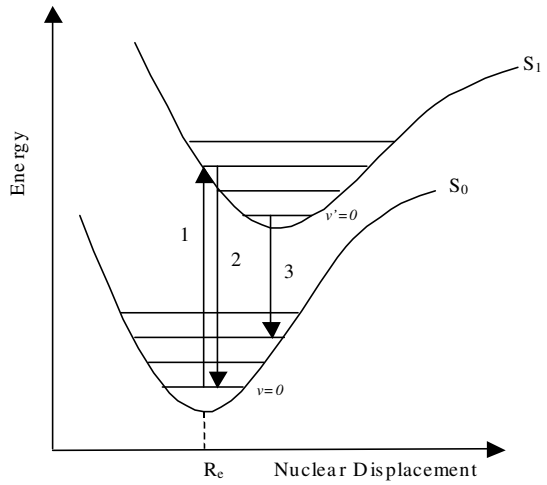

Figure 1.10 Representations of Franck-Condon type vertical transition (1), resonance fluorescence (2), and relaxed fluorescence (3)

The point where the vertical line (line 1 in Figure 1.10 cuts the electronic excited state (S_1) curve is the one in which the nuclei are most probably at the same initial separation R_e. Hence, this vibrational state is the most probable state for the termination of the transition, and is called the Franck-Condon state.

The excited molecule is in a nonequilibrium condition, and thus, must dissipate its excess energy. If the excited molecule is relaxed to a state of the same

spin (for example, from singlet S_1 state to the singlet ground state S_0) by emitting a photon, the pathway of relaxation is called fluorescence. Two types of fluorescence can be identified: resonance fluorescence and relaxed fluorescence. The emission that occurs instantaneously following photoexcitation is called resonance fluorescence (line 2 in Figure 1.10). However, typically excited states live long enough to undergo vibrational relaxation to the equilibrium nuclear position of the electronic excited state. The Franck-Condon vertical transition that occurs from this position is called relaxed fluorescence (line 3 in Figure 1.10). Thus, resonance fluorescence occurs at the λ_{max} of the absorption spectrum but the λ_{max} of relaxed fluorescence is red shifted. The shift between resonance and relaxed fluorescence is known as the Stokes shift.

The transition from the lowest vibrational level of the ground state (S_1, $v = 0$) to the lowest vibrational level of the first singlet excited state (S_1, $v' = 0$) is often called the '0-0' transition. Kasha's Rule[56] states that polyatomic molecular entities luminesce with appreciable yield only from the lowest excited state of a given multiplicity (from S_1, $v' = 0$ in the case of singlet multiplicity).

Almost all quantum-chemical calculations produce the 0-0 vertical electronic transition energies of the molecules in the gas phase- without accounting for any macroscopic effects (e.g., solvent effects). If the absorption spectrum of the molecule in the gas phase is not known, the theoretical transition energies can be compared to the absorption band maximum in a nonpolar solvent, thereby making the implicit assumption that the solvatochromic shift is approximately equal to the energy difference between the maximum and the 0-0 peak positions.

1.4.1.3 Excited State Electronic Structures of Heterocyclic Systems

The lowest singlet excited state plays a key role in absorption, emission, transport, and nonlinear optical processes of the π-conjugated systems. For these systems, the lowest singlet excited state is reached after a vertical transition mainly from the HOMO level to the LUMO level.

The bonding-antibonding pattern of the HOMO wave function is reflected into the ground state geometry. In contrary, the LUMO wave function displays the

exactly opposite bonding-antibonding pattern. Thus, in the lowest singlet excited state, the π-bond densities are strongly modified. Indeed, the spatial extent of the electron distribution increases, the total electron density becomes more diffuse, and often more polarizable. The change in electron density causes a new force field on the stationary nuclear configuration of the ground state. The nuclei must move to reorganize to the new electronic configuration. Consequently, the equilibrium geometry in the lowest singlet excited state is markedly different from that in the ground state. This phenomenon is called geometry relaxation.

Excited-state optimized geometries are important for the investigation of emission properties because structural relaxation after photoexcitation cannot be reproduced by ground-state optimizations. Indeed, the geometry optimization at the S_1 state is essential for the computation of emission energies, which are sources of light emission in luminescent compounds, such as nT. However, the nature of the lowest lying one-photon allowed excited state of the considered oligomers is still controversial. Thus, one of the goals of this study is to contribute to the present picture of the B-type excited state of single conjugated chains.

Knowledge about redistribution of π-electron density and geometry relaxation upon an electronic excitation are very important for a proper assignment of spectral transitions and to understand molecular behavior in the excited state. For the polyheterocycles, the electronic excitation to the lowest singlet excited state is often characterized by a significant reduction in C-C bond length alternation. The geometry relaxation is expected to increase the bond order of the interring bond(s) [57]. Hence, the capability of an oligomer to support a "quinoid-like' ' resonance structure will increase in the excited state [57].

Excitation energies are one of the many features of a molecular excited state, which are of interest to both physicists and chemists. For π-conjugated systems, energy gap transitions (singlet $\pi^* \leftarrow \pi$ transitions) are the lowest allowed excitations with minimum energy. Thus, the energy gap provides an estimate for λ_{max} in the UV/VIS absorption spectra. Excitation energies of different oligomers are well separated since band-gap transition energy-shifts to the red with increasing chain length and gradually saturates to a constant for long chains [58].

1.4.1.4 Why are Sophisticated Quantum-Chemical Calculations Needed?

For π-conjugated materials, small variations in chemical structure play an essential role on the optical properties. Thus, it is very important to consider the chemical nature fully. Quantum-chemical approaches, which allow this kind of consideration, have become an important tool for investigation of structure/property relationships in the field of π-conjugated materials. The theoretical works that employ the methods of quantum chemistry have provided a tremendous input to the field. These have helped in understanding of the electronic and optical characteristics of the conjugated materials, or better yet, in guiding the experimental efforts toward novel compounds with enhanced characteristics such as higher electrical conductivity, special optical properties or increased environmental stability [59].

Although oligomers are much smaller than polymers, they are large systems from the quantum chemical point of view. Thus, for a long time only very crude methods have been used. These calculations have been successful in understanding qualitative behavior of oligomers but fail in correctly predicting the absolute values of, for example, excitation energies. However, accurate calculations of molecular vertical excitation energies are essential for the modeling of spectroscopic probes, addressing structure-property relations and predicting structures with desired optical properties [1]. Thus, the computational methodology used is required to incur small errors overall. In addition, it must be well matched to both large and small π-systems to enable us to saturation effects [60]. The development of efficient quantum chemistry methods, and the improvements in computer technology have enabled sophisticated (high level) calculations on both small and large members of oligomers.

Excited state properties is the area where theory has to play an important role [61] since experimental study of excited state geometry is very difficult even for simple polyatomic molecules [62]. Generating a qualitatively acceptable description of excited states is a challenging task [63]. In treatment of the electronically excited states, more sophisticated methods that consider electron correlation effects [64], and consideration of strong connection between (and mutual influence of)

electronic and geometric structures are crucially needed. These effects, which are often negligible in short π systems, become relevant in molecules that contain large numbers of π electrons like conjugated oligomers.

Polyacetylene can be accepted as a fundamental model of organic conjugated systems. Therefore, we have chosen an oligomer of it, octatetraene (Figure 1.11), to exemplify the importance of the electron correlation effects. The ordering of the lowest singlet excited states in octatetraene has been analyzed [1].

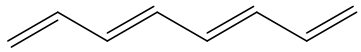

Figure 1. 11 The molecular structure of octatetraene (belongs to the C_{2h} point group)

The singlet ground state S_0 has A_g symmetry. At the one-electron level, the lowest (one-photon allowed) excited state is expected to be of B_u symmetry (Figure 1.12). Any (one-photon forbidden) A_g excited state lies higher in energy. Here, it is assumed that the lowest singlet excited state can be described by only one singly excited configuration in which an electron is promoted from HOMO to LUMO. However, an entirely different picture emerges when electron correlation is switched on, *i. e.* when more than one excited configuration is used in description of the lowest singlet excited state. The lowest excited singlet state S_1 (the $2A_g$ state) becomes one-photon forbidden vs. the ground state [65]. Indeed, polyenes and polyacetylene do not luminesce according to Kasha's rule.

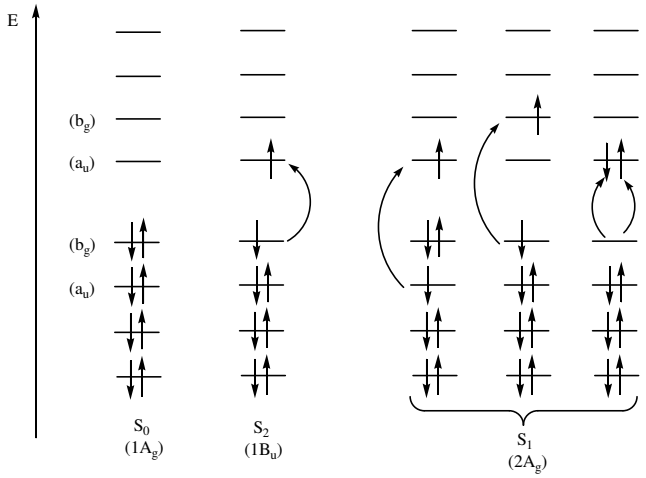

Figure 1.12 The main electronic configurations contributing to the ground state S_0 and the lowest singlet excited states S_1 and S_2 in the case of octatetraene

Consequently, an accurate description of the lowest singlet excited state of π-conjugated systems requires very precise consideration of electron correlation, although the excited configuration that includes only a single HOMO-LUMO transition plays a dominant role. Employing elaborate theoretical methods is thus crucial to increase the accuracy of the information on the nature of the lowest singlet excited state. Although, the computational demand associated with the calculations that employs these methods is very large, and places severe limitations on the size of the systems whose excited states can be studied [66], it is known that considerably large systems such as C70 cluster [67c] have been studied by these techniques.

In the following, the physical properties, applications, and literature information on aromatic five-membered heterocyclic oligomers, namely oligothiophenes **nT**s, oligofurans **nF**s, and oligopyrroles **nP**s (where *n* stands for the number of oligomer units) will be given.

1.4.2 Subclasses of Aromatic Five-Membered Heterocyclic Oligomers

1.4.2.1 Thiophene Oligomers

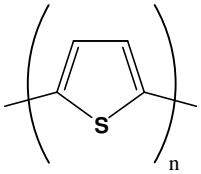

nT

Figure 1.13 Molecular structures of oligothiophenes (**nT**) and polythiophene (very large n)

1.4.2.1.1 Polythiophene

Polythiophene (PTh) [68-70] (Figure 1.13) is among the most widely studied conjugated organic polymers, experimentally [71-73] and theoretically [74-76]. It has very promising properties such as environmental stability, structural versatility, high conductivity (upon doping), non-linear optical property, and moderate band gap. In fact, PTh exhibits the smallest band gap (2.00 eV at absorption edge and 2.70 eV at maximum absorption [77]) of the polymers of the three systems examined. Not surprisingly, PTh backbone is a prime candidate to construct low band-gap polymers [78]. These properties of PTh have led to multiple developments aimed at applications such as photovoltaic cells [79], FET [80], and supercapacitor electrodes [81].

1.4.2.1.2 Physical Properties of Thiophene Oligomers

Although oligothiophenes (**nT**, Figure 1.13) with n=1-6 have been synthesized since 1947 [82], beginning with the realization of the desirable electronic and optical characteristics in 1990s, they have become the most carefully studied aromatic five-membered heterocyclic oligomers [41, 83, 84].

UV/VIS absorption and fluorescence spectra of oligothiophenes have been reported many times with change in phase, solvent, and/or temperature (Table 1.2-4).

Table 1.2 Experimental Absorption Energies (in eV) of thiophene oligomers (**nT**)

1T	2T	3T	4T	5T	6T
5.34[a]	4.09[a]	3.50[a]	3.17[a]	2.98[a]	2.81[a]
	4.12[b]	3.49[b]	3.18[b]	2.99[b]	2.87[b]
	4.05[c]	3.49[c]	3.16[c]	2.99[c]	2.85[c]
5.37[d]	4.09[d]	3.50[d]	3.16[d]	2.97[d]	2.84[d]
5.10[e]	4.11[e]	3.50[e]	3.18[e]	2.98[e]	2.87[e]
5.37[f]	4.12[f]	3.53[f]	3.22[f]		
5.37[g]	4.11[g]	3.54[g]	3.17[g]	3.01[g]	2.89[g]
	4.07[h]	3.49[h]	3.17[h]	2.97[h]	
5.37[i]	4.09[i]	3.53[i]	3.16[i]	3.00[i]	

[a] ref. 85, in dioxane; [b] ref. 86, in dioxane; [c] ref. 87,88, in dioxane; [d] ref. 89, in dioxane, 1T data in acetonitrile; [e] ref. 90, 91, 92, in CH_2Cl_2; [f] ref. 93, in *n*-hexane; [g] ref. 94, in benzene; [h] ref 87, in benzene; [i] ref. 36, in acetonitrile; [j] ref 87, in $CHCl_3$.

Table 1.3 Experimental Fluorescence Energies (in eV) of thiophene oligomers (**nT**)

2T	3T	4T	5T	6T
3.43[a]	2.91[a]	2.59[a]	2.57[a]	2.47[a]
	3.04[b]	2.76[b]	2.57[b]	2.45[b]
3.43[c]	2.86[c]	2.56[c]		2.42[c]
3.44[d]	2.93[d]	2.63[d]		
3.44[e]	2.94[e]	2.62[e]	2.59[e]	

[a] ref. 85, 89, in dioxane; [b] ref. 88 in dioxane; [c] ref. 91, in $CHCl_2$; [d] ref. 93, in *n*-hexane; [e] ref. 36, in acetonitrile.

Table 1.4 Solid-state and low temperature absorption data (in eV) of thiophene oligomers (**nT**)

2T	3T	4T	6T
3.67[a]	3.08[b]	2.75[c]	2.76[d]
		2.61[e]	2.27[e]
		2.62[f]	2.28[f]

[a] ref. 95, solid solution in n-hexane at 4.2 K; [b] ref. 96, solid solution in n-decane at 4.2 K; [c] ref. 97, solid solution in n-tetradecane at 4.2 K; [d] ref. 98, single crystals grown from vapor phase; [e] ref. 99, ultrathin films; [f] ref. 100,single crystals.

Optical properties of oligothiophenes (and other heterocyclic π-conjugated oligomers) depend first on the number of the chain units. As seen from the Tables 1.2-4, the experimental longest wavelength absorptions and emissions show

systematic red shifts (shift to lower energies) with increasing size of oligothiophenes. However, saturation of the optical properties is expected when the oligomer size reaches the ECL. For the polythiophene system, there is no consensus on the ECL. Some [101, 102] have offered that it is not longer than 11 units based on the observation that the absorption spectra and doped conductivities of the 11-mer and 12-mer were very similar to those for polythiophenes. Others [103] have concluded that the ECL is about 20 depending on the experimental absorption and emission data of long substituted oligothiophenes. ECL of PTh has been also estimated experimentally to be of 21 monomer units at 10 K and 15 monomer units at room temperature [104]. Others [55] have calculated the ECL of PTh as 21. Meier and co-workers [7] have reported the ECL of **nT** to be around 17 monomer units using the experimental UV/VIS absorption and fluorescence data of unsubstituted **nT** (n=1-6), which was taken as reference in comparing theoretical results in this study.

Fluorescence studies provide information only about the fluorescent lowest singlet excited state S_1 state. Since the fluorescence spectra is more structured and sharper than the respective absorption spectra, molecular structure of S_1 state is expected to be more rigid and planar than the ground state S_0 state. The experimentally determined nonzero Stokes shifts also confirm this conclusion. Spectroscopic data shows that the lowest singlet state S_1 is of B symmetry, and any A-type state other than the ground state lies above it.

There are a very large number of theoretical investigations on the thiophene oligomers. Some have investigated the geometrical conformation in the ground state. Many other have dealt with the excitation energies [50, 105-107] and the ordering of the excited states [108, 109]. However, a few concentrated on the excited state geometries [110, 111] and molecular orbitals [112].

Theory and experiment have shown that **nT**s are not planar but subject to a strong rotational disorder [113]. However, Others [114] have concluded that rotational defects in poly(α-thiophene)s do not likely contribute significantly to the material properties because any mesoscopic or macroscopic material response is averaged over a large number of rotations of each thiophene ring. Thus, we thought that if the dihedral angle between oligomers units were taken to be 180º, this would

not very seriously affect the optical and electronic properties, but would considerably reduce the computational time because of the symmetry requirements.

1.4.2.1.3 Applications of Thiophene Oligomers

In 1990s, it was realized that α-oligothiophenes constitute interesting models of the electronic properties of polythiophene. However, realization of their possible applications in molecular electronics is the main reason for intensive research work in the area of thiophene oligomers that have been neglected for so many years [115].

Today, the use of unsubstituted oligothiophenes as active components of molecular electronic devices [116] that are employed in a broad range of fields is possible: field-effect transistors (FETs) [117], photovoltaic cells [118, 119], light modulators [120], molecular electronics [121], optical devices [122], nonlinear optics [123], Schottky diodes [124, 125], plastic electronics [126], light-emitting diodes [127, 128]. In oligothiophene based FETs, the conductivity and the mobility of charges increase with increasing chain length, and exceed those of polythiophene [129].

Many of the α-conjugated oligothiophenes exhibit biological activity: some of them generate skin pigmentation, act as herbicides or inhibit feed germination, while others are phototoxic against nematodes, algae, human erythrocytes, insect larvae and eggs [130]. This phototoxic ability of the thiophene oligomers (especially **3T** and **4T** [131]) is because they generate singlet oxygen when illuminated [132]. In addition, **2T** and **3T** is known to act as biosensitizers [133, 134], and the latter also acts as singlet oxygen synthesizer.

1.4.2.2 Furan Oligomers

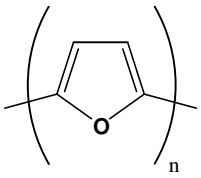

nF

Figure 1.14 Molecular structures of oligofurans (**nF**) and polyfuran (very large n)

1.4.2.2.1 Polyfuran

Polyfuran (PFu) (Figure 1.14) received little attention mainly due to the experimental difficulties in synthesis of a well-defined polymeric material and doping [135, 136]. However, high quality PFu has been obtained in recent years [71]. The band gap of PFu was determined to be 2.35 eV [137], which is lower than that of PPr. Conductivity of PFu upon doping was reported to be 102 S/cm [138]. This has to be compared to maximal conductivities of 500 S/cm for PPy and 2000 S/cm for PTh. Plasma polymerized furan that possesses good dielectric properties have been used as thin film capacitor [139].

1.4.2.2.2 Physical Properties of Furan Oligomer

As for PFu, oligofurans (**nF**) (Figure 1.14) have received attention only to a minor extent. Indeed, there had been very limited absorption data for the oligofurans [140] until recently. However, Seixas de Melo *et.al* [36] have given comprehensive photophysical data on furan oligomers containing up to five rings (Table 1.5). Others [55] have calculated the ECL of PFu as 21 monomer units, as for PTh.

Table 1.5 Absorption and Fluorescence data (in eV) of furan oligomers (**nF**) [36]

	1F	**2F**	**3F**	**4F**	**5F**
Abs (acetonitrile)	5.93	4.4	3.78	3.43	3.25
Abs (ethanol)		4.41	3.77	3.44	
Abs (dioxane)		4.38	3.75	3.41	
Abs (benzene)			3.71	3.38	
Fluo (acetonitrile)		3.96	3.34	3	

1.4.2.3 Pyrrole Oligomers

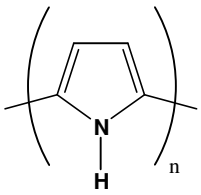

nP

Figure 1.15 Molecular structure of oligopyrroles (**nP**) and polypyrrole (very large n)

1.4.2.3.1 Polypyrrole

An important step in the development of conjugated polyheterocycles is the synthesis of highly conducting polypyrrole (PPy) (Figure 1.15) films in 1979 [141]. Together with PTh, polypyrrole [141a] has received intense research interest due to its ease of synthesis, chemical stability, high conductivity upon doping, and non-linear optical properties [70, 71, 74, 142-145]. The band gap of PPy has been given as 2.50 eV from the thin-film measurements [146]. This value indicates that it has a significantly larger band gap, and thus lower conductivity than PTh. Polypyrrole currently has many applications [147]. For instance, it has been used as an active component in an all-polymer battery system [148], in information storage devices

[149], in optoelectronics [150], and in LED materials [151].

1.4.2.3.2 Physical Properties of Pyrrole Oligomers

Despite the importance of PPy in the field of conducting polymers, less experimental work has been devoted to the investigation of oligopyrroles (**nP**) (Figure 1.15) probably due to their sensitivity to heat and light. However, pyrrole oligomers have interesting electronic and/or (nonlinear) optical properties [32].

UV/VIS spectroscopic investigations on a series of **nP** (n=1-3, 5, 7) [152] (Table 1.6) in acetonitrile (polar aprotic solvent) at room temperature have allowed first estimations of the properties of **nP**.

Table 1.6 Absorption data (eV) of pyrrole oligomers (**nP**) [152]

1P	2P	3P	5P	7P
5.96	4.49	3.91	3.38	3.26

Using this experimental data, others [7] have predicted to the ECL of the PPr to be 13.

There are few electronic structure calculations on medium and large sized pyrrole oligomers using DFT/hybrid functionals [9b, 12, 37, 38, 153]. For the $1B_u$ transition frequencies of oligomers with various sizes, experimental results reported in the literature for PPy [154].

1.5 Scope of the Study

The oligothiophenes (**nT**), oligofurans (**nF**), and oligopyrroles (**nP**) containing up to six monomer units are the concerns of this study.

Within a wide range of heteroaromatic five-membered oligomers that differ in chemical composition by substitutions, only the unsubstituted analogs were considered. Although substitution of molecules with the alkyl groups enhances solubility [102] (by decreasing attractive interactions between chains and creating favorable interactions with the solvent), this has several disadvantages. It can

weaken π-conjugation by inducing torsion about formal single bonds, inhibit a tight packing of molecules in the solid state [155], and decrease the electronically active function of the molecules.

All oligomers considered have α-linkages between monomer units. Indeed, in literature, regioisomeric oligomers including β-linkages were studied only to a minor extent since this kind of linkage does not occur in the corresponding polymers and the degree of conjugation is strongly decreased relative to the α-linked oligomers [156]. The systems considered are planar and in anti conformation (i.e. monomers point in opposite directions).

We did not address torsional disorder defects (nor do most computational studies [55]), which may be present to some extent in the actual materials [157].

All species studied were in the neutral, undoped forms. Doped materials are, of course, more conductive, and thus, more promising in terms of applications than their undoped counterparts, however there is a few experimental optical data that can be used for comparison [158]. Furthermore, computational treatment of closed-shell systems are much more easy and common than that of anionic or cationic systems.

We did not concentrate on the intermolecular interactions that may have very important impacts when the solid phase is considered. However, the differences in band gaps between the case of an isolated chain, and crystalline environments have found to be small [159], which implies that such effects may be small for conjugated systems in general. Because of our limited computer facility, only isolated molecules in gas phase were taken into account through this work. We have compared our quantum-chemical calculation results to experimental measurements carried out in solutions or in inert matrices, in order to prevent the effects of strong intermolecular interactions that are known to affect the electronic and optical properties [160].

Quantum chemical simulations reproduce geometries for isolated molecules without surrounding medium. Although models that describe solvents effects are available [161], we choose not to include such simulations into the present contribution, as they are beyond our computational capacities, especially for the longer oligomers.

The main purpose of the present work is to systematically analyze the structural, electronic and optical properties of thiophene, furan and pyrrole

oligomers in the ground state and the first singlet excited state to ascertain changes that these systems undergo both as a result of increasing chain lengths and differences in chemical compositions. We focus on the comparison between bond lengths, excitation and emission energies. In addition, the validity and limitations of different theoretical methods were explored to make a conclusion on the choice of method to be used in defining the geometrical and electronic parameters of π-conjugated oligomers, especially when treating the lowest singlet excited states. In fact, this study can be considered as the first comprehensive theoretical study on the first singlet excited states of this class of oligomers.

In this first chapter, we gave a brief introduction about π-conjugated, mainly aromatic five-membered heterocyclic, oligomers. In Chapter 2, the quantum-chemical methods used in this study and the computational procedure will be briefly described. The results of this study and their discussions will be presented in Chapter 3. The last chapter is devoted to the conclusions.

CHAPTER 2

THEORETICAL CALCULATION METHODS

2.1 Introduction

"What are the electrons really doing in molecules ?"

R. S. Mulliken

Theoretical chemistry concentrates on the description of chemical phenomena using mathematical methods and fundamental laws of physics. This branch of chemistry is an exciting and ever-more-important area of modern chemistry education and research. It lies at the interfaces among chemistry, physics, mathematics, and computational science. Thus, theoretical chemistry is expected to have major impacts over the next ten to twenty years within the disciplines of materials chemistry and biological chemistry that currently are two of the "hottest" research areas in chemical science [162].

Computational chemistry uses computer as an experimental tool to obtain results relevant to chemical problems with the help of theoretical models. As the computer technology improves, handling of more problems in computational chemistry will be possible.

Remaining part of this chapter has three different considerations. In the first part, some of the basic ideas in theoretical chemistry will be given. Theoretical methods used to compute the molecular properties will be mentioned in the second part with focus on the methods used in this work. In the last part, the computational procedure followed will be discussed.

2.2 Background

No understanding of the mechanisms and dynamics of a chemical bond were possible before the advent of Schrödinger' s wave equation in 1926. The shorthand notation for the time-dependent Schrödinger equation [163] is

$$i\hbar \frac{\partial \Psi(\boldsymbol{r},t)}{\partial t} = \hat{H}\Psi(\boldsymbol{r},t) = E\Psi(\boldsymbol{r},t) \tag{2.1}$$

where $\Psi(\boldsymbol{r},t)$ is the wave function, $\hat{H}$ is the Hamiltonian operator, E is the total energy, $\boldsymbol{r}$ are spatial coordinates and t is the time. Exact solution of the Schrödinger equation (*i.e.*, the exact wave function of the system under consideration) enables full description of the system.

For the stationary states, the time-independent Schrödinger equation is given as

$$\hat{H}\Psi(\mathbf{r}) = E\Psi(\mathbf{r}) \tag{2.2}$$

where

$$\hat{H} = \hat{T}_e + \hat{T}_n + \hat{V}_{ne} + \hat{V}_{ee} + \hat{V}_{nn} \tag{2.3}$$

For a molecule with N electrons and M nuclei, the kinetic energy operators of the electrons T_e and the nuclei (T_n), the electron nucleus attraction energy operator V_{ne}, the repulsion energy operator of the electron-electron V_{ee} and the nucleus-nucleus repulsion V_{nn} are given in atomic units as

$$\hat{T}_e = -\sum_{i=1}^{N} \frac{1}{2}\nabla_i^2 \,,\; \hat{T}_n = -\sum_{a=1}^{M} \frac{1}{2M_a}\nabla_a^2$$

$$\hat{V}_{ne} = -\sum_{i}^{N}\sum_{a}^{M} \frac{Z_a}{r_{ia}} \,,\; \hat{V}_{ee} = \sum_{i}^{N}\sum_{j>i}^{N} \frac{1}{r_{ij}} \,,\; \hat{V}_{nn} = \sum_{a=1}^{M}\sum_{b>a}^{M} \frac{Z_a Z_b}{R_{ab}} \tag{2.4}$$

where i and j are indices of electrons whereas a and b are indices of atomic nuclei. M_a is the ratio of the mass of nucleus a to an electron, and Z_a is the atomic number of nucleus a. The distance between the ith and the jth electron is r_{ij} ; the distance between the ath nucleus and the bth nucleus is R_{ab} ; r_{ia} specifies the distance between electron i and nucleus a.

In quantum mechanics, equations of motion can be solved (analytically) exactly only for systems containing a single electron.

Born-Oppenheimer approximation [164] is one of the most important approximations that are made to facilitate the solution of the Schrödinger equation.

In the Born-Oppenheimer approximation, the nuclei are considered as moving on a potential energy surface of electronic motion, which means that the electronic and nuclear motions are separated. Thereby, the task of solving full Schrödinger equation is reduced to solving just the electronic Schrödinger equation at interested nuclear coordinates. For an isolated N-electron atomic or molecular system, the electronic Schrödinger equation is given by

$$\hat{H}_{elec}\Psi_{elec} = E_{elec}\Psi_{elec} \tag{2.5}$$

where $E_{elec} = E_{elec}(\{R_a\})$ is the electronic energy and $\Psi_{elec} = \Psi_{elec}(\{r_i\},\{R_a\})$ is the electronic wave function, both of which have parametrical dependence on nuclear coordinates. $\hat{H}_{elec}$ is the electronic Hamiltonian operator:

$$\hat{H}_{elec} = -\sum_{i=1}^{N}\frac{1}{2}\nabla_i^2 - \sum_{i}^{N}\sum_{a}^{M}\frac{Z_a}{r_{ia}} + \sum_{i}^{N}\sum_{j>i}^{N}\frac{1}{r_{ij}} \tag{2.6}$$

The total energy E_{tot} is given as

$$E_{tot} = E_{elec} + \sum_{a=1}^{M}\sum_{b>a}^{M}\frac{Z_a Z_b}{R_{ab}} \tag{2.7}$$

Since all of remaining parts deal with the electronic Schrödinger, the subscripts "$elec$" will be omitted.

2.2.1 The Hartree-Fock Theory

The Hartree-Fock theory describes the many electron system as a system of nearly independent particles. This first approximation to solve electronic Schrödinger equation uses the variational principle. The electronic energy expectation value is required to be above the exact energy,

$$E = \langle \Psi | \hat{H} | \Psi \rangle \geq E_{exact} \tag{2.8}$$

The trial function Ψ is chosen such that it is anti-symmetric upon exchange of two electrons, and given as a “Slater determinant” [165] of an N electron system,

$$\Psi = \frac{1}{\sqrt{\mathbf{N!}}}\begin{vmatrix} \phi_1(x_1) & \phi_2(x_1) & \dots & \phi_N(x_1) \\ \phi_1(x_2) & \phi_2(x_2) & \dots & \phi_N(x_2) \\ \dots & \dots & \dots & \dots \\ \phi_1(x_N) & \phi_2(x_N) & \dots & \phi_N(x_N) \end{vmatrix} \tag{2.9}$$

where each ϕ_i is the ith spin molecular orbital, and x_k includes the space and spin coordinates for k^{th} electron.

After solving this problem, final *Hartree-Fock equations* [166, 167] are obtained as

$$\hat{F}_i\phi_i = \varepsilon_i\phi_i \tag{2.10}$$

where ε_i are the molecular orbital energies. Fock operator, $\hat{F}_i$, an effective one-electron energy operator, is given as

$$\hat{F}_i = \hat{h}_i + \sum_j^N \left(\hat{J}_j - \hat{K}_j\right) \tag{2.11}$$

The one-electron operator $\hat{h}_i$ defines the kinetic energy and the potential energy for the electrostatic attraction between the nuclei and the electron in ϕ_i. The potential energy for the electrostatic repulsion between the electrons with the electron density function $(\phi_i)^2$ and the electron with the electron density function $(\phi_j)^2$ is given by the Coulomb integral operator $\hat{J}_j$. The exchange integral operator $\hat{K}_j$ arises from the requirement that Ψ be antisymmetric with respect to the permutation of the coordinates of any two electrons.

$$\hat{h}_i = -\frac{1}{2}\nabla_i^2 - \sum_a \frac{Z_a}{|\mathrm{R}_a - \mathrm{r}_i|} \tag{2.12}$$

$$\hat{J}_i\,|\phi_j(x_2)\rangle = \left\langle \phi_i(x_1)\,|\,\frac{1}{|\mathrm{r}_1 - \mathrm{r}_2|}\,|\,\phi_i(x_1)\right\rangle |\,\phi_j(x_2)\rangle \tag{2.13}$$

$$\hat{K}_i\,|\phi_j(x_2)\rangle = \left\langle \phi_i(x_1)\,|\,\frac{1}{|\mathbf{r}_1 - \mathbf{r}_2|}\,|\,\phi_j(x_1)\right\rangle |\,\phi_i(x_2)\rangle \tag{2.14}$$

The Hartree-Fock equations can be solved iteratively. Starting with a set of MOs, equation 2.10 gives an improved set. These new MOs are used to get better ones. This calculation continues until a convergence limit. This iterative method of solving the Hartree-Fock equations is called the *Self-consistent Field* (SCF) method.

By this way, the Hartree-Fock energy is obtained as

$$E_{HF} = \sum_{i}^{N} h_{ii} + \frac{1}{2}\sum_{i}^{N}\sum_{j}^{N}(J_{ij} - K_{ij}) + V_{nn} \tag{2.15}$$

2.2.2 Restricted and Unrestricted Hartree-Fock Wave Functions

If the system interested is of a closed-shell system (a system which has an even number of electrons whose spins are paired, and which, thus, has a singlet type wave function), two electrons with different spins are normally restricted to occupy a single spatial orbital. Such a wave function is known as restricted Hartree-Fock (RHF) wave function [168, 169].

If there is no restriction on the form of the spatial orbitals, the trial function is called as unrestricted Hartree-Fock (UHF) wave function [168, 169]. In a UHF wave function, each electron is allowed to occupy a different spatial orbital. The term "different orbitals for different spins (DODS)" is also used to define UHF wave function. UHF wave function is generally used for open-shell systems (a system in which there is at least one space orbital occupied by a single electron).

Restricted open-shell Hartree-Fock (ROHF) [168, 169] wave function is formed by assigning a single spatial orbital for each spin-paired electron and for each unpaired electron in an open-shell system. Since the ROHF wave function is a spin eigenfunction of the Hamiltonian operator, it is commonly used in treating doublet and triplet systems.

A closed-shell singlet wave function can always be written as a single determinant. However, open-shell singlet wave functions require at least two determinants.

For closed-shell systems, if the same basis set is used to describe the spatial orbitals of spin-paired electrons, the UHF wave function will collapse to the RHF wave function. Thus, it is very important to assign different sets of basis functions to the spatial parts of different spin orbitals while forming UHF wave function to get an improvement over RHF wave function.

R, U, and RO letters are put before the name of method, namely RHF, UHF, and ROHF. This procedure can be extended to other methods. However, since in most calculations closed-shell systems are considered, R letter is commonly not written.

2.2.3 The Basis Set Approximation

Most molecular quantum chemical methods begin calculation with a choice of a set of basis functions χ_α, which are used to express the MOs as a linear combination of atomic orbitals (LCAO) [168-170].

$$\phi_i = \sum_{\alpha}^{K} c_{\alpha i} \chi_\alpha \tag{2.16}$$

There are two types of commonly used basis functions: Slater type orbitals (STO) and Gaussian type orbitals (GTO). Slater type orbitals [[171]] have the form

$$\chi_{\zeta,n,l,m}(r,\theta,\varphi) = NY_{l,m}(\theta,\varphi)\mathrm{r}^{n-l}e^{-\zeta\mathrm{r}} \tag{2.17}$$

Gaussian type orbitals [172] are defined as

$$\chi_{\zeta,n,l,m}(r,\theta,\varphi) = NY_{l,m}(\theta,\varphi)\mathrm{r}^{(2n-2-l)}e^{-\zeta\mathrm{r}^2} \tag{2.18}$$

A LC-STO SCF MO calculation takes more computer time than a LC-GTO SCF MO calculation. Hence, in most calculations GTO are used [169].

A complete basis set (infinite number of basis functions) is ideal to get results with the highest accuracy. Since a complete basis is out of question, one tries to use as many functions as he/she can. However, a good choice of the number and type of basis functions (even though these count not very many) is an important criterion to describe the system with enough accuracy.

A minimum basis set consists of one basis function for each inner-shell and valence-shell AO of each atom in a molecule. For nitrogen or oxygen (in fact for any first row atom), this means 1s, 2s, $2p_x$, $2p_y$, and $2p_z$ functions. For sulfur, 3s, $3p_x$, $3p_y$, and $3p_z$ functions are added to the minimal basis set of nitrogen or oxygen.

A double-zeta (DZ) basis set is obtained by replacing each basis function of a minimal basis set by two basis functions that differ in their orbital exponents ζ (zeta).

A triple-, quadruple-, or quintuple-zeta basis sets contain three, four, or five times as many functions as the minimum basis set, respectively.

A split-valence (SV) basis set uses two (or more) basis functions for each valence AO but only one basis function for each inner-shell (core) AO. Split-valence sets are called valence double zeta (VDZ), valence triple zeta (VTZ), …according to the number of basis functions used for each valence AO. In most chemical experiment, change in energy upon perturbation (not absolute value of energy) is measured. In calculation of energy change, contribution of core electrons is very small compared to valence electrons. Thus, SV basis sets usually produces results with reasonable accuracy.

A polarized basis set contains additional basis functions whose *l* quantum numbers are greater than the maximum *l* of the valence shell of the ground-state atom. A diffuse function is one with a very small orbital exponent.

In this study 6-31G* and 6-31+G* basis sets [173] are used. Both of these basis sets are extensions of the 6-31G basis set. As understood from the number before dash, a contraction of six primitive Gaussians is used to represent core orbitals. The numbers after dash indicate that a contraction of three primitive Gaussians and one Gaussian are used to define valence orbitals. A set of polarization functions are added to the basis functions of non-hydrogen atoms, as seen from the * sign. The + symbol is used to indicate that four highly diffuse functions (s, p_x, p_y, and p_z) are added on each non-hydrogen atom. For example, calculations on furan using 6-31G* basis set includes 83 basis functions (contracted Gaussians) and 156 primitive Gaussians. The 6-31G* basis set has been proved to form a good compromise between the reproduction of experimental first singlet excitation energies (within 0.05 eV error range for biphenyl [64]) and computational effort. It is the smallest basis set able to give a reliable description of the structural parameters for the heterocyclic five-membered rings [54].

2.3 Computational Methods

2.3.1 *Ab Initio* Methods

In *ab initio* methods, there is no reference to experimental data. Experimental data is used to compare calculation results.

The *ab initio* HF method uses the approximations mentioned in Sections 2.2.1-2.2.3. The electronic energies are calculated from the Hartree-Fock equations using a single determinant description of the (restricted) electronic wave function and a suitable basis set. This method provides the best single-deteminant wave function and the lowest energy possible within a given basis set for the ground state of most molecules near the equilibrium geometry.

The main disadvantages of the HF method are [174]:

- *Expense.* There are very many integrals to be calculated, thus it is time- and memory-consuming.
- *Accuracy.* Even though absolute energies computed with high accuracy, relative energies such as excitation energies are much less well reproduced.
- *Applicability.* Certain molecules or states have an electronic structure that has to be described by considering electron correlation.

2.3.2 Semi-Empirical Methods

Semi-empirical methods give qualitatively, and for some systems, quantitatively correct predictions. They can be used to correlate and/or extrapolate the properties of compounds. Furthermore, semi-empirical methods suggest a way to overcome the difficulties in applying *ab initio* methods to medium or large molecules. Reducing the number of integrals by approximations reduces computational time [175]. The approximations made in semi-empirical methods are [169]:

- Only valence electrons are considered explicitly. Core electrons are taken into account by reducing nuclear charge or introducing functions that treat them as negative charge clouds.

- The minimum basis set (STO-3G) is used for the valence electrons. Most semi-empirical methods use only s- and p-type functions.
- The zero differential overlap (ZDO) approximation is made. The ZDO approximations assigns all products of basis functions (μ,ν) depending on the same electron coordinates (*i*) when located on different atoms (A, B) to zero.

$$\mu_A(i)\nu_B(i) = 0 \tag{2.19}$$

By ZDO approximation, the overlap matrix is reduced to a unit matrix. Furthermore, all three-center one-electron, three- and four-center two-electron integrals are set to zero.

To compensate for these approximations, the remaining integrals are made into parameters. The values of these parameters are assigned to the results of higher-level calculations or experiments. The number of neglected integrals and the way the parameterization is done determines the type of semi-empirical method. A semi-empirical method may only be applied to the chemical species for which it is parameterized.

One- and two-center integrals are considered using NDDO, INDO, and CNDO approximations [169]. To transform these approximations into working computational models, three methods can be used:

- Functional form of the atomic orbitals can be used to calculate the remaining integrals.
- Few experimental data can be used to assign values of parameters which correspond to the integrals.
- Many experimental data can be used in fitting values of parameters which correspond to the integrals

Commonly used semi-empirical methods are the INDO/S, MINDO, MNDO, AM1, and PM3 methods. The semi-empirical methods that are used in this study, namely AM1 and ZINDO/S methods, will be explained in the following.

2.3.2.1 Austin Model 1 (AM1)

Austin Model 1 (AM1) [176-179] is one of the modified MNDO methods (MNDO, AM1, and PM3) which employ the Neglect of Diatomic Differential Overlap (NDDO) approximation. Using μ and ν to denote either an s- or p-type orbital, the NDDO approximation is defined by the following equations [169].

Overlap integrals

$$S_{\mu\nu} = \langle \mu_A | \nu_B \rangle = \delta_{\mu\nu}\delta_{AB} \tag{2.20}$$

One electron operator

$$\hat{h}_i = -\frac{1}{2}\nabla_i^2 - \sum_a \frac{Z_a'}{|\mathbf{R}_a - \mathbf{r}_i|} \tag{2.21}$$

Here Z_a' is the nuclear charge on center *a*, that is reduced by core electrons.

In AM1, all one-center two-electron integral parameters are taken from the atomic spectra, while the rest are fitted to the molecular data. AM1 has been parameterized for many atoms including H, C, N, O, and S.

2.3.2.2 Zerner's Intermediate Neglect of Differential Overlap Method Parameterized for Spectroscopy (ZINDO/S)

Intermediate Neglect of Differential Overlap parameterized for spectroscopy (INDO/S) [180] semi-empirical method is a parameterization of the INDO approximation for the calculation of electronically excited states and their properties. The INDO approximation, in addition to the NDDO, neglects all two-center two-electron integrals that are not of Coulomb type.

The INDO/S method is typically set up for a treatment of the excited states within the singly excited configuration interaction (CIS) approximation [181].

The ZINDO/S [182, 183] has been parameterized for many atoms including H, C, N, O, S, and transition metals.

A ZINDO/S excitation energy calculations performed on a conjugated system [184] have given very accurate 0-0 excitation energies.

2.3.4 Electron Correlation Methods

A very large part of the error in the HF energy originates from the inadequate inclusion of electron correlation. Even though there exists some instantaneous electron correlation because the HF wave function obeys the Pauli principle (*Fermi hole* around an electron), electron-electron interactions are considered only in an average way in the HF method. However, the repulsion between electrons is effective at every instant, and thus, they are furher apart than described by the HF wave function. Indeed, in an atom, presence of an electron in a region of space decreases very much the possibility of finding any other electron around that region. This correlated motion of electrons that is said to form a *Coulomb hole* surrounding each electron in an atom constitutes the basis of *electron correlation*. Thus, to go beyond the Hartree-Fock approximation, one must consider first the ways to include electron correlation to the HF energy.

Taking fully into account the correlated motion of electrons, one can find the lowest possible energy using a very large and flexible basis set (i.e., the exact nonrelativistic energy, E_{nonrel}). Within such a basis set, an HF calculation produces the energy at HF limit (E_{HF}). Using these the correlation energy, E_{corr} is defined as

$$E_{corr} \equiv E_{nonrel} - E_{HF} \tag{2.22}$$

For neutral atoms, the absolute value of E_{corr}, $|E_{corr}|$ increases linearly with the number of electrons.

2.3.4.1 Configuration Interaction (CI)

Configuration interaction (CI) [185, 186] is one of the methods used to provide instantaneous electron correlation. In the configuration interaction method, correction to the HF single determinant wave function is supplied by adding excited electronic configurations. The CI wave function Ψ is written as:

$$\Psi = \sum_i c_i \Phi_i \tag{2.23}$$

where c_i are variational coefficients, and each Φ_i is called a configuration state function (CSF). In the case of i=0, the CSF Φ_0 is taken as the HF wave function.

The CSFs are given as a (linear combination of) Slater determinant(s) which is(are) formed using a set of occupied and virtual spin-orbitals. These are classified as singly, doubly, triply, quadruply … excited according to whether 1, 2, 3, 4, … electrons are excited from occupied to unoccupied orbitals of single determinant ground state Φ_0. The excited Slater determinants are often referred to as Singles (S), Doubles (D), Triples (T), and Quadruples (Q) with a maximum excitation of N electrons (N-multiple). A representation for these determinants is given in Figure 2.1.

In practical calculations, while forming the trial CI wave function, only configurations that will contribute most to the description of the interested state are included. The unexcited CSF is expected to make the largest contribution. Thus, one usually includes singly and doubly excited configurations in addition to the HF wave function. The most common type of CI calculation is the configuration interaction singles and doubles (CI-SD) [187-189].

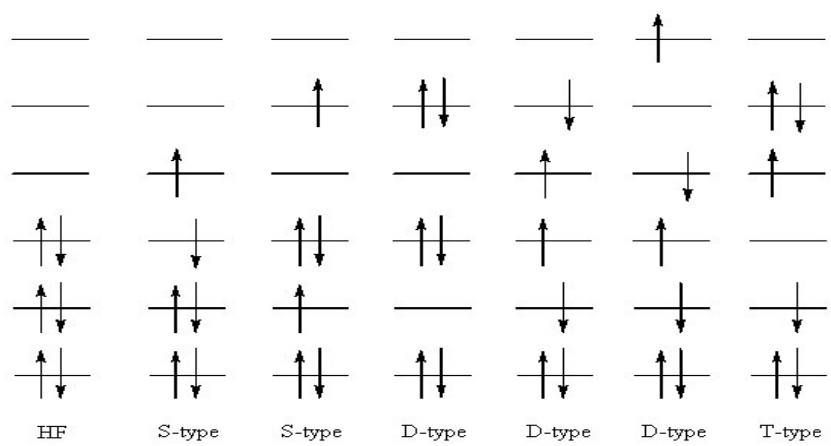

Figure 2.1 Representation of excited Slater determinants generated from a HF reference

The unknown coefficients, c_i (in equation 2.23), are determined by the linear variation principle from the solution of a set of secular equations

$$\sum \left(H_{ij} - E_k \delta_{ij} \right) c_i = 0, \;\; i = 0, 1, 2, 3... \tag{2.24}$$

where H_{ij} is an "interaction" matrix element between two configurations

$$H_{ij} = \left\langle \Phi_i \middle| \hat{H} \middle| \Phi_j \right\rangle \tag{2.25}$$

Here, all excited configurations are set orthogonal to the HF wave function. In addition, they are orthogonal to each other. This guarantees that the energy ordering

of the states will be the same as in the exact wave function.

The lowest root of the secular determinant of the equation 2.24 gives the (improved) ground state energy. The next root is the lowest excited state energy, and so on. Substituting one of the roots into the secular equation one gets a set of variational coefficients, and thereby the wave function of the state of interest.

Because of slow convergence, lack of size consistency, and disappointing results of CI-SD calculations, CI calculations have lost their former dominance in correlation energy calculations [168], and several other correlation method are developed such as Mϕller Plesset perturbation theory (MPn) [190] and coupled-cluster theory (CC) [191-193].

2.3.4.2 Configuration Interaction Singles (CIS)

The configuration interaction singles (CI-Singles or CIS [194]) method (also called the Tamm-Dancoff approximation) is a computationally simple, widely used procedure for treating excited states.

The CIS linear variation wave function is formed using only the singly excited configurations:

$$\Psi_{CIS} = \sum_a \sum_i c_{ia} \varphi_i^a \tag{2.26}$$

where the sums go over all the occupied and virtual spin-orbitals, c_{ia} are variational coefficients, and φ_i^a denote a singly excited Slater determinant in which the occupied spin-orbital i in Φ_0 is replaced by the virtual spin-orbital a.

As seen in equation 2.26, the HF wave function does not appear in the CIS wave function. The CIS theory assigns all Hamiltonian matrix elements between the HF wave function and singly excited configurations to zero ("Brillouin' s Theorem"). Hence, the resulting CIS wave function does not provide an improvement over the HF wave function for the ground state, but improves the electronically excited states.

The CIS method can be used to calculate vertical excitation/emission energies, excited state geometries and vibrational frequencies. However, CIS excited state geometries and vibrational frequencies have been said to be more

accurate than CIS vertical excitation energies [195]. The excited state structural parameters and excitation energies of some conjugated molecules obtained with CIS method have been found to be in very good agreement with experimental data [196-199].

2.3.5 Density Functional Theory

Although the electronic wavefunction of an N-electron molecule depends on 3N spatial and N spin coordinates, the molecular energy can be written in terms of integrals involving only six spatial coordinates. Thus, alternative functions that has fewer variables than the wavefunction and that can be used to calculate the energy and other properties of a system would be more appropriate in practical applications [168]. A proposed function is the electron probablity density ρ_0(x,y,z), a function of only three variables. The theory in which the electron probability density is used to calculate the ground state molecular properties of interacting many-electron systems is called (stationary) Density Functional Theory (DFT) [200]. DFT is a powerful, and formally exact theory. Being a non-interacting theory and not yielding a correlated N-body wave function, it is different from quantum chemical methods.

It was proved by Hohenberg and Kohn [201] that the ground state molecular energy, wave function, and all other molecular electronic properties are uniquely determined by the ground state electron probablity density ρ_0 for molecules with a nondegenerate ground state. This means that all the molecular properties can be written as a functional of ρ_0 such as the ground state energy $E_0 = E_0[\rho_0]$. Discovering the form of functionals connecting the electron density with the energy is the main aim in DFT.

The ground state electronic energy functional in DFT is written as

$$E_0 = E_0[\rho_0] = \overline{V}_{Ne}[\rho_0] + \overline{T}[\rho_0] + + \overline{V}_{ee}[\rho_0] \tag{2.27}$$

where nuclear-electronic attraction energy functional is given as

$$\overline{V}_{Ne}[\rho_0] = \langle \Psi_0 | \sum_{i=1}^{N} v(\mathrm{r}_i) | \Psi_0 \rangle = \int \rho_0(\mathrm{r}) v(\mathrm{r}) d\mathrm{r} \tag{2.28}$$

Here, $v(\mathbf{r})$ is the nuclear-electronic attraction potential for an electron located at point

r. The average electronic kinetic energy functional $\overline{T}[\rho_0]$ and the average interelectronic repulsion functional $\overline{V}_{ee}[\rho_0]$ are unknown in the Hohenberg-Kohn theorem.

Kohn and Sham [202] devised a method to form the practical expressions for these two unknown functionals. In Kohn-Sham (KS) method, an auxiliary reference system is considered. This system is thought to consist of N noninteracting electrons each of which experiences the same external potential ν_s that is chosen to make the electron density of the reference system ρ_s equal to the electron density of the real molecule ρ_0. After some arithmetics, the ground state energy functional is given as

$$E_0[\rho] = \int \rho_0(\mathbf{r})v(\mathbf{r})d\mathbf{r} - \frac{1}{2}\iint \frac{\rho(\mathbf{r}_1)\rho(\mathbf{r}_2)}{r_{12}} d\mathbf{r}_1 d\mathbf{r}_2 + \overline{T}_s[\rho] + E_{xc}[\rho] \tag{2.29}$$

where

$$\overline{T}_s[\rho] = -\frac{1}{2}\left\langle \theta_i^{KS} \middle| \nabla^2 \middle| \theta_i^{KS} \right\rangle \tag{2.30}$$

and $E_{xc}[\rho]$ is the *exchange-correlation energy functional*.

Using the Kohn-Sham orbitals, θ_i^{KS} the ground state electron density is defined as

$$\rho = \rho_s = \sum_{i=1}^{N} \left| \theta_i^{KS} \right|^2 \tag{2.31}$$

Employing the equations 2.29 and 2.31, the ground state electronic density and energy can be calculated if the KS orbitals and the exchange-correlation functional is known.

The KS orbitals can be found solving the *Kohn-Sham equations* [202]

$$\left[-\frac{1}{2}\nabla^2 + V_{ne}(\mathbf{r}) + \int \frac{\rho(\mathbf{r}')}{|\mathbf{r}-\mathbf{r}'|} d\mathbf{r}' + \nu_{xc} \right] \theta_i^{KS} = \varepsilon_i \theta_i^{KS} \tag{2.32}$$

where the *exchange-correlation potential* ν_{xc} is found as the functional derivative of the exchage-correlation energy.

$$\nu_{xc}(\mathrm{r}) = \frac{\delta E[\rho(\mathrm{r})]}{\delta \rho(\mathrm{r})} \tag{2.33}$$

Both ν_{xc} and E_{xc} can be written as the sum of their exhange and correlation parts:

$$v_{xc} = v_x + v_c$$
$$E_{xc} = E_x + E_c \tag{2.34}$$

The exchange and correlation contribution to E_{xc} are negative with $|E_x|$ being much larger than $|E_c|$. The exchange term can be given as the exchange energy in the HF theory by replacing the HF orbitals with the KS orbitals.

The main problem in KS-DFT is that the correct functional form of the exchange-correlation energy $E_{xc}[\rho]$ is not known. The approximate functionals proposed for $E_{xc}[\rho]$ in literature are: local density approximation (LDA), local-spin-density approximation (LSDA), generalized gradient approximation (GGA), and hybrid methods.

2.3.5.1 Generalized Gradient Approximation (GGA)

For the systems in which the variation of electron density with position is too large to be ignored, the gradients are used;

$$E_{xc}^{GGA}\left[\rho^{\alpha},\rho^{\beta}\right] = \int f\left(\rho^{\alpha}(\mathbf{r}),\rho^{\beta}(\mathbf{r}),\nabla\rho^{\alpha}(\mathbf{r}),\nabla\rho^{\beta}(\mathbf{r})\right)d\mathbf{r} \tag{2.35}$$

where f is a function of the spin densities and their *gradient*s. The exchange and correlation parts of the exchange-correlation energy are modelled separately in the *generalized gradient approximation*, GGA.

The names of some commonly used functionals for the exchange part E_x^{GGA} and E_c^{GGA} are given in Table 2.1.

Table 2.1 Acronyms for some popular functionals in DFT.

Exchange functionals, E_x^{GGA}	Correlation functionals, E_c^{GGA}
B88 (Becke 88) [203]	LYP (Lee-Yang-Parr) [204]
PW86 (Perdew-Wang 86) [205]	P86 (Perdew 86) [206]
PW91 (Perdew-Wang 91) [207]	PW91 (PerdewWang 91) [208, 209]
	B96 (Becke 96) [210]

In forming the exchange-correlation functional, any exchange functional can be combined with any correlation functional.

2.3.5.2 Hybrid methods

This class of exchange-correlation functionals is very widely used. A hybrid functional mixes the HF exchange energy expression E_x^{HF} with the gradient-corrected exchange and correlation functionals. For example, the commonly used Becke's three parameter hybrid functional that employs the Lee, Yang, and Parr correlation functional B3LYP [211] is defined as

$$E_{xc}^{B3LYP} = aE_x^{LSDA} + (1-a)E_x^{HF} + b\Delta E_x^{B88} + c\Delta E_c^{LYP} \tag{2.36}$$

where $\Delta E_x^{B88} = E_x^{B88} - E_x^{LSDA}$, $\Delta E_c^{LYP} = E_C^{LYP} - E_c^{LSDA}$ and the empirical values of the parameters are: a = 0.80, b = 0.72, and c = 0.81. B3LYP hybrid functional has been shown to be one of the most accurate methods for aromatic hydrocarbons and polyenes [212, 213].

2.3.5.3 Time-Dependent Density Functional Theory (TDDFT)

Generally, in all time-dependent theories, the following secular equation is solved [67a].

$$\left\| \begin{pmatrix} \mathbf{A} & \mathbf{B} \\ \mathbf{B} & \mathbf{A} \end{pmatrix} - \Delta E \begin{pmatrix} 1 & 0 \\ 0 & -1 \end{pmatrix} \right| = 0 \tag{2.37}$$

where ΔE are the excitation energies. The elements of **A** and **B** matrices are given as

$$\begin{aligned} A_{ai,bj} &= \left\langle \varphi_i^a \middle| \hat{H} \middle| \varphi_j^b \right\rangle - E_0^{SCF}\delta_{ij}\delta_{ab} \\ B_{ai,bj} &= \left\langle \varphi_0 \middle| \hat{H} \middle| \varphi_{ij}^{ab} \right\rangle \end{aligned} \tag{2.38}$$

Here φ_i^a and φ_j^b denotes the wave function which have a single excitation from the occupied spin-orbitals *i* and *j* to the virtual spin-orbitals *a* and *b*, respectively; φ_0 stands for the SCF wave function; φ_{ij}^{ab} denotes the wave function with a double excitation from the occupied spin-orbitals *i* and *j* to the virtual spin-orbitals *a* and *b*.

In the CI-Singles method (Section 2.3.4.2), the matrix B is ignored. Hence, the problem of solving the secular equation (equation 2.37) is reduced to the variational problem of finding eigenvalues of matrix A as the excitation energies. In the time-dependent Hartree-Fock (TDHF) [214] (or random phase approximation (RPA)

[215]), full solution of the equation 2.37 is required, and thus the problem is a non-variational problem. The wave functions are taken as the Slater determinants of the HF orbital with proper excitations. In the case of the time-dependent density functional theory (TDDFT) [216], the solutions can be derived along the same lines as the RPA except that the matrices A and B are formed with appropriate DFT expressions.

TDDFT extends the concept of the stationary DFT to time-dependent situations. Within the adiabatic approximation, for any interacting many-particle system subject to a given time-dependent potential all physical observables are uniquely determined by knowledge of the time-dependent density and the state of the system at an arbitrary, single instant in time [217]. When the adiabatic approximation is employed in TDDFT, the exchange-correlation functionals in stationary DFT (Sections 2.3.5.1-2) appear to work best for low-lying excited states of clear valence type [67e, 218].

The TDDFT, a promising method for predicting excitation energies, has been used to study excitation processes in conjugated systems [43]. Because of the low computational costs and complexity, TDDFT is applicable to large systems [219, 220] for which traditional wave function-based methods are not feasible. Although, the TDDFT in its current form and employing standard functionals should be used with great caution for large unsaturated π systems (17 π bonds) [221, 222], we have chosen this method in treatment of excited states since it has been shown to describe the characteristic features and trends in relatively small π-systems [223] like ours (maximum of 12 π bonds).

2.4 Computational Procedure

All quantum-chemical calculations in this work were performed using Gaussian 98 program package [224] with the implemented basis sets [225]. Gaussian 98, a sophisticated simulation program, is capable of performing calculations at almost all levels of theory. However, since Gaussian 98 program does not include AM1 parameters for sulfur [179], AM1 geometry optimizations were carried using HyperChem program. HyperChem [226] is able to perform calculations at molecular

mechanics, semi-empirical and *ab initio* levels.

As stated in Section 2.2.3, the 6-31G* and 6-31+G* basis sets were used throughout this study.

The ground state full geometry optimizations of the thiophene, furan, and pyrrole oligomers containing up to six rings (total of 18 structures) were done at AM1, (closed-shell) RHF, and DFT (B3LYP) levels. The inputs of AM1 calculations were prepared by rough optimizations employing the MM+ force field that is an extension of MM2 developed by Allinger [227] with the HyperChem package. For these AM1 semi-empirical geometry optimizations, the convergence limit on the energy was taken to 10^{-5} kcal mol^{-1}, and the RMS gradient of 0.001 kcal mol^{-1}. The results of AM1 geometry optimizations were used as input for the RHF and B3LYP geometry optimizations. Taking the B3LYP ground state geometries as initial guesses, the vibrationally relaxed first singlet excited state geometries were fully optimized at CIS level. In these RHF, B3LYP, and CIS calculations, the requested convergence on the density matrix was 10^{-8}, and the threshold values for the maximum force and the maximum displacement were 0.00045 and 0.00018 a. u., respectively. AM1, RHF, and B3LYP ground state geometries provided three sets of coordinates for the evaluation of the vertical excitation, and CIS excited state geometries that for the emission energies.

To compute vertical excitation and emission energies, we performed single point CI calculations in which all singly excited configurations from an active space with the 10 highest occupied orbitals and the 10 lowest unoccupied orbitals (CI=10/10) were included. In all cases, the first singlet excitation/emission that have the largest calculated oscillator strength was taken as the excitation/emission energy (analogous to the maximum $\lambda_{abs}/\lambda_{fluo}$ in experimental measurements). The vertical excitation energies from the ground state (S_0) to the first singlet excited state (S_1) were calculated at four levels of theory: ZINDO/S, CIS, TD-B3LYP and TD-B3LYP/6-31+G*. The emission energy ($S_0 \leftarrow S_1$) calculations were done at CIS, TD-B3LYP and TD-B3LYP/6-31+G* levels.

CHAPTER 3

RESULTS AND DISCUSSION

3.1 Geometry Optimizations

The results obtained from the geometry optimizations performed both at the ground state (S_0) and the lowest singlet excited state (S_1) of oligothiophene (**nT**), oligofuran (**nF**), and oligopyrrole (**nP**) systems will be discussed in the following.

3.1.1 Ground State Geometries

The ground state (S_0) AM1, HF/6-31G*, and B3LYP/6-31G* fully optimized geometries of the **nT**, **nF**, and **nP** (n=1-6) are given in Tables 3.1-3. Although the geometrical parameters considered in Tables 3.1-3 are only the carbon-carbon bond lengths, the full geometrical data in the cartesian coordinate system might be found in Appendices A-C. For all systems, the chains have planar geometry and in *anti* conformation (i.e., monomers point in opposite directions). Thus, the oligomers with an even number of rings belong to the C_{2h} point group, and those with an odd number of rings belong to the C_{2v} point group. The geometric parameters are labeled according to Figure 3.1.

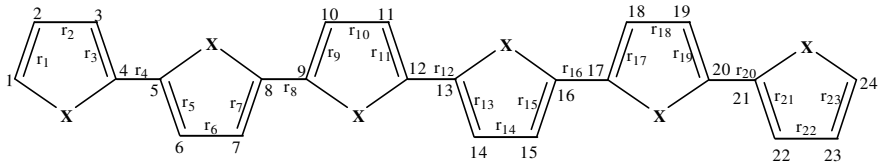

Figure 3.1 Numbering of sites and bonds between carbon atoms in the hexamers of oligoheterocycles (X=S, O, or NH). In general, r_i reflects the bond length between carbon atoms C_i and C_{i+1}.

Table 3.1 Optimized bond lengths (Å) in the ground state (S_0) and the lowest singlet excited state (S_1) of thiophene oligomers (**nT**)

r_i[a]/method[b]	r_1	r_2	r_3	r_4	r_5	r_6	r_7	r_8	r_9	r_{10}	r_{11}	r_{12}
Thiophene **(1T)**												
S_0												
AM1	1.377	1.432										
RHF	1.345	1.437										
B3LYP	1.367	1.430										
S_1												
CIS	1.428	1.364										
Bithiophene **(2T)**												
S_0												
AM1	1.379	1.426	1.388	1.424								
RHF	1.344	1.433	1.352	1.464								
B3LYP	1.367	1.424	1.378	1.451								
S_1												
CIS	1.377	1.388	1.420	1.381								
Terthiophene **(3T)**												
S_0												
AM1	1.379	1.426	1.388	1.424	1.390	1.420						
RHF	1.344	1.433	1.353	1.462	1.351	1.429						
B3LYP	1.368	1.423	1.380	1.447	1.379	1.416						
S_1												
CIS	1.358	1.409	1.390	1.402	1.413	1.369						
Quarterthiophene **(4T)**												
S_0												
AM1	1.379	1.426	1.389	1.424	1.390	1.419	1.390	1.423				
RHF	1.344	1.433	1.353	1.462	1.351	1.428	1.352	1.460				
B3LYP	1.368	1.423	1.380	1.446	1.380	1.415	1.381	1.442				
S_1												
CIS	1.351	1.420	1.373	1.424	1.393	1.380	1.407	1.391				
Quinquethiophene **(5T)**												
S_0												
AM1	1.379	1.426	1.389	1.424	1.390	1.419	1.390	1.423	1.390	1.419		
RHF	1.344	1.433	1.353	1.462	1.351	1.428	1.352	1.460	1.352	1.428		
B3LYP	1.368	1.423	1.380	1.446	1.380	1.414	1.381	1.442	1.382	1.414		
S_1												
CIS	1.348	1.425	1.365	1.438	1.378	1.394	1.392	1.401	1.404	1.376		
Sexithiophene **(6T)**												
S_0												
AM1	1.379	1.426	1.389	1.424	1.390	1.419	1.390	1.423	1.390	1.419	1.390	1.423
RHF	1.344	1.433	1.353	1.462	1.351	1.428	1.352	1.460	1.352	1.428	1.352	1.459
B3LYP	1.368	1.423	1.380	1.446	1.380	1.414	1.381	1.441	1.382	1.413	1.382	1.441
S_1												
CIS	1.346	1.428	1.360	1.447	1.368	1.405	1.379	1.416	1.392	1.382	1.400	1.398

[a] r_i is the bond length between carbon atoms C_i and C_{i+1}. See the numbering in Figure 3.1. Note that $r_{4n-i} = r_i$ due to symmetry, where n is the number of monomer units. Thus, only bond lengths for half of

the molecule are shown in each case. [b] All methods except AM1 employ the 6-31G* basis set.

To test the accuracy of the computed geometrical parameters for the ground state (S_0) of oligothiophenes (**nT**) (Table 3.1), we compared them with the experimental data. The errors in the C-C bond lengths in AM1, RHF/6-31G*, and B3LYP optimized S_0 geometries of some selected **nT** (n = 2, 4, 6) are given in Table 3.2.

Table 3.2 Relative and average errors in the computed geometrical parameters of some selected thiophene oligomers (**nT**)[a].

method[b]/r_i[c]	AM1			RHF			B3LYP		
	2T	**4T**	**6T**	**2T**	**4T**	**6T**	**2T**	**4T**	**6T**
r_1	0.022	0.043	0.033	-0.014	0.008	-0.002	0.010	0.032	0.022
r_2	-0.018	-0.028	0.010	-0.011	-0.021	0.017	-0.020	-0.031	0.007
r_3	-0.044	-0.035	-0.013	-0.080	-0.071	-0.049	-0.054	-0.044	-0.022
r_4	-0.024	-0.030	-0.017	0.016	0.008	0.021	0.003	-0.008	0.005
r_5		0.021	0.013		-0.018	-0.026		0.011	0.003
r_6		0.013	0.014		0.022	0.023		0.009	0.009
r_7		0.018	0.020		-0.021	-0.019		0.009	0.011
r_8		-0.023	-0.018		0.014	0.019		-0.004	0.000
r_9			0.014			-0.024			0.006
r_{10}			0.016			0.025			0.010
r_{11}			0.023			-0.015			0.015
r_{12}			-0.021			0.015			-0.003
error[d]	0.027	0.026	0.018	0.030	0.023	0.021	0.022	0.019	0.009
error[e]		0.022			0.023			0.015	

[a] Experimental X-ray data are from references **2T** [228], **4T** [229], and **6T** [230]. For calculation of relative and average errors, see text.[b] All methods except AM1 employ the 6-31G* basis set. [c] r_i is the bond length between carbon atoms C_i and C_{i+1}. See the numbering in Figure 3.1. Note that $r_{4n-i} = r_i$ due to symmetry, where n is the number of monomer units. Thus, only errors for half of the molecule are shown in each case. [d] Average absolute error in computed C-C bond lengths of each oligomer. [e] Average absolute error in C-C bond lengths computed by the indicated method.

Table 3.2 illustrates the relative and absolute average errors in computed C-C bond length values. Relative errors were calculated as the difference between computed and experimental bond lengths while average absolute errors were obtained using the formula in equation 3.1.

$$Average \quad Absolute \quad Error = \frac{1}{N}\sum_{i=1}^{N}\left|r_i^{calc} - r_i^{\exp}\right| \tag{3.1}$$

Here, N is the number of unequal C-C bonds in the molecule, and r_i^{calc} and r_i^{exp} are computed and experimental bond lengths, respectively.

As seen from Table 3.2, there is no regular pattern in the errors in C-C bond lengths for the same oligomer, or for the same method. In addition, no correlation between and within errors for intraring and interring bonds is observed. However, the smallest average absolute errors are obtained when DFT geometries are considered. In other words, B3LYP/6-31G* optimized ground state geometries of **nT** are probably the most reliable geometries. It is almost impossible to reach a crude conclusion on the method that gives the smallest errors since, in the solid state, geometries are influenced by packing effects [231], which are not considered in quantum-chemical calculations –single molecules in gas phase are considered.

To compare the AM1, RHF/6-31G*, and B3LYP/6-31G* optimized ground state geometries of **nT**, the bond length alternation (BLA), Δr_i in **6T** calculated at these levels of theory as a function of the site position are plotted (Figure 3.2).

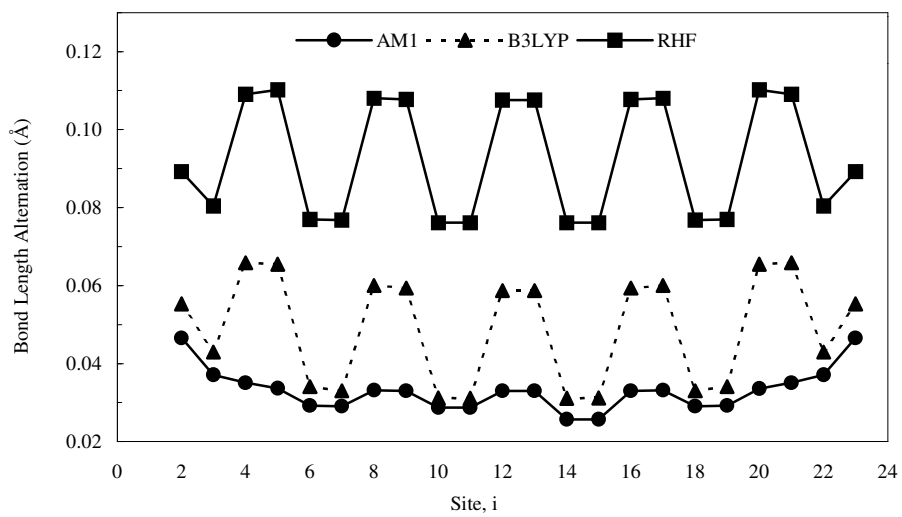

Figure 3.2 Evolution with site position, *i* (see Figure 3.1), of the bond-length alternation, $\Delta r_i = (-1)^i (r_i - r_{i-1})$ in the ground state of sexithiophene (**6T**) calculated at AM1, RHF/6-31G*, and B3LYP/6-31G* levels.

Figure 3.2 clearly illustrates that the ground state geometry optimized at AM1 level has the smallest BLA values. This means that the difference in length between single and double bonds is smallest, and thus the extension of π-conjugation is highest in the AM1 geometry. In addition, Δr_i values calculated for the intraring sites (i = 2, 3, 6, 7, etc.) and interring sites (i = 4, 5, 8, 9, etc.) are almost equal ignoring the chain end regions (about 0.03 Å for both types of sites in **6T**). Hence, it can be concluded that, in the case of thiophene oligomers, the AM1 method produces geometries giving almost equal weight to the cyclic and linear π-conjugation. (Conjugation in and between rings are called as cyclic and linear conjugation, respectively)

In the ground state geometries of thiophene oligomers (**nT**), the DFT intraring Δr_i values quite similar (~0.03 Å) to those predicted by the AM1. However, the interring BLAs are significantly larger (~0.06 Å) due to the longer interring single bonds than intraring ones predicted by the DFT method. The HF method, on the other hand, gives much larger BLA at both the intraring (~0.08 Å) and interring (~0.11 Å) sites. However, the difference (0.11- 0.08 = 0.03 Å) is the same as that given by DFT (0.06 – 0.03 = 0.03 Å). This difference is simply the difference between an interring and an intraring single bond. In other words, the vertical shift of the HF BLA values in Figure 3.2 is due to the too short double bonds predicted by this method (see also Table 3.1). This discussion shows that the ground state geometries obtained at these levels of theory have more localized π-electron densities. Put differently, both HF and DFT methods disfavor linear π-conjugation, whereas within the rings the DFT method predicts a significantly larger π-conjugation for **nT**. This result has been reached in other theoretical studies [12], and considered as the reason for the observed saturation of physical properties as chain length of oligomers increase.

Comparison of BLA parameter in *cis*-polyacetylene with that obtained in heterocyclic oligomers would give an idea on the effect of heteroatom inclusion to the carbon backbone. There is only one BLA parameter in *cis*-polyacetylene (*cis*-PA), and it is 0.095 Å [2]. For thiophene oligomers (**nT**), all levels of theory used in geometry optimizations produces smaller BLA values (except BLA values in

interring sites of RHF/6-31G* optimized geometry) than *cis*-PA. A smaller BLA parameter means a smaller length difference between single and double bonds in the carbon backbone, and thus a more conjugated system. Consequently, it can be concluded that the thiophene oligomers are more conjugated (and stable) systems than *cis*-PA because of the (stabilizing) effect of sulfur atoms.

The data and discussion above shows that the ground state geometries of thiophene oligomers (**nT**) obtained at RHF/6-31G* and B3LYP/6-31G* levels are better than AM1. Others [232] have proved that DFT methods (eg. those employ the B3LYP hybrid functional) compute equilibrium geometries in excellent agreement with experiment for both conjugated organic oligomers and polymers. Thus, we choose the B3LYP/6-31G* optimized ground state geometries of thiophene oligomers in discussion of geometrical changes with the increase in chain length.

In Figure 3.3, we plot the BLA values, Δr_i of all **nT** (n=1-6) calculated at B3LYP/6-31G* level as a function of the site position.

a)

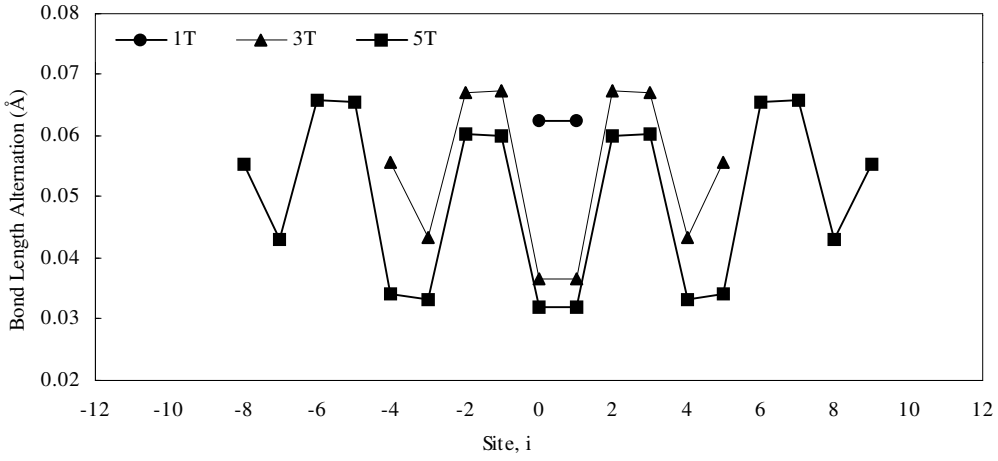

b)

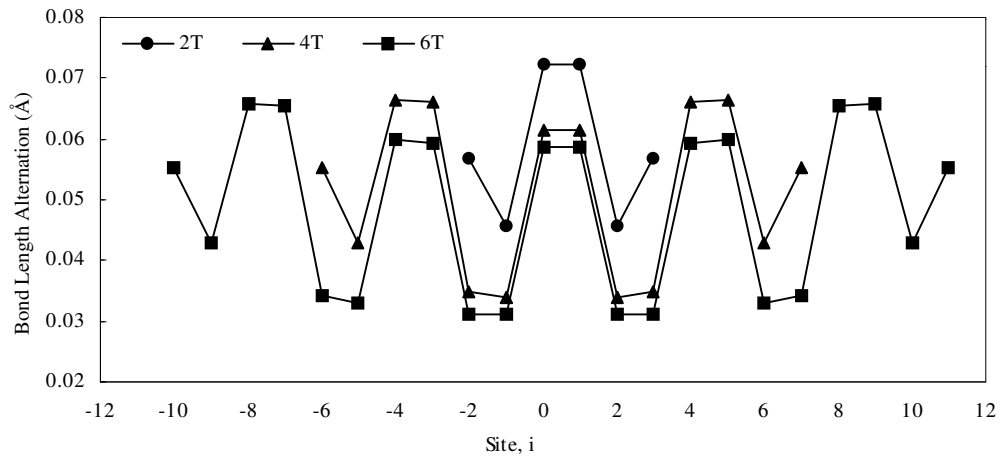

Figure 3.3 Evolution with site position, *i* of the bond-length alternation, $\Delta r_i = (-1)^i (r_i - r_{i-1})$ in the ground state of **1T** (a), **2T** (b), **3T** (a), **4T** (b), **5T** (a), and **6T** (b) calculated at B3LYP/6-31G* level. In order to compare oligomers of different lengths, the numbering in Figure 3.1 has been changed. The sites at 0 and 1 above refer to; in (a) intraring, in (b) interring sites at the center of the oligomers.

Dependence of the BLA on the chain length of thiophene oligomers is shown in Figure 3.3. In thiophene (**1T**), which belongs to the C_{2v} point group, one Δr_i value, 0.06 Å, was recognized since it has only two different bond lengths (one for single C-C bond and one for two double C-C bonds). Starting with **2T**, interring sites appear with a BLA of 0.07 Å. In **4T**, BLA parameters at the center of oligomers are nearly 0.03 Å and 0.06 Å for intraring and interring sites, respectively. For oligomers **5T** and **6T**, extension of this constant region increases linearly with the chain length. Thus, it can be concluded that no major changes in the structural parameters of the central unit should occur when the size of the oligomer is increased [233].

Consequently, for the thiophene oligomers containing up to six monomer units the ground state geometries obtained at B3LPY/6-31G* level are most probably the best geometries employed among the three levels of theory. Stabilizing effect of sulfur atoms in **nT** with respect to *cis*-PA carbon backbone is confirmed. In addition, centrally localized geometrical parameters for oligomers longer than tetramer (**4T**) was deduced from the discussion above.

What is the situation in the optimized ground state geometries of the other π-

conjugated oligomer systems -oligofurans (**nF**) and oligopyrroles (**nP**)? We will first discuss the oligofurans (**nF**). The AM1, RHF/6-31G*, and B3LYP/6-31G* optimized ground state geometries of furan oligomers (**nF**) (n=1-6) are given in Table 3.3. To our knowledge, there is no experimental data on the geometrical parameters of furan oligomers. Thus, we do not have any chance to test the accuracy of theoretically obtained geometric data for oligofurans. However, comparison among the geometries optimized at these three levels of theory may give us an idea about the level of theory that is most reasonable. To ease the comparison we, once again, choose BLA instead of carbon-carbon bond lengths. The bond length alternation, Δr_i, in the AM1, RHF/6-31G*, and B3LYP/6-31G* optimized ground state geometries of sexifuran (**6F**) was calculated and plotted as a function of the site position (Figure 3.4).

Table 3.3 Optimized bond lengths (Å) in the ground state (S_0) and the lowest singlet excited state (S_1) of furan oligomers (**nF**)

r_i[a]/method[b]	r_1	r_2	r_3	r_4	r_5	r_6	r_7	r_8	r_9	r_{10}	r_{11}	r_{12}
Furan **(1F)**												
S_0												
AM1	1.380	1.448										
RHF	1.339	1.441										
B3LYP	1.361	1.436										
S_1												
CIS	1.425	1.367										
Bifuran **(2F)**												
S_0												
AM1	1.381	1.444	1.386	1.424								
RHF	1.339	1.438	1.345	1.449								
B3LYP	1.362	1.430	1.371	1.438								
S_1												
CIS	1.367	1.395	1.415	1.375								
Terfuran **(3F)**												
S_0												
AM1	1.381	1.443	1.386	1.424	1.387	1.439						
RHF	1.339	1.438	1.345	1.447	1.345	1.434						
B3LYP	1.362	1.430	1.372	1.435	1.373	1.423						
S_1												
CIS	1.352	1.415	1.384	1.391	1.405	1.374						
Quarterfuran **(4F)**												
S_0												
AM1	1.381	1.443	1.386	1.424	1.387	1.439	1.387	1.424				
RHF	1.339	1.437	1.345	1.447	1.346	1.433	1.346	1.445				
B3LYP	1.362	1.430	1.372	1.435	1.373	1.422	1.374	1.431				
S_1												
CIS	1.346	1.424	1.367	1.410	1.385	1.385	1.401	1.381				
Quinquefuran **(5F)**												
S_0												
AM1	1.381	1.443	1.386	1.424	1.388	1.439	1.387	1.424	1.388	1.438		
RHF	1.339	1.437	1.345	1.447	1.346	1.433	1.346	1.445	1.346	1.433		
B3LYP	1.362	1.430	1.372	1.435	1.374	1.422	1.375	1.431	1.375	1.421		
S_1												
CIS	1.343	1.430	1.358	1.424	1.370	1.398	1.387	1.391	1.396	1.380		
Sexifuran **(6F)**												
S_0												
AM1	1.381	1.443	1.386	1.424	1.388	1.439	1.387	1.424	1.388	1.438	1.388	1.424
RHF	1.339	1.437	1.345	1.447	1.346	1.433	1.346	1.445	1.346	1.433	1.346	1.445
B3LYP	1.362	1.430	1.372	1.435	1.373	1.422	1.374	1.431	1.375	1.421	1.375	1.431
S_1												
CIS	1.342	1.433	1.353	1.432	1.361	1.409	1.374	1.404	1.385	1.387	1.393	1.388

[a] r_i is the bond length between carbon atoms C_i and C_{i+1}. See the numbering in Figure 3.1. Note that $r_{4n-i} = r_i$ due to symmetry, where n is the number of monomer units. Thus, only bond lengths for half of

the molecule are shown in each case. [b] All methods except AM1 employ the 6-31G* basis set.

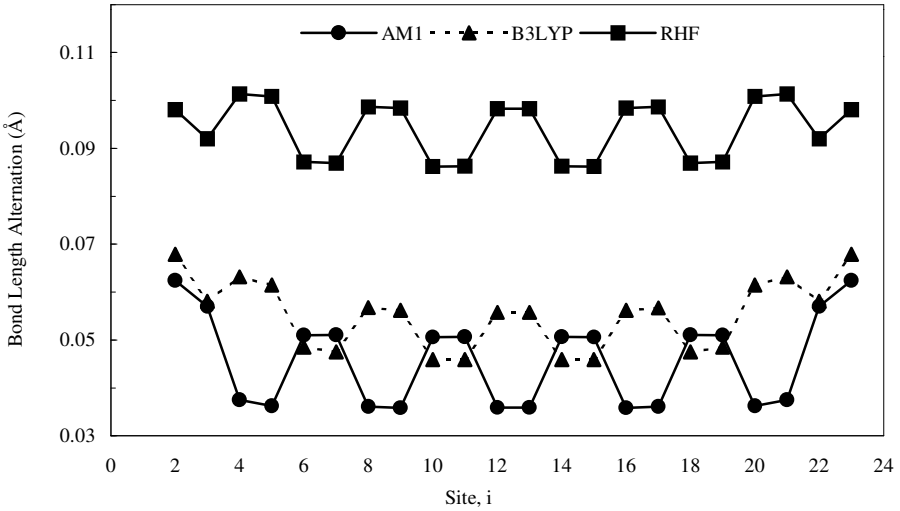

Figure 3.4 Evolution with site position, *i* (see Figure 3.1), of the bond-length alternation, $\Delta r_i = (-1)^i (r_i - r_{i-1})$ in the ground state of sexifuran (**6F**) calculated at AM1, RHF/6-31G*, and B3LYP/6-31G* levels.

As seen from Figure 3.4, the BLA pattern of sexifuran (**6F**) predicted by AM1 is strikingly different than those of DFT and HF methods, and also from the AM1 BLAs of **6T** (Figure 3.2). In AM1 geometry, the BLAs for interring and intraring bonds are about 0.04 and 0.05 Å, respectively. The difference is –0.01 Å, which means that the interring single bonds are shorter than the single bonds in the rings, leading to a reversal of the expected pattern. As a result, linear π-conjugation outweighs the cyclic conjugation. We believe that this behavior is due to an artifact in the semi-empirical AM1 method.

The DFT and HF methods produce the normal patterns, with the HF BLA are shifted vertically up as in the case of thiophene oligomers, and for the same reason; the HF double bonds are too short in 6F, also.

The BLA values in three different geometries of **6F** are smaller than that in *cis*-PA (0.095 Å) [2]. Similar to **nT**, for furan oligomers (**nF**) oxygen atom (heteroatom) stabilizes the π-conjugated carbon skeleton, making the π-conjugation strength of these oligomers larger.

As we did for the thiophene oligomers, the B3LYP/6-31G* optimized ground

state geometries are chosen in investigating change of geometrical parameters of furan oligomers with the chain length. In Figure 3.5, we plot the BLA values, Δr_i of all **nF** (n=1-6) calculated at B3LYP/6-31G* level as a function of site position.

a)

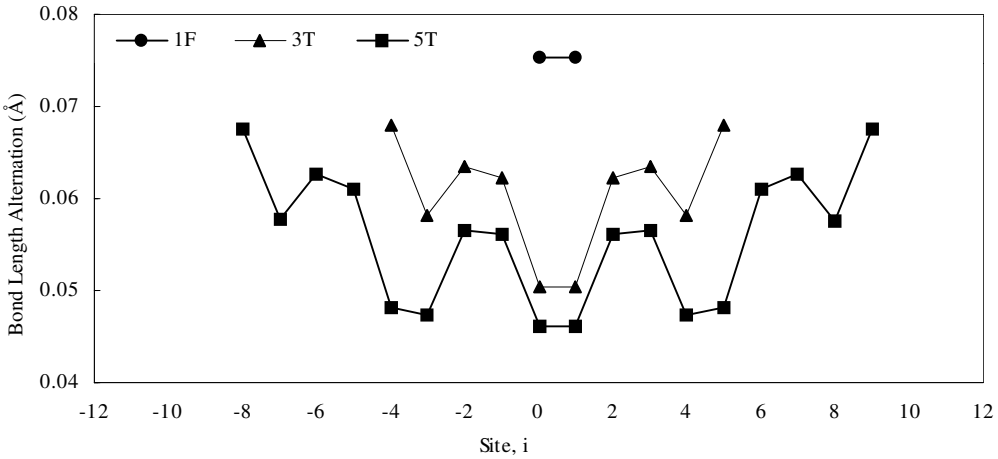

b)

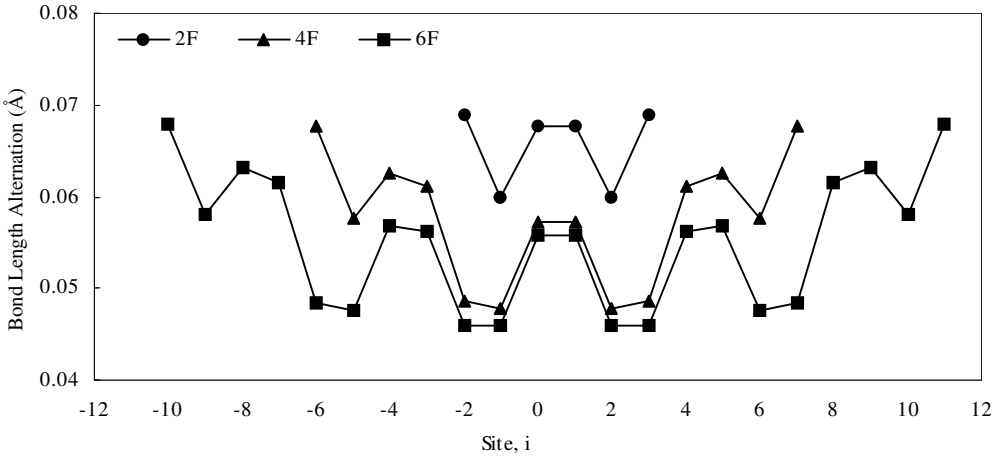

Figure 3.5 Evolution with site position, *i* of the bond-length alternation, $\Delta r_i = (-1)^i (r_i - r_{i-1})$ in the ground state of **1F** (a), **2F** (b), **3F** (a), **4F** (b), **5F** (a), and **6F** (b) calculated at B3LYP/6-31G* level. In order to compare oligomers of different lengths, the numbering in Figure 3.1 has been changed. The sites at 0 and 1 above refer to; in (a) intraring, in (b) interring sites at the center of the oligomers.

In furan oligomers (**nF**), B3LYP generated structures show a regular BLA pattern (ignoring the chain-end effects) along the carbon backbone, as in thiophene oligomers (**nT**). For terfuran (**3F**) and higher oligomers, the BLAs calculated at the center of the oligomers start to saturate to constant values of 0.05 Å and 0.06 Å for

intraring and interring sites, respectively (Figure 3.5). Furan (**1F**) and bifuran (**2F**) are too short to reach these values. For oligomers longer than **3F**, extension of this constant region increases linearly with the chain length.

Summarizing the results above for the furan oligomers (**nF**), the B3LYP/6-31G* geometries were chosen in investigation of change of geometric parameters with the chain length. Centrally constant geometrical parameters are indicative of exsistence of a limit at which the π-conjugation extension stops. Stabilizing effect of oxygen atoms to the π-conjugated carbon backbone of **nF** was observed.

We will now discuss the results obtained for the ground state geometries of the last oligomer system, oligopyrrole (**nP**)s. The AM1, RHF/6-31G*, and B3LYP/6-31G* optimized ground state geometries of pyrrole oligomers (**nP**) (n=1-6) are given in Table 3.4. We are not aware of any experimental data on the geometrical parameters of pyrrole oligomers. Thus, comparisons among the geometrical parameters obtained upon geometry optimizations will be done in order to investigate the relative accuracies of these methods. The bond length alternation (BLA) parameters, Δr_i, in the AM1, RHF/6-31G*, and B3LYP/6-31G* optimized ground state geometries of the largest pyrrole oligomer considered, namely (sexipyrrole) **6F,** were calculated and plotted as a function of the site position (Figure 3.6).

Table 3.4 Optimized bond lengths (Å) in the ground state (S_0) and the lowest singlet excited state (S_1) of pyrrole oligomers (**nP**)

r_i[a]/method[b]	r_1	r_2	r_3	r_4	r_5	r_6	r_7	r_8	r_9	r_{10}	r_{11}	r_{12}
Pyrrole **(1P)**												
S_0												
AM1	1.402	1.435										
RHF	1.358	1.427										
B3LYP	1.378	1.426										
S_1												
CIS	1.440	1.366										
Bipyrrole **(2P)**												
S_0												
AM1	1.403	1.431	1.410	1.439								
RHF	1.357	1.424	1.366	1.458								
B3LYP	1.378	1.421	1.390	1.448								
S_1												
CIS	1.382	1.389	1.436	1.378								
Terpyrrole **(3P)**												
S_0												
AM1	1.403	1.430	1.410	1.439	1.412	1.426						
RHF	1.357	1.423	1.366	1.457	1.365	1.420						
B3LYP	1.378	1.421	1.390	1.446	1.390	1.416						
S_1												
CIS	1.369	1.404	1.404	1.399	1.421	1.370						
Quarterpyrrole **(4P)**												
S0												
AM1	1.404	1.430	1.410	1.439	1.412	1.426	1.412	1.439				
RHF	1.357	1.423	1.366	1.457	1.365	1.420	1.365	1.455				
B3LYP	1.379	1.421	1.391	1.445	1.391	1.415	1.392	1.443				
S1												
CIS	1.363	1.413	1.387	1.420	1.401	1.378	1.418	1.389				
Quinquepyrrole **(5P)**												
S_0												
AM1	1.404	1.430	1.410	1.439	1.412	1.426	1.412	1.439	1.412	1.426		
RHF	1.357	1.423	1.366	1.457	1.365	1.420	1.365	1.455	1.365	1.420		
B3LYP	1.379	1.421	1.391	1.445	1.391	1.415	1.392	1.442	1.392	1.415		
S_1												
CIS	1.361	1.417	1.378	1.434	1.388	1.390	1.404	1.400	1.412	1.375		
Sexipyrrole **(6P)**												
S_0												
AM1	1.404	1.430	1.410	1.439	1.412	1.426	1.412	1.439	1.412	1.426	1.412	1.439
RHF	1.357	1.423	1.366	1.457	1.365	1.420	1.365	1.455	1.365	1.420	1.365	1.455
B3LYP	1.379	1.421	1.391	1.445	1.391	1.415	1.392	1.442	1.392	1.414	1.392	1.442
S_1												
CIS	1.359	1.420	1.373	1.443	1.379	1.400	1.391	1.414	1.401	1.381	1.410	1.398

[a] r_i is the bond length between carbon atoms C_i and C_{i+1}. See the numbering in Figure 3.1. Note that $r_{4n-i} = r_i$ due to symmetry, where n is the number of monomer units. Thus, only bond lengths for half of

the molecule are shown in each case. [b] All methods except AM1 employ the 6-31G* basis set.

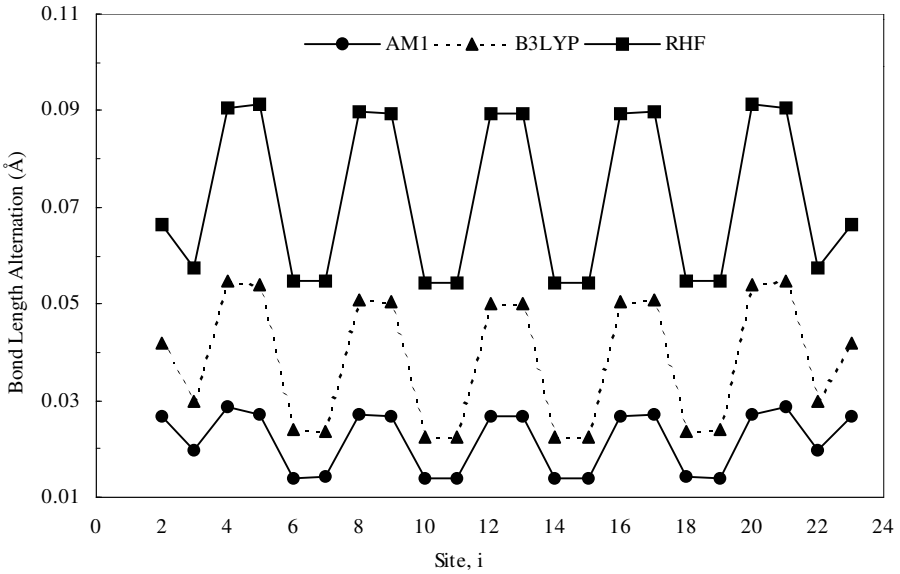

Figure 3.6 Evolution with site position, *i* (see Figure 3.1), of the bond-length alternation, $\Delta r_i = (-1)^i (r_i - r_{i-1})$ in the ground state of sexithiophene (**6P**) calculated at AM1, RHF/6-31G*, and B3LYP/6-31G* levels.

The smallest BLA parameters were obtained in AM1 optimized ground state geometry of sexipyrrole (**6P**). In the central part of this geometry, Δr_i values are about 0.01 and 0.03 Å for the intraring and interring sites. Since BLA is a measure of the strength of π-conjugation, AM1 method may be concluded, for pyrrole oligomers (**nP**), to give largest importance to conjugation phenomena among the three methods considered. For the ground state geometry of **6P** obtained at B3LYP/6-31G* level of theory, Δr_i values are of about 0.02 and 0.05 Å for the intraring and interring sites at the central part. Corresponding values are about 0.05 and 0.09 Å in the RHF/6-31G* optimized geometry of **6P**. Considerable differences between Δr_i values for the interring and intraring sites indicates that all three methods make a clear distinction between cyclic and linear π-conjugation strengths.

The BLA values in three different geometries of **6P** are smaller than that in *cis*-PA (0.095 Å) [2]. Similar to **nT** and **nF**, for pyrrole oligomers (**nP**) nitrogen atom (heteroatom) stabilizes the conjugated π-system, making the π-conjugation strength of these oligomers larger.

The B3LYP/6-31G* optimized ground state geometries are chosen in

investigating change of geometrical parameters of pyrrole oligomers with the chain length, as we did for the thiophene and furanoligomers. In Figure 3.7, we plot the BLA values, Δr_i of all **nP** (n=1-6) calculated at B3LYP/6-31G* level as a function of the site position.

a)

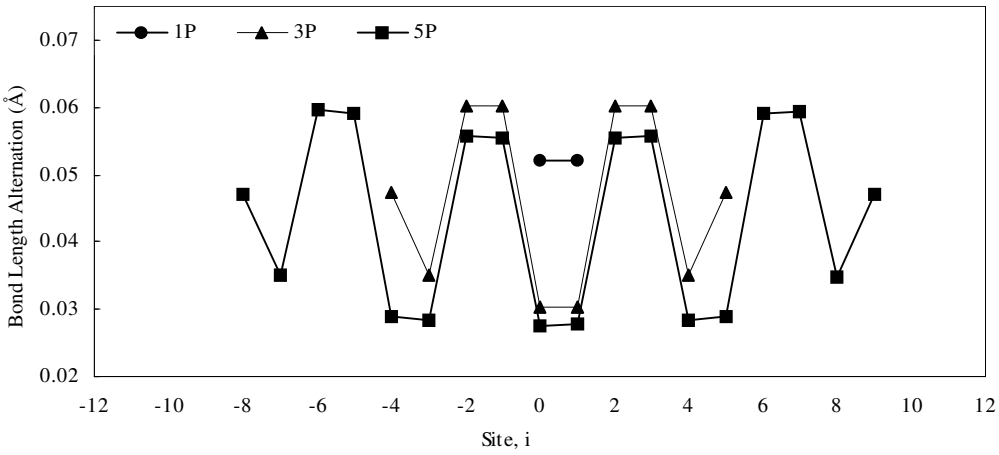

b)

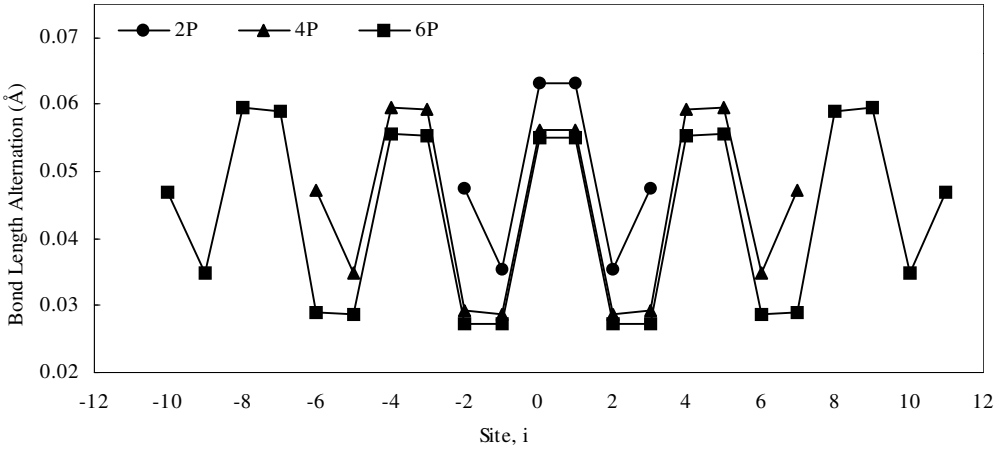

Figure 3.7 Evolution with site position, *i* of the bond-length alternation, $\Delta r_i = (-1)^i (r_i - r_{i-1})$ in the ground state of **1P** (a), **2P** (b), **3P** (a), **4P** (b), **5P** (a), and **6P** (b) calculated at B3LYP/6-31G* level. In order to compare oligomers of different lengths, the numbering in Figure 3.1 has been changed. The sites at 0 and 1 above refer to; in (a) intraring, in (b) interring sites at the center of the oligomers.

Increasing the chain length of pyrrole oligomers (**nP**) changes the geometrical parameters. However, when the tetramer (**4P**) of oligopyrroles is reached the geometrical parameters in the center of oligomers become constant. The saturated values are 0.02 Å and 0.05 Å for intraring and interring sites, respectively (Figure

3.7).

In summary, similar to thiophene and furan oligomers, centrally constant geometrical parameters when the chain length of oligomers is increased and stabilizing effect of heteroatom with respect to *cis*-PA are the important results of the discussion above for pyrrole oligomers.

To compare the effect of heteroatoms in the ground state geometries of **nT** (S), **nF** (O), and **nP** (NH), we plot the BLA parameters, Δr_i calculated for the B3LYP/6-31G* optimized ground state geometries in the largest oligomers (**6T**, **6F**, **6P**) as a function of the site position, i (Figure 3.8).

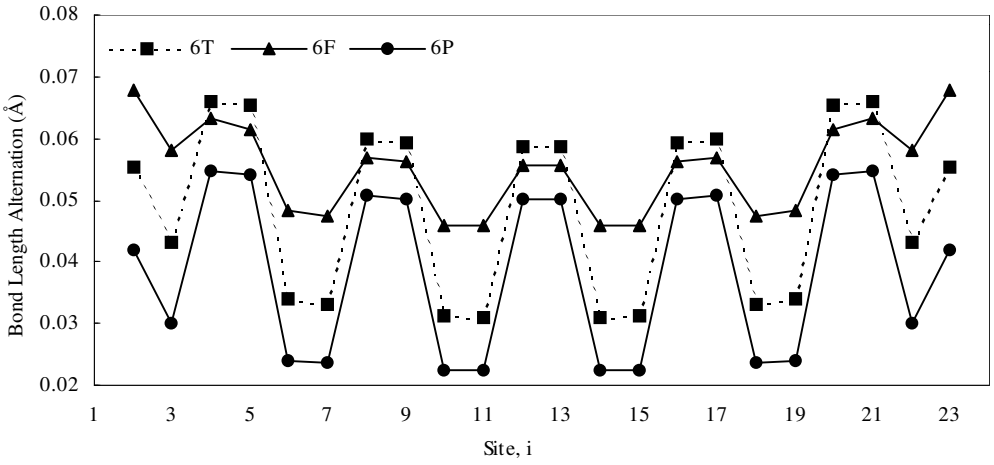

Figure 3.8 Evolution with site position, *i* (see Figure 3.1), of the bond-length alternation, $\Delta r_i = (-1)^i (r_i - r_{i-1})$ in the ground state of **6T**, **6F**, and **6P** (b) calculated at B3LYP/6-31G* level

As seen in Figure 3.8 the BLA parameters for the interring sites increase in the order of **nP**, **nT**, and **nF**, while the corresponding order for the intraring sites is **nT**, **nF**, and **nP**. The first ordering (for interring sites) has no meaning in terms of the change in the physical properties of these systems with the change in the heteroatom. Thus, it can be concluded that the heteroatom has not much effect on the linear π-conjugation. However, the second ordering (for intraring sites) is exactly the same ordering that physical properties of the oligomers change, e.g., absorption energies increase in this order (see Section 3.3.1). The effect of heteroatoms to the cyclic π-conjugation is, hence, very important. Indeed, the ordering above shows that the furan oligomers have the lowest cyclic π-

conjugation, which has been verified by experimental data [12].

3.1.2 Lattice Relaxation

If the geometry of a molecule in the excited state is different than that in the ground state, geometry (or lattice) relaxation phenomena is said to occur. In the area of π-conjugated oligomers, geometry relaxation takes the aromatic-like ground state geometry to the quinoid-like oligomer conformation in the lowest singlet excited state [108, 234]. In other words, the geometry that is found to be optimal for the ground state does not constitute the optimal geometry in the lowest excited states.

In a previous theoretical work on the thiophene oligomers (**nT**), occurrence of geometry relaxation has been seen [196]. To extend this work, we investigated the lattice relaxation phenomenon in the lowest singlet excited state (S_1) of five-membered heterocyclic oligomers. We plot the changes in the bond lengths between the ground state (B3LYP/6-31G*) and excited state (CIS/6-31G*) values as a function of bond number along the carbon backbone, i, for **nT**, **nF**, and **nP** (n=6) in Figures 3.9-11.

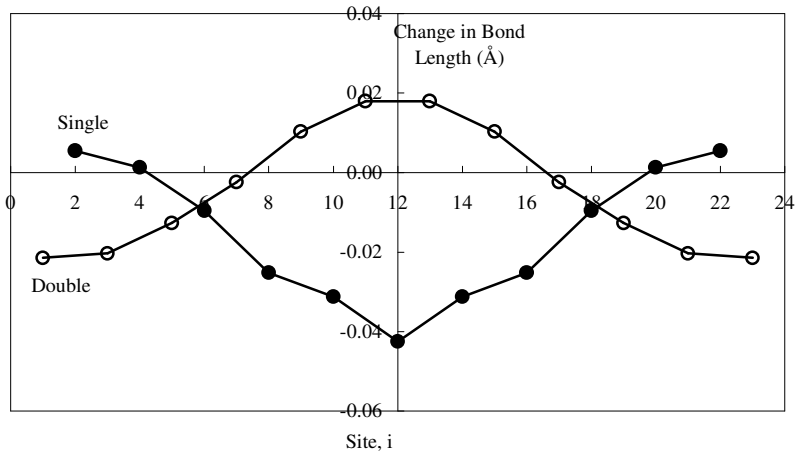

Figure 3.9 Evolution with site position, *i* (see Figure 3.1), of changes in single and double bond lengths (as indicated) between the ground state (B3LYP/6-31G*) and lowest singlet excited state (CIS/6-31G*) values shown for **6T**.

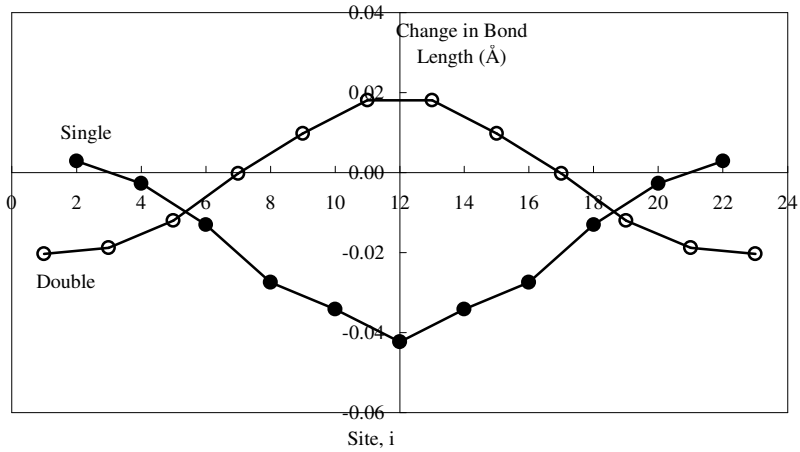

Figure 3.10 Evolution with site position, *i* (see Figure 3.1), of changes in single and double bond lengths (as indicated) between the ground state (B3LYP/6-31G*) and lowest singlet excited state (CIS/6-31G*) values shown for **6F** as indicated.

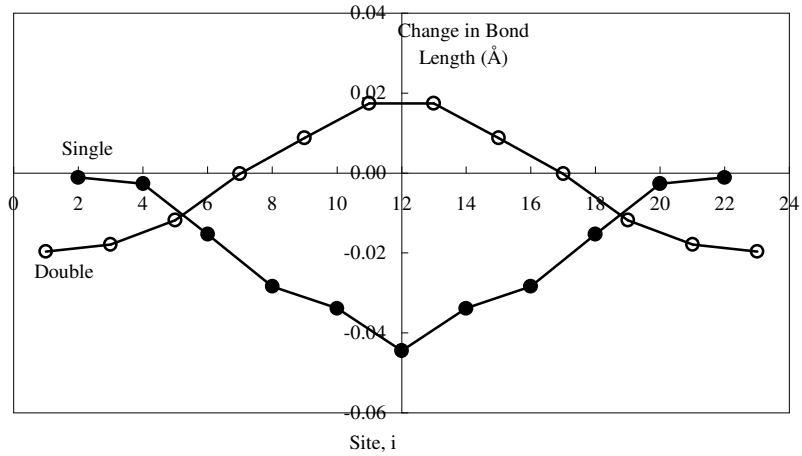

Figure 3.11 Evolution with site position, *i* (see Figure 3.1), of changes in single and double bond lengths (as indicated) between the ground state (B3LYP/6-31G*) and lowest singlet excited state (CIS/6-31G*) values shown for **6P**.

As illustrated in Figures 3.9-11, the S_0-double bonds gradually lengthen in S_1, becoming largest around the center of the chain (in bonds r_{11}, r_{13}) as one proceeds to the middle of the oligomer. Concurrently, the S_0-single bonds shorten in S_1 as one approaches the center of the oligomer. The decrease in S_0-single bonds occurs at a faster rate than the increase in the S_0-doubles causing a much larger BLA near the center. In addition, the interring single bonds (r_4, r_8, r_{12}, r_{16}, r_{20}) undergo the largest

changes. Hence, the greatest lattice distortion in the lowest singlet excited state can be concluded to occur in the middle of the oligomers. The centrally located character of the lattice distortion does not change as the oligomer type changes. However, it becomes more extended with the increase in the chain length of the oligomers.

The occurrence of relatively large carbon-carbon bond length modifications near the central rings is indicative of a localized character of π-electron distribution in the lowest singlet excited state in the aromatic five-membered heterocyclic oligomers. The trend further shows that there is a similarity in the variation of bond lengths between the B3LYP ground state and CIS excited state results: the C—C single bond lengths are shortened and the C═C double bond lengths are elongated towards the center and as the oligomers become longer.

3.1.3 Excited State Geometries

There are no experimental data available for the excited state geometries of the oligothiophene (**nT**), oligofuran (**nF**), and oligopyrrole (**nP**) systems. Furthermore, theoretical works on the excited states of **nF** and **nP** is very rare. In the case of **nT**, few calculations have been published for the excited states [196, 235, 236], and even fewer include changes in molecular structure upon excitation, i.e. optimization of excited-state geometries [196-198, 237]. However, excited-state optimized geometries are important since this is the only way that theoretical investigation of photophysical behavior of molecules in excited state can be done. In investigation of, for example, emission properties, structural relaxation after photoexcitation cannot be reproduced by ground-state optimizations. In fact, optimized ground-state geometries can be used in obtaining absorption energies, but the optimization of the excited state is essential for the computation of emission energies.

Fluorescence properties of π-conjugated systems are largely concerned for light-emitting diode (LED) applications. The lowest singlet excited state (S_1) is, thus, of particular importance since fluorescence occurs only from this state due to Kasha's rule. Therefore, S_1 state is investigated in term of geometries and electronic transition to and from this state. In this section, we will explore the S_1 state

geometries of aromatic five-membered heterocyclic oligomers **nT**, **nF**, and **nP** (n=1-6). We performed the geometry optimizations for the S_1 states of all oligomers at the CIS/6-31G* level.

The carbon-carbon bond lengths in the lowest singlet excited state geometries of **nT** (Table 3.1), **nF** (Table 3.3), and **nP** (Table 3.4) were given in Section 3.1.1. The full geometrical data in cartesian coordinate system may be found in Appendix D. Instead of bond lengths, the bond length alternation parameters, Δr_i will be considered in discussion of the S_1 state geometries as we did in the ground state geometries.

For CIS/6-31G* optimized lowest singlet excited state geometries of thiophene, furan, and pyrrole oligomers (**nT**, **nF**, and **nP**, n=3-6), we plot the BLA parameters, Δr_i as a function of the site position, i in Figure 3.12-14.

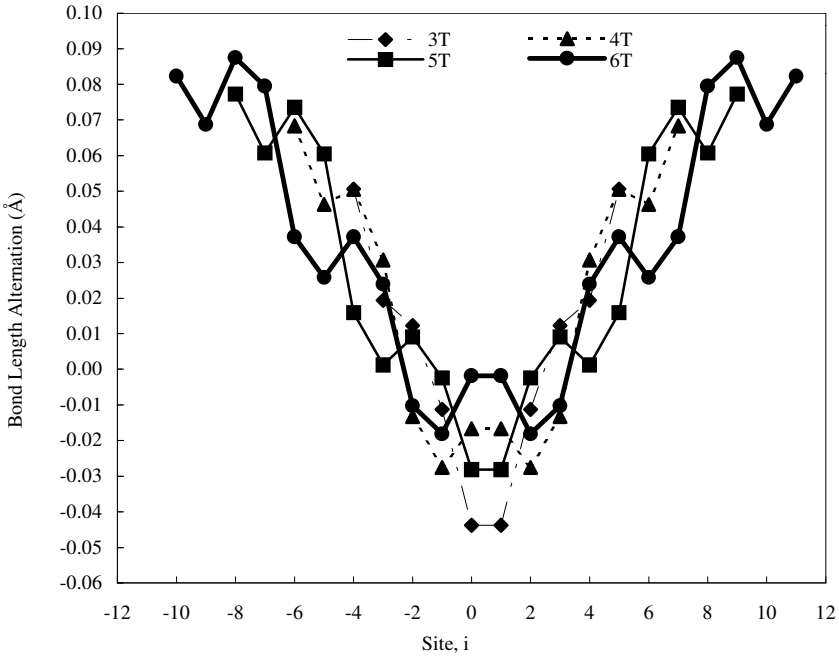

Figure 3.12 Evolution with site position, *i*, of the bond-length alternation, $\Delta r_i = (-1)^i (r_i - r_{i-1})$ in the lowest singlet excited state of **3T**, **4T**, **5T** and **6T** calculated at CIS/6-31G* level. In order to compare oligomers of different lengths, the numbering in Figure 3.1 has been changed. The sites at 0 and 1 above refer to; in (a) intraring, in (b) interring sites at the center of the oligomers.

At the chain end regions of the lowest singlet excited state (S_1) geometries of thiophene, furan, and pyrrole oligomers (**nT**, **nF**, and **nP**) an aromatic-like structure is recognized (Figure 3.12-14). More precisely, the BLA pattern in the ground state geometries is almost conserved for the chain ends. The magnitude of BLA parameters decreases significantly or even becomes zero when going from chain ends to the middle of the oligomers. Indeed, the absolute values of BLA parameters in the central region of S_1 state geometries of **nT**, **nF**, and **nP** range between 0.04 Å to 0.00 Å. The zero BLA cases, which are observed at some parts of the S_1 state geometries, indicate a nearly benzenoid-like geometry in which single and double bond lengths are equal. At the center part, most Δr_i values are negative, and that indicates a quinoid-like geometry. Indeed, the most important feature of the S_1 state geometries of **nT**, **nF**, and **nP** is the increase in the contribution of quinoid-like resonance structure to the equilibrium geometry with respect to that in the ground state.

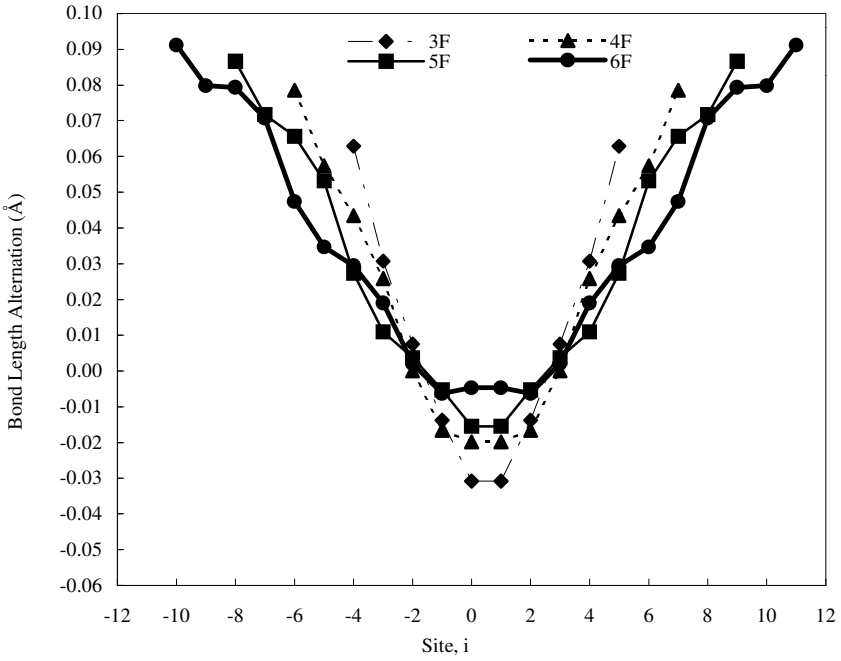

Figure 3.13 Evolution with site position, *i*, of the bond-length alternation, $\Delta r_i = (-1)^i (r_i - r_{i-1})$ in the lowest singlet excited state of **3F**, **4F**, **5F** and **6F** calculated at CIS/6-31G* level. In order to compare oligomers of different lengths, the numbering in Figure 3.1 has been changed. The sites at 0 and 1 above refer to; in (a) intraring, in (b) interring sites at the center of the oligomers.

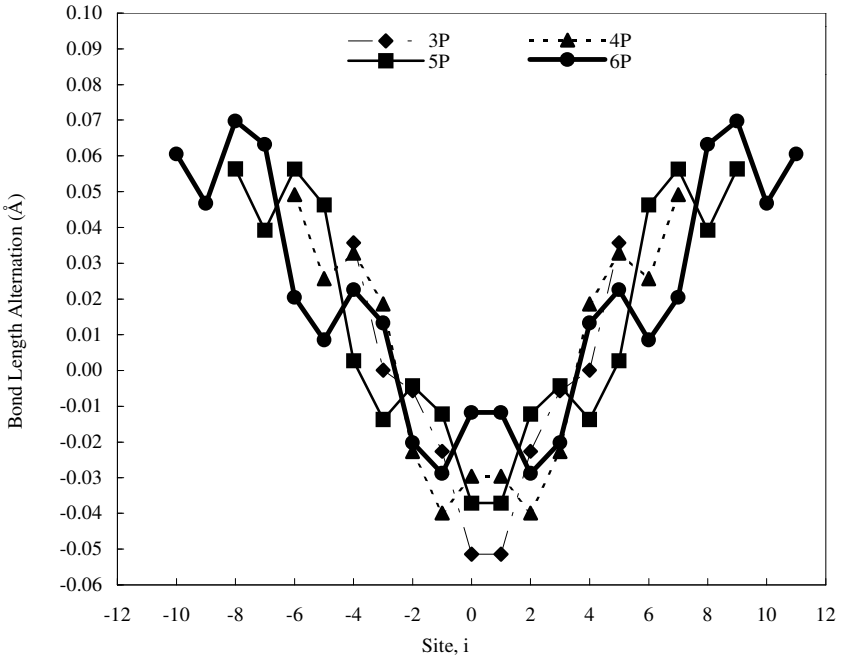

Figure 3.14 Evolution with site position, *i*, of the bond-length alternation, $\Delta r_i = (-1)^i (r_i - r_{i-1})$ in the

lowest singlet excited state of **3P**, **4P**, **5P** and **6P** calculated at CIS/6-31G* level. In order to compare oligomers of different lengths, the numbering in Figure 3.1 has been changed. The sites at 0 and 1 above refer to; in (a) intraring, in (b) interring sites at the center of the oligomers.

As the chain length increases from trimers to seximers, benzenoid character of structures increase as understood from zero Δr_i values. However, the magnitude of the negative BLA values decreases. Hence, a decrease in the quinoid character of the S_1 state can be concluded with the increase in the number of monomer units in the oligomers.

To discuss the effect of heteroatoms on the S_1 state of **nT**, **nF**, and **nP**, we, again, plot the BLA parameters, Δr_i as function of the site positions, i, for the largest members of the oligomers, namely, for **6T**, **6F**, and **6P** (Figure 3.15).

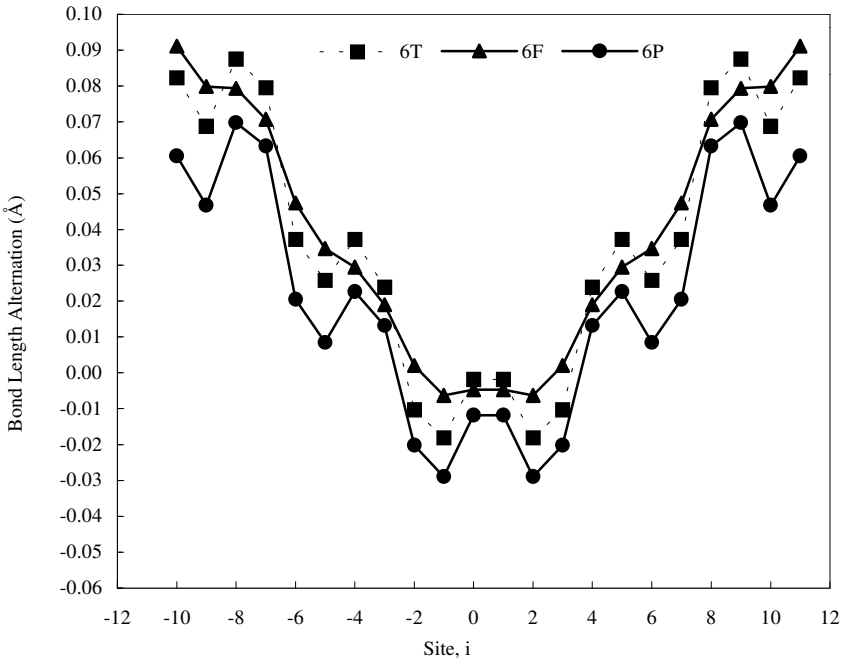

Figure 3.15 Evolution with site position, *i* (the numbering in Figure 3.1 is changed by assigning *i*=0 to the carbon atom at the center of an oligomer), of the bond-length alternation, $\Delta r_i = (-1)^i (r_i - r_{i-1})$ in the lowest singlet excited state of **6T**, **6F** and **6P** calculated at CIS/6-31G* level.

It can be seen in Figure 3.15 that the BLA parameters for the intraring sites is largest for **6F**, than **6T**, and **6P**. For the interring sites, Δr_i increases in the order **6T**, **6F**, and **6P**. Since the fluorescence energies of π-conjugated oligomer increases in the latter order (see Section 3.3.2), the effect of heteroatoms to the interring sites in

the S_1 state is important, the reverse of the situation in S_0 state. In fact, the heteroatoms in **nT** (S), **nF** (O), and **nP** (NH) affect the linear π-conjugation in S_1 state. This, again, may be related to the increase in the rate of participation of heteroatoms in conjugated π-systems that extends to whole molecule of S_1 state with respect to that in S_0 state.

3.2 Molecular Orbital Analysis

There is a strong connection between the ground state and lowest singlet excited state geometries and the frontier molecular orbitals of the five-membered heterocyclic oligomers. As shown in Chapter 1, HOMO wave function reflects the bonding pattern in the ground state geometry while LUMO that in the lowest singlet excited state. Furthermore, the bond length alternation parameter, Δr_i that is used in investigation of the geometries in S_0 and S_1 states is related to the π-electron density distribution. In fact, the BLA parameter reflects the uneven distribution of the π-electron density along the conjugated chain.

The HOMO belongs to b_g (b_1), and the LUMO to a_u (a_2) species in C_{2h} (C_{2v}) groups, respectively. Based upon the one-electron promotion from HOMO to LUMO, one expects the lowest S_1 state to belong to the B_u (C_{2h}) or B_2 (C_{2v}) symmetries, depending on whether the oligomers contain an even or an odd number of monomers, respectively.

The oligomers studied in this work with an even number of rings belong to the C_{2h} point group, and those with an odd number of rings belong to the C_{2v} point group. Thus, the symmetry of the ground state S_0 of these closed-shell systems is. In addition, the lowest singlet excited state S_1 has B_u symmetry.

The S_1 state corresponds predominantly to a transition between the HOMO and the LUMO levels. Other excitations may also be involved in the determination of the excited state wave function. We note that the single excitations between highest occupied MOs (HOMO, HOMO-1, HOMO-2) and lowest unoccupied MOs (LUMO, LUMO+1, LUMO+2) are the most important contributions to the wave function of S_1 state. In order to gain a better insight for the electronic structure of the five-membered heteroaromatic oligomers, we plotted these frontier MOs of *trans-cisoid*

acetylene hexamer (**6A**) (Figure 3.16) and the largest members of the considered oligomers (**6T**, **6F**, and **6P**).

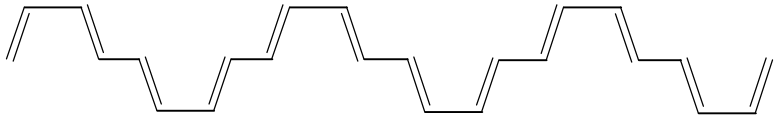

Figure 3.16 Molecular structure of *trans-cisoid* acetylene hexamers, **6A**.

In Figures 3.17-19 we present HOMO (b_g), HOMO-1 (a_u), and HOMO-2 (b_g) of **6A**, **6T**, **6F**, and **6P** in three dimensions.

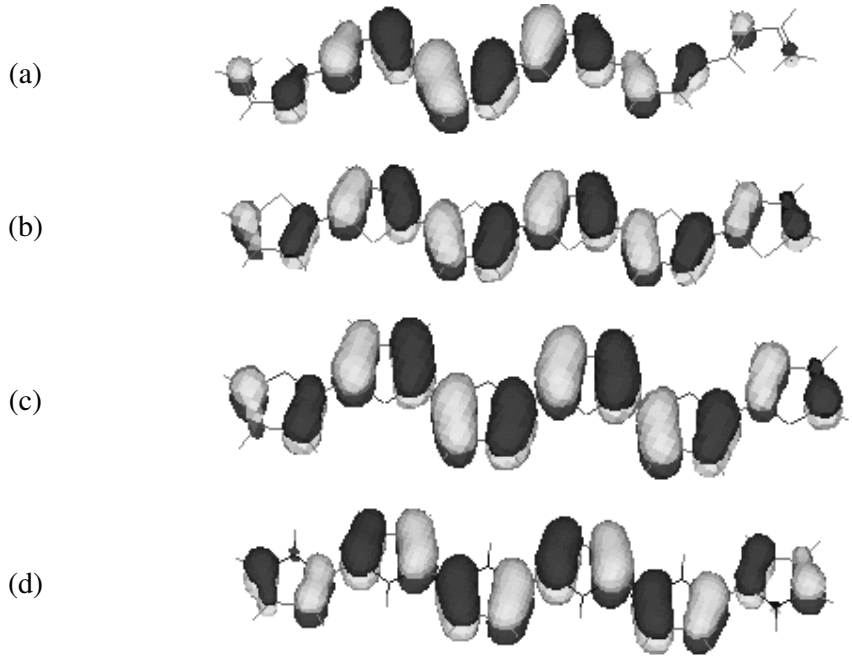

Figure 3.17 (a) Schematic representation of the HOMO for trans-cisoid acetylene hexamer, **6A**. (b) Schematic representation of the HOMO for aromatic thiophene hexamer, **6T**. (c) Schematic representation of the HOMO for aromatic furan hexamer, **6F**. (d) Schematic representation of the HOMO for aromatic pyrrole hexamer, **6P**.

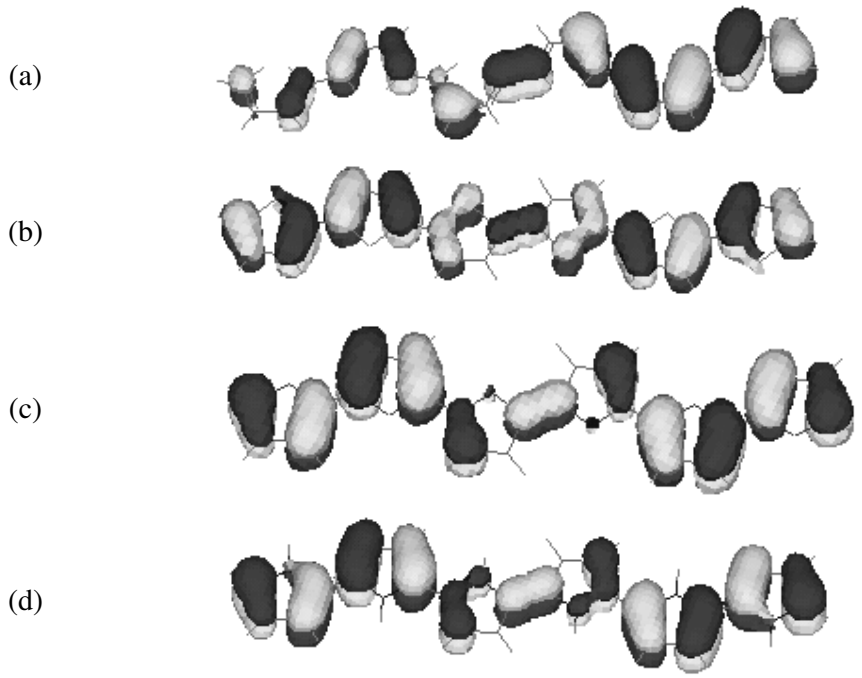

Figure 3.18 (a) Schematic representation of the HOMO-1 for trans-cisoid acetylene hexamer, **6A**. (b) Schematic representation of the HOMO-1 for aromatic thiophene hexamer, **6T**. (c) Schematic representation of the HOMO-1 for aromatic furan hexamer, **6F**. (d) Schematic representation of the HOMO-1 for aromatic pyrrole hexamer, **6P**.

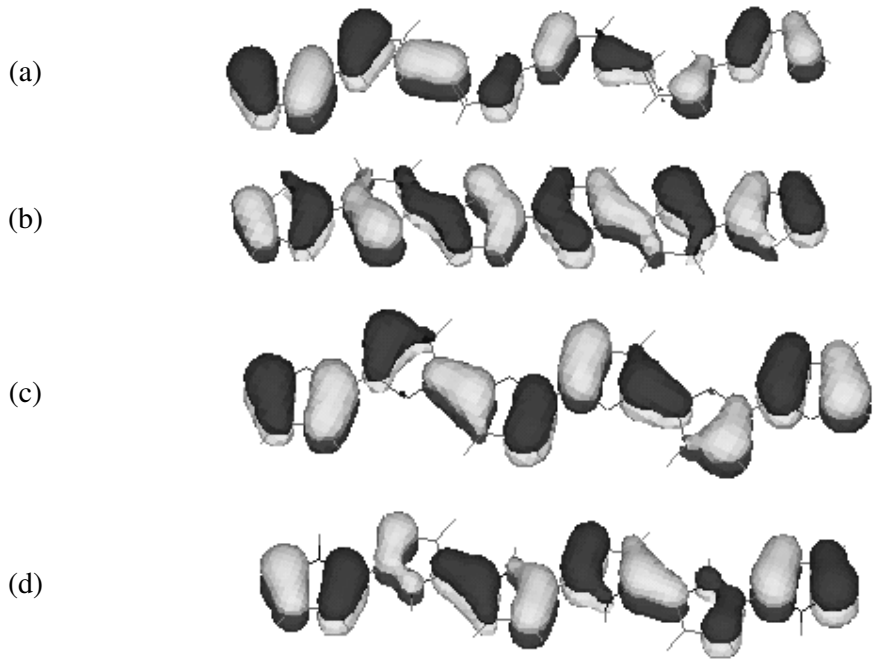

Figure 3.19 (a) Schematic representation of the HOMO-2 for trans-cisoid acetylene hexamer, **6A**. (b) Schematic representation of the HOMO-2 for aromatic thiophene hexamer, **6T**. (c) Schematic representation of the HOMO-2 for aromatic furan hexamer, **6F**. (d) Schematic representation of the

HOMO-2 for aromatic pyrrole hexamer, **6P**.

It is clear from Figures 3.17-19 that lowest occupied molecular orbitlas are not affected very much by the inclusion/change in heteroatom. Especially, the HOMO remains basically unaltered as one goes from **6A** backbone to **6T/6F/6P**. This points to the fact that we would expect that the HOMO of eigenvalue would not change very much by an introduction of S, O, or NH into the oligomer. All four compounds clearly display the aromatic structure, i.e., with double bonds along the 1—2 and 3—4 bonds in monomer units.

In Figures 3.20-22 we present LUMO (a_u), LUMO+1 (b_g), and LUMO+2 (a_u) of **6A**, **6T**, **6F**, and **6P** in three dimensions.

(a)

(b)

(c)

(d)

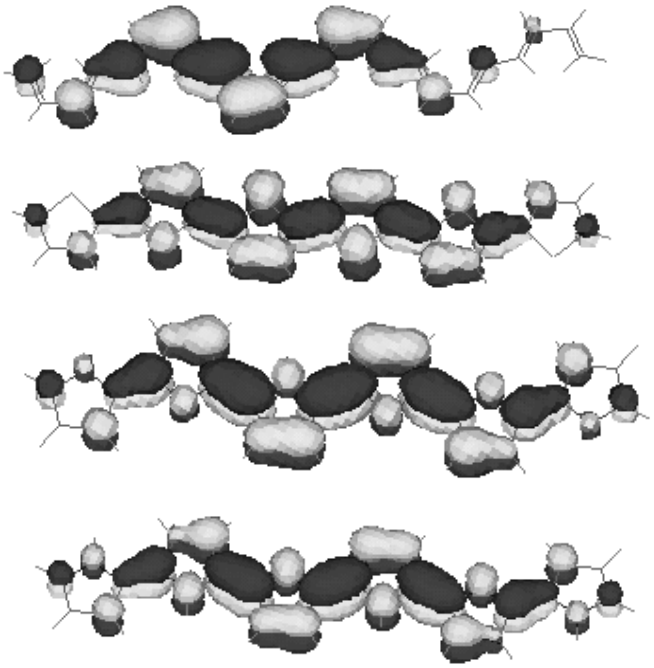

Figure 3.20 (a) Schematic representation of the LUMO for trans-cisoid acetylene hexamer, **6A**. (b) Schematic representation of the LUMO for aromatic thiophene hexamer, **6T**. (c) Schematic representation of the LUMO for aromatic furan hexamer, **6F**. (d) Schematic representation of the LUMO for aromatic pyrrole hexamer, **6P**.

(a)

(b)

(c)

(d)

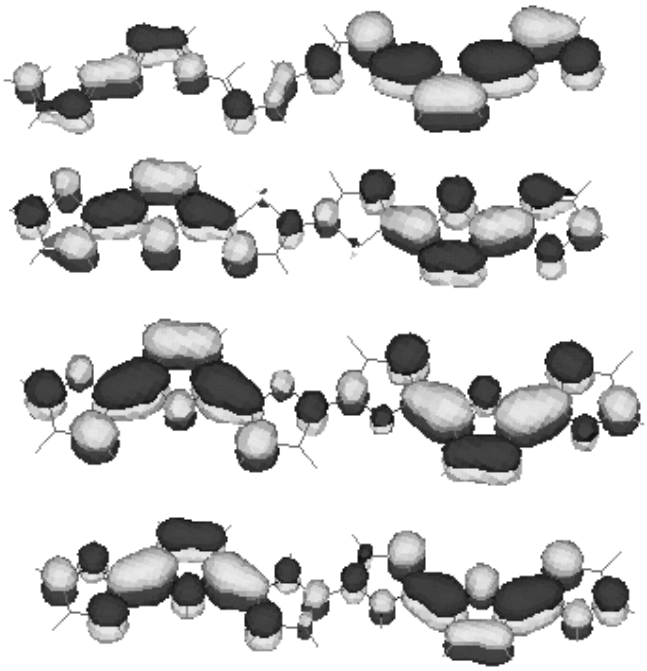

Figure 3.21 (a) Schematic representation of the LUMO+1 for trans-cisoid acetylene hexamer, **6A**. (b) Schematic representation of the LUMO+1 for aromatic thiophene hexamer, **6T**. (c) Schematic representation of the LUMO+1 for aromatic furan hexamer, **6F**. (d) Schematic representation of the LUMO+1 for aromatic pyrrole hexamer, **6P**.

(a)

(b)

(c)

(d)

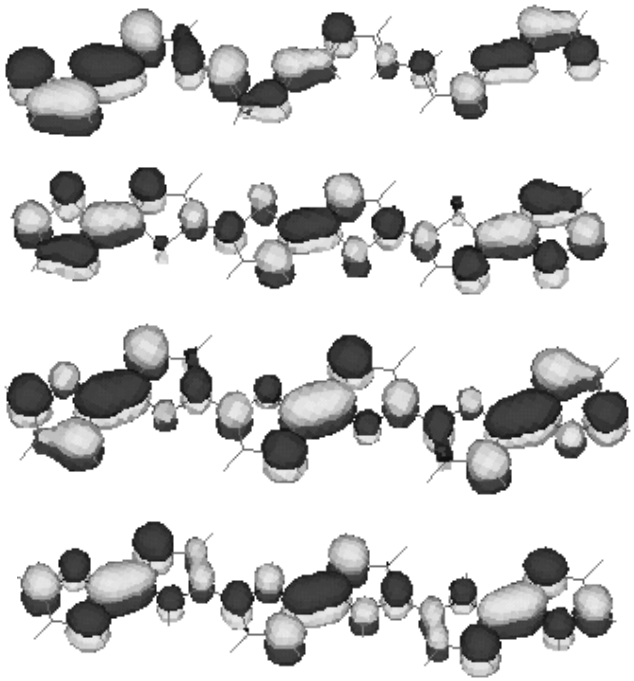

Figure 3.22 (a) Schematic representation of the LUMO+2 for trans-cisoid acetylene hexamer, **6A**. (b) Schematic representation of the LUMO+2 for aromatic thiophene hexamer, **6T**. (c) Schematic representation of the LUMO+2 for aromatic furan hexamer, **6F**. (d) Schematic representation of the

LUMO+2 for aromatic pyrrole hexamer, **6P**.

LUMO (Figure 3.20) is especially important because in the excited state this orbital becomes the lowest orbital that is most likely to be occupied by an excited electron [228]. Not surprisingly the LUMOs for **6A**, **6T**, **6F**, and **6P** are not nearly as the same, as is the case for HOMOs. In particular, one notes that the difference between LUMO for **6A** and **6T/6F/6P** is that the heteroatom now contributes to the LUMO in these heterocycles. In fact, the out-of-plane p_x atomic orbital of the heteroatom destabilizes the LUMO of **6T/6F/6P** (relative to **6A**), with the net effect that excitation energy actually increases for **6T/6F/6P** (relative to **6A**). However, the LUMO, LUMO+1 and LUMO+2 (Figures 3.20-22) show nearly same localization character in **6A**, **6T**, **6F**, and **6P**. The quinoid structure of the LUMO, LUMO+1, and LUMO+2 explains why the geometry of the singlet-excited states becomes more quinoid-like in the central part of the oligomer.

3.3 Transition Energies

3.3.1 Excitation Energies ($S_1 \leftarrow S_0$)

Excitation energy ($S_1 \leftarrow S_0$) can be defined as the energy of a transition from the electronic ground state to an excited state. For π-conjugated systems, it is commonly accepted that an electronic excitation occurs mainly from HOMO to LUMO. Thus, HOMO-LUMO orbital energy differences have been used in estimating the $S_1 \leftarrow S_0$ transition energies of these systems. However, others [238] have shown that vertical transition energies calculated employing a configuration interaction technique give better accord with the experimental absorption energies than those obtained by the crude method above. Thus, we performed single point vertical excitation energy calculations employing the methods that account for electron correlation.

The excitation energies and oscillator strengths of oligothiophene (**nT**), oligofuran (**nF**), and oligopyrrole (**nP**) systems containing up to six monomer units were computed at ZINDO/S, CIS/6-31G*, TDDFT/6-31G*, and TDDFT/6-31+G* levels. In each of these single point calculations, three different sets of coordinates, that is, the AM1, RHF/6-31G*, and B3LYP/6-31G* optimized ground state

geometries, are used. The results are reported in Tables 3.5-7 together with the experimental data.

The vertical transition energies obtained in quantum chemical simulations for fixed ground state geometries correspond to the absorption maxima in experimental spectra [153, 239]. A comparison of absorption data from solid-state films with quantum chemical calculations is not straightforward for crystalline materials. It has been shown for, e.g., parasexiphenyl that the absorption spectra strongly depend on texturing of the investigated film, which is due to the wave propagation effects [240]. Although few experimental data in the gas phase is available, we did not choose them as reference data in comparing our theoretical results since complete data in a specified phase that can be used most of the oligomers is required. Because there is plenty of experimental absorption data in solution, we used them as reference to the theoretical $S_1 \leftarrow S_0$ excitation energies.

The agreement between the calculated and experimental singlet excitation energies of aromatic five-membered heterocyclic oligomers depends on the method used in ground state geometry optimization, the excitation energy calculation method, and the type of basis set. In the following, we will use all these criteria in comparing the computed and experimental excitation energies. In addition, we consider the expectation [37] that experimental results in non-polar solvents are 0.2-0.3 eV smaller than those in the gas phase.

Table 3.5 Absorption energies (ΔE_{abs}) and oscillator strengths (f) of thiophene oligomers (**nT**) computed at various levels of theory[a]

Method[a]	Geom[b]	**1T**		**2T**		**3T**		**4T**		**5T**		**6T**	
		ΔE_{abs}	f	ΔE_{abs}	f	ΔE_{abs}	f	ΔE_{abs}	f	ΔE_{abs}	f	ΔE_{abs}	f
ZINDO/S	AM1	4.76	0.21	3.63	0.79	3.01	1.21	2.67	1.61	2.46	1.95	2.32	2.28
	RHF	4.95	0.20	3.97	0.74	3.43	1.13	3.12	1.50	2.95	1.82	2.84	2.14
	B3LYP	4.77	0.20	3.73	0.79	3.12	1.24	2.77	1.64	2.56	1.99	2.42	2.33
CIS	AM1	6.51	0.12	4.69	0.57	3.96	1.00	3.58	1.45	3.36	1.87	3.21	2.29
/6-31G*	RHF	6.58	0.11	5.01	0.53	4.36	0.94	4.03	1.36	3.84	1.77	3.72	2.18
	B3LYP	6.34	0.12	4.67	0.56	3.94	0.99	3.56	1.44	3.33	1.86	3.17	2.28
TDDFT	AM1	6.10	0.09	4.09	0.44	3.32	0.82	2.89	1.21	2.63	1.59	2.44	1.96
/6-31G*	RHF	6.13	0.08	4.28	0.41	3.56	0.78	3.16	1.14	2.92	1.49	2.75	1.82
	B3LYP	5.93	0.09	4.03	0.43	3.27	0.81	2.84	1.22	2.57	1.61	2.38	1.99
TDDFT	AM1	5.88	0.10	3.91	0.42	3.17	0.76	2.77	1.13	2.52	1.49		
/6-31+G*	RHF	5.92	0.10	4.11	0.40	3.42	0.73	3.05	1.07				
	B3LYP	5.73	0.10	3.87	0.42	3.14	0.77	2.74	1.15	2.48	1.53		
exp[c]		5.10		4.11		3.50		3.18		2.98		2.87	

[a] Method employed to calculate absorption energies. [b] Method used in optimizing the ground state geometry. All values are in eV. TDDFT methods have been employed using B3LYP hybrid functional. [c] ref. 91, in CH_2Cl_2.

For thiophene oligomers (**nT**), excitation energies obtained by ZINDO/S method are always smaller than the experimental data (Table 3.5). This trend can be related to the overestimation of the linear π-conjugation character of **nT**. Contrary to ZINDO/S, configuration interaction singles (CIS) predictions of excitation energies are always higher than the experimental absorption energies. This result can be rationalized by the fact that CI-singles method accounts for the electron correlation only by singly excited configurations. For both ZINDO/S and CIS predictions, the trends do not change as the ground state geometry changes. Accuracy of results changes when the initial geometry used in the ZINDO/S and CIS/6-31G* single point calculations (together with other single point calculations) is changed. However, the better agreement with the experimental data is obtained when the ZINDO/S//RHF/6-31G* and CIS/6-31G*//B3LYP/6-31G* levels of theory are employed. The former level has smaller absolute error than the latter.

Time dependent density functional theory (TDDFT) method was employed to

lower the errors in CIS and ZINDO/S. Indeed, TDDFT/6-31G*//AM1 level is found to give the smallest errors for **nT** when the average errors in these twelve calculations are compared. This result shows that use of larger basis set does not improve the accuracy in excitation energies of **nT**, except **1T** and **2T** as seen from the TDDFT/6-31+G* results.

Table 3.6 Absorption energies (ΔE_{abs}) and oscillator strengths (f) of furan oligomers (**nF**) computed at various levels of theory[a]

Method[a]	Geom[b]	**1F**		**2F**		**3F**		**4F**		**5F**		**6F**	
		ΔE_{abs}	f	ΔE_{abs}	f	ΔE_{abs}	f	ΔE_{abs}	f	ΔE_{abs}	f	ΔE_{abs}	f
ZINDO/S	AM1	4.79	0.21	3.68	0.70	3.06	0.93	2.74	1.22	2.55	1.51	2.43	1.76
	RHF	5.09	0.19	4.07	0.63	3.49	0.82	3.21	1.09	3.05	1.34	2.95	1.56
	B3LYP	4.91	0.20	3.83	0.68	3.20	0.89	2.88	1.19	2.69	1.46	2.57	1.71
CIS	AM1	6.66	0.19	4.88	0.73	4.09	1.03	3.68	1.44	3.43	1.80	3.27	2.17
/6-31G*	RHF	7.22	0.19	5.55	0.72	4.81	1.00	4.44	1.40	4.22	1.76	4.08	2.13
	B3LYP	6.92	0.19	5.17	0.74	4.37	1.04	3.94	1.45	3.69	1.82	3.53	2.20
TDDFT	AM1	6.26	0.14	4.33	0.57	3.49	0.85	3.03	1.21	2.74	1.54	2.54	1.87
/6-31G*	RHF	6.78	0.14	4.87	0.57	4.03	0.82	3.58	1.15	3.31	1.44	3.13	1.72
	B3LYP	6.51	0.14	4.57	0.58	3.71	0.85	3.23	1.21	2.93	1.53	2.73	1.85
TDDFT	AM1	5.87	0.16	4.14	0.57	3.35	0.83	2.92	1.18	2.64	1.49	2.46	1.81
/6-31+G*	RHF	6.27	0.17	4.65	0.57	3.87	0.80	3.46	1.10	3.21	1.38	3.04	1.66
	B3LYP	6.06	0.17	4.37	0.58	3.56	0.83	3.12	1.17	2.84	1.48	2.65	1.79
exp[c]		5.93		4.40		3.78		3.43		3.25			

[a] Method employed to calculate absorption energies. [b] Method used in optimizing the ground state geometry. All values are in eV. TDDFT methods have been employed using B3LYP hybrid functional. [c] ref. 36, in acetonitrile.

For furan oligomers (**nF**) (Table 3.6), ZINDO/S and CIS/6-31G* calculated excitation energies show the same trend as in **nT**. More precisely, while ZINDO/S results are always smaller than the experimental data CIS method overestimates the excitation energies. In ZINDO/S predictions of excitation energies of **nF**, the smallest errors were obtained when the ground state geometries obtained at RHF/6-31G* were employed. However these geometries produces highest errors when employed with CIS method with which the best agreement with the experimental data are obtained when AM1 geometries are used. Among all levels of theory,

TDDFT/6-31G*//B3LYP/6-31G* calculated excitation energies have, in average, the smallest absolute errors for **nF**. This means, similar to the case in **nT**, inclusion of diffuse function to 6-31G* basis set (designated by 6-31+G*) does not improve the accuracy of the results for **nF**.

Table 3.7 Absorption energies (ΔE_{abs}) and oscillator strengths (f) of pyrrole oligomers (**nP**) computed at various levels of theory[a]

Method[a]	Geom[b]	**1P**		**2P**		**3P**		**4P**		**5P**		**6P**	
		ΔE_{abs}	f	ΔE_{abs}	f	ΔE_{abs}	f	ΔE_{abs}	f	ΔE_{abs}	f	ΔE_{abs}	f
ZINDO/S	AM1	4.99	0.25	3.76	0.74	3.16	1.03	2.85	1.38	2.67	1.69	2.55	1.97
	RHF	5.29	0.24	4.14	0.70	3.60	0.96	3.32	1.27	3.16	1.57	3.07	1.83
	B3LYP	5.15	0.25	3.95	0.74	3.36	1.02	3.05	1.36	2.87	1.68	2.76	1.96
CIS	AM1	6.92	0.19	5.10	0.77	4.36	1.17	3.97	1.64	3.74	2.08	3.59	2.51
/6-31G*	RHF	7.39	0.18	5.70	0.76	5.02	1.14	4.68	1.60	4.47	2.04	4.35	2.49
	B3LYP	7.18	0.19	5.40	0.78	4.67	1.19	4.29	1.67	4.06	2.11	3.92	2.57
TDDFT	AM1	6.51	0.14	4.49	0.59	3.68	0.91	3.24	1.28	2.97	1.62	2.78	1.95
/6-31G*	RHF	6.95	0.14	4.97	0.59	4.18	0.88	3.76	1.22	3.51	1.53	3.35	1.84
	B3LYP	6.76	0.14	4.74	0.60	3.93	0.91	3.49	1.28	3.21	1.61	3.03	1.94
TDDFT	AM1	5.91	0.19	4.24	0.58	3.49	0.84	3.09	1.18	2.84	1.50	2.67	1.81
/6-31+G*	RHF	6.17	0.18	4.69	0.57	3.98	0.80	3.60	1.11	3.38	1.40	3.23	1.68
	B3LYP	6.05	0.18	4.48	0.59	3.73	0.84	3.33	1.18	3.09	1.49	2.93	1.80
exp[c]		5.96		4.49		3.91				3.38			

[a] Method employed to calculate absorption energies. [b] Method used in optimizing the ground state geometry. All values are in eV. TDDFT methods have been employed using B3LYP hybrid functional. [c] ref. 152 in acetonitrile.

Table 3.7 illustrates the excitation energies and corresponding oscillator strengths of pyrrole oligomers (**nP**) computed using four levels of theory at three different geometries. Negative errors in the excitation energies computed by ZINDO/S method and positive errors in CIS/6-31G* results are also observed for **nP**, as for **nT** and **nF**. In ZINDO/S single point calculations, the smallest errors obtained when the RHF/6-31G* optimized ground state geometry is used. However, the CIS/6-31G*//AM1 level gives excitation energies that have the best agreement with the experimental data within data obtained by CIS method. The absolute errors

in excitation energies computed by ZINDO/S method is smaller than those computed at CIS/6-31G* level.

Accuracy of TDDFT method changes with the change in geometry and/or basis set for each member of pyrrole oligomers. However, the smallest errors among all levels of theory are obtained by TDDFT/6-31G*//AM1 method when averaged over the data for four members (**1P-3P, 5P**).

If, for all **nT**, **nF**, and **nP**, the average errors in excitation, $S_1 \leftarrow S_0$, energies depending on a given geometry are compared, it is found that the data obtained using the DFT geometries show the best agreement with experimental data. When the same type of comparison is done for $S_1 \leftarrow S_0$ energies computed by a given level of theory, TDDFT/6-31G* computed data is found to have the smallest errors, although TDDFT/6-31+G* is the second.

For all systems, as the oligomer length increases an exponential decrease in excitation energies accompanied by an increase in the oscillator strengths occurs. This general trend is observed in all theoretical and experimental excitation energies. For these data, we performed least-squares exponential fit to the equation (equation 1.4) given by Meier *et. al.* [7] as (for definitions of shorthand symbols refer to Section 1.1.3)

$$\lambda(n) = \lambda_\infty + (\lambda_1 - \lambda_\infty)e^{-b(n-1)}$$

In fitting procedure to this function, firstly, the parameters λ_∞ and b were obtained using the data series $\lambda(n)$ and n, where the maximum n value is the length of longest oligomer for which corresponding $\lambda(n)$ data available. We, then, calculated $\lambda(n)$ values for n=1-30. The effective conjugation length (ECL) values were obtained as the n value at which the difference between λ_∞ and $\lambda(n)$ is smaller than 1 nm (accuracy of an ordinary spectrometer). This kind of an exponential fit has already been performed [7] for the experimental excitation energies of **nT** and **nP**. In this study, their work is extended to all of the computed excitation energies and to the experimental data of **nT**, **nF**, and **nP**. However, we give here only the fits that were found to give best agreement with the experimental fits for each oligomer series, and, of course, experimental fits (Figure 3.23-25).

Tables 3.5-7 together with Figure 3.23-25 illustrate that the excitation energies $S_1 \leftarrow S_0$ increase in the order **nT**, **nF**, and **nP**.

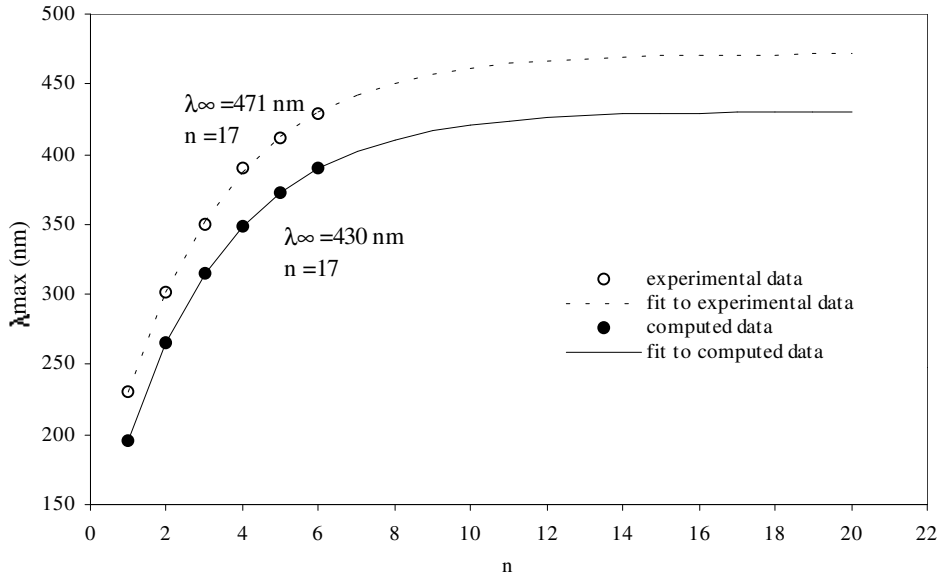

Figure 3.23 Convergence of the computed (—, CIS/6-31G*//B3LYP/6-31G*) and experimental (---, in CH_2Cl_2) excitation energies ($S_1 \leftarrow S_0$) in thiophene oligomers (**nT**). Computed (●) and experimental (○) data is included.

For thiophene oligomers, we obtained the effective conjugation length (ECL) as 17 (17), while the corresponding the wavelength (λ_∞) was found as 430 (471) nm, where the values in parentheses are for the experimental fits (Figure 3.23). The experimental band gap in polythiophene (PTh) is 2.00 eV [77]. Converting λ_∞ values to eV units we obtain, 2.88 eV and 2.63 eV for fits of theoretical (this study) and experimental data, respectively. The small error in the experimental fit values for PTh supports the validity of the equation 1.4. Furthermore, the small difference between experimental fit and our theoretical fit results for PTh show the accuracy of our data.

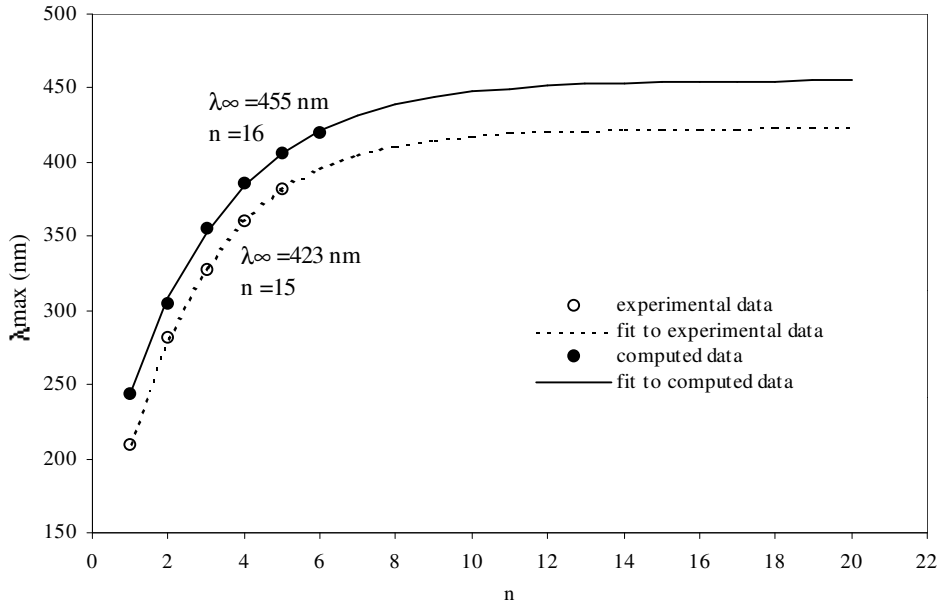

Figure 3.24 Convergence of the computed (—, CIS/6-31G*//RHF/6-31G*) and experimental (---, in acetonitrile) excitation energies ($S_1 \leftarrow S_0$) in furan oligomers (**nF**). Computed (●) and experimental (○) data is included

In the case of furan oligomers, ECL was calculated to be 16 (15) and λ_∞ is 455 (423) nm, where the values in parentheses are for the experimental fits (Figure 3.23). In eV units, these latter values correspond 2.72 eV and 2.93 eV for least squares fits for theoretical (this study) and experimental data, respectively. The experimental band gap in polyfuran (PFu) is 2.35 eV [137]. Since there is a small difference between experimental fit value and the experimental data for PFu, the equation 1.4 may be said to be valid for **nF**. Furthermore, the small difference between experimental fit and our theoretical fit results for PFu show the accuracy of our data.

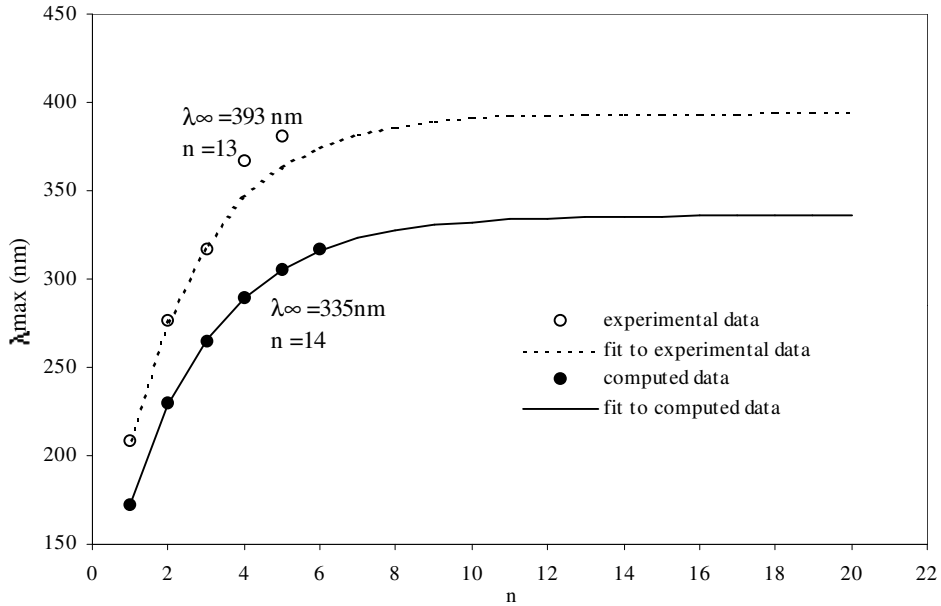

Figure 3.25 Convergence of the computed (—, CIS/6-31G*//B3LYP/6-31G*) and experimental (---, in CH_2Cl_2) excitation energies ($S_1 \leftarrow S_0$) in pyrrole oligomers (**nP**). Computed (●) and experimental (○) data is included.

For the pyrrole oligomers, ECL and λ_∞ are 14 (13) and 336 (394) nm, respectively. Converting λ_∞ values to eV units we obtain, 3.69 eV and 3.15 eV for fits of theoretical and experimental data, respectively. The experimental band gap in polypyrrole (PPr) is 2.35 eV [146]. The error in the experimental fit value is large, which indicates that equation 1.4 should not be used for **nP**. However, there is a small difference between experimental and our theoretical fit results, showing the accuracy of our data.

In average, smallest deviations from the experimental data resulted from the excitation energy calculation with TDDFT/6-31G* based on the B3LYP geometries. Although the quality of the TDDFT calculated excitation energy results are limited by approximations and/or empirical parameters entering in the exchange correlation energy [43, 241], our result exemplifies the importance of this method in the area of π-conjugated oligomers.

3.3.2 Emission Energies ($S_1 \rightarrow S_0$)

The emissive properties of conjugated oligomers are generally highly interesting in the context of display applications. It is proven in a previous study on the thiophene oligomers [196] that geometry relaxation occurring in the first singlet state has significant effect on the emission properties of these compounds. Thus, to have better agreement between theoretical and experimental emission energies, geometry must be allowed to relax in (the lowest singlet) excited state. Consequently, although vertical transition energy calculations on the ground state geometries might be sufficient to reproduce the excitation energies (or absorption maxima), the emission energies (or fluorescence maxima) are reproduced quantitatively accurate only after a vertical transition energy calculation based on the optimized geometry of the (lowest singlet) excited state.

Do different levels of theory chosen in optimizing the S_1 state geometry make any change in the computed physical properties? To answer this question, we compared several single point calculations on the S_1 geometries of bifuran (**2F**) obtained at configuration interaction singles (CIS/6-31G*) and time-dependent Hartree-Fock (TDHF/6-31G*) levels (Table 3.8).

Table 3.8 Predicted vertical emission energy (eV) in the $S_1 \rightarrow S_0$ transition of bifuran (**2F**) at various levels of theory[a]

Level of theory	E ($S_1 \rightarrow S_0$)
CIS/6-31G*//CIS/6-31G*	4.58
CIS/6-31+G*//CIS/6-31G*	4.35
TDDFT/6-31G*//CIS/6-31G*	4.57
TDDFT/6-31+G*//CIS/6-31G*	3.98
TDHF/6-31G*//CIS/6-31G*	4.25
TDHF/6-31+G*//CIS/6-31G*	4.05
CIS/6-31G*//TDHF/6-31G*	4.57
CIS/6-31+G*//TDHF/6-31G*	4.34
TDDFT/6-31G*//TDHF/6-31G*	4.18
TDDFT/6-31+G*//TDHF/6-31G*	3.97
TDHF/6-31G*//TDHF/6-31G*	4.24
TDHF/6-31+G*//TDHF/6-31G*	4.05
exp[b]	3.96

[a] Based on the optimized geometry of the S_1 excited state. [b] Ref.36, in acetonitrile.

The emission energy ($S_1 \rightarrow S_0$) calculations using the same level of theory (for example, TDDFT/6-31+G*) but different excited state geometries (CIS/6-31G* and TDHF/6-31G* optimized S_1 state geometries) produce very similar results (3.98 and 3.97 eV for the cases stated in parentheses). This trend may be seen in other computation results in Table 3.8. Thereby, it is proved that the method used in geometry optimization S_1 state does not much affect the resulting geometrical parameters, and the computed emission energies ($S_1 \rightarrow S_0$). Hence, we employed the CIS/6-31G* optimized S1 geometries in computing $S_1 \rightarrow S_0$ energies of all species discussed below.

Emission energies for $S_1 \rightarrow S_0$ transition, or in other words, fluorescence energies were computed using single point calculations on the fixed geometries of the lowest singlet excited state (S_1). In fact, using the CIS/6-31G* fully optimized geometry of the first singlet excited state as the initial geometry, we calculated $S_1 \rightarrow S_0$ emission energies at CIS/6-31G*, TDDFT/6-31G*, and TDDFT/6-31+G* levels of theory. The calculated transition energies and oscillator strengths together with experimental data are shown in Tables 3.9-11.

Table 3.9 Emission energies (ΔE_{ems}) and oscillator strengths (f) of thiophene oligomers (**nT**) computed at various levels of theory. [a]

level of theory[b]	**1T**		**2T**		**3T**		**4T**		**5T**		**6T**	
	ΔE_{ems}	f	ΔE_{ems}	f	ΔE_{ems}	f	ΔE_{ems}	f	ΔE_{ems}	f	ΔE_{ems}	f
CIS/6-31G*	6.34	0.12	4.67	0.56	3.94	0.99	3.56	1.44	3.33	1.86	3.17	2.28
TDDFT/6-31G*	5.16	0.09	3.57	0.44	2.95	0.84	2.61	1.27	2.39	1.68	2.24	2.06
TDDFT/6-31+G*	4.99	0.11	3.41	0.43	2.82	0.79	2.50	1.20	2.29	1.59	2.16	1.95
exp[c]			3.43		2.91		2.59		2.57		2.47	

[a] All values are in eV. TDDFT methods have been employed using B3LYP hybrid functional. [b] Single point calculations at CIS/6-31G* optimized S_1 geometries. [c] ref. 85, in acetonitrile.

Table 3.10 Emission energies (ΔE_{ems}) and oscillator strengths (f) of furan oligomers (**nF**) computed at various levels of theory. [a]

level of theory[b]	**1F**		**2F**		**3F**		**4F**		**5F**		**6F**	
	ΔE_{ems}	f	ΔE_{ems}	f	ΔE_{ems}	f	ΔE_{ems}	f	ΔE_{ems}	f	ΔE_{ems}	f
CIS/6-31G*	6.03	0.21	4.58	0.81	3.89	1.10	3.54	1.50	3.69	1.82	3.53	2.20
TDDFT/6-31G*	5.74	0.14	4.18	0.60	3.44	0.90	3.03	1.29	2.77	1.63	2.60	1.96
TDDFT/6-31+G*	5.39	0.17	3.98	0.61	3.28	0.87	2.91	1.24	2.67	1.57	2.52	1.89
exp[c]			3.96		3.34		3.00					

[a] All values are in eV. TDDFT methods have been employed using B3LYP hybrid functional. [b] Single point calculations at CIS/6-31G* optimized S_1 geometries. [c] ref. 36, in acetonitrile

For oligothiophenes and oligofurans (**nT** and **nF**, n=1-6), CIS/6-31G* calculated emission energies have the largest errors of all. The best level of theory in computing the emission energies $S_1 \rightarrow S_0$ is TDDFT/6-31G* (Tables 3.9-10) for n $\geq$ 4. This shows that, for n $\geq$ 4, a larger basis set (6-31+G*) does not improve the results. For n $\leq$ 4, the best agreement with the experimental data is obtained when the TDDFT/6-31+G* level is employed. Both results show that an extension in the basis set has important effects on the computed properties of small oligomers, while this kind of improvement is not significant for larger oligomers.

Table 3.11 Emission energies (ΔE_{ems}) and oscillator strengths (f) of pyrrole oligomers (**nP**) computed at various levels of theory. [a]

level of theory[b]	**1P**		**2P**		**3P**		**4P**		**5P**		**6P**	
	ΔE_{ems}	f	ΔE_{ems}	f	ΔE_{ems}	f	ΔE_{ems}	f	ΔE_{ems}	f	ΔE_{ems}	f
CIS/6-31G*	6.42	0.23	4.75	0.84	4.16	1.25	4.29	1.67	4.06	2.11	3.92	2.57
TDDFT/6-31G*	6.06	0.15	4.29	0.62	3.61	0.96	3.22	1.36	2.99	1.72	2.84	2.05
TDDFT/6-31+G*	5.54	0.20	4.02	0.61	3.40	0.89	3.06	1.25	2.86	1.58	2.73	1.88

[a] All values are in eV. TDDFT methods have been employed using B3LYP hybrid functional. [b] Single point calculations at CIS/6-31G* optimized S_1 geometries.

For the pyrrole oligomers (**nP**, n=1-6), there is no experimental data available for comparison with the computed emission energies, $S_1 \rightarrow S_0$. However, as the trends in the computed data do not change with the oligomer type, we can accept that the results deduced for **nT** and **nF** hold for **nP**.

Tables 3.9-11 clearly show that the emission energies $S_1 \rightarrow S_0$ increase in the order **nT**, **nF**, and **nP**. Furthermore, in each oligomer series, an exponential decrease in emission energies $S_1 \rightarrow S_0$ is seen as the chain length increases.

In many previous experimental and theoretical works, aromatic five-membered heterocyclic oligomers have been expected to show nonzero Stokes shifts. As stated in Chapter 1, Stokes shift is defined as the energy difference between the absorption and emission maxima. Indeed, Stokes shift is a result of geometry relaxation phenomenon in the excited state, and thus equal to the relaxation energy.

Table 3.12 Stokes shifts (eV) obtained as the difference between the absorption energies calculated at TDDFT/6-31G*//RHF/6-31G* and the fluorescence energies calculated at TDDFT/6-31G*//CIS/6-31G* levels for oligothiophene (**nT**), oligofuran (**nF**), and oligopyrrole (**nP**), where n=1-6.

	T1	T2	T3	T4	T5	T6
Stokes shift	0.97	0.71	0.6	0.55	0.53	0.51
	F1	F2	F3	F4	F5	F6
Stokes shift	1.04	0.69	0.59	0.56	0.54	0.52
	P1	P2	P3	P4	P5	P6
Stokes shift	0.89	0.68	0.58	0.55	0.52	0.5

In Table 3.12, we give the Stokes shifts obtained as the difference between the absorption energies calculated at TDDFT/6-31G*//RHF/6-31G* and the fluorescence energies calculated at TDDFT/6-31G*//CIS/6-31G* levels. We obtained the relaxation energies to be on the order of 0.5 eV for the considered oligomers. This actually constitutes a lower limit since no ring rotation relaxation is taken into account.

CHAPTER 4

CONCLUSION

We have presented an extensive semi-empirical, *ab initio*, and DFT study on the ground state, the one-photon allowed lowest singlet excited state, and transitions between these states for a series of thiophene oligomers (**nT**), furan oligomers (**nF**), and pyrrole oligomers (**nP**). At each step of the work, same types of calculations were performed at several levels of theory to compare the validity of theoretical methodologies. Comparison with the experimental data where available have allowed us to test the accuracy of different methods.

In investigation of geometries in the S_0 and S_1 states, we have used bond length alternation (BLA), Δr_i parameters. The ground state geometries were optimized at AM1, RHF/6-31G*, and B3LYP/6-31G* levels. B3LYP method is believed to give the most reasonable ground state geometries. When going from chain ends to the middle part of oligomers, saturation of geometrical parameter is observed. The heteroatoms in **nT**, **nF**, and **nP** were shown to have a stabilizing effect on the conjugated π-system of the ground state. In the lowest singlet excited state geometries, most significant changes in geometrical parameters occur in the middle part of the oligomers with respect to those in the ground state. Excitation from the ground state to the first singlet excited is accompanied with a change from one kind of isomer to another (aromatic→quinoid) because of the elongation of the double bonds and shortening of the single bonds.

We have presented the shapes of molecular orbitals for trans-cisoid acetylene hexamers (**6A**) and the largest members of each oligomer system (**6T**, **6F**, **6P**) to gain a better insight to electronic structure of the oligomer systems. These plots showed that there is no change in the shapes of highest occupied molecular orbitals including HOMO as the oligomer type changes. However, the shape of LUMO and other lowest unoccupied orbitals is different for **6A**, **6T**, **6F**, and **6P**. This proves

the importance of the heteroatoms in determining physical properties of oligoheterocycles.

The excitation ($S_0 \rightarrow S_1$) energy calculations at ZINDO/S, CIS/6-31G*, TDDFT/6-31G*, and TDDFT/6-31+G* levels using the AM1, RHF/6-31G*, and B3LYP/6-31G* geometries as inputs have allowed us to predict the absorption energies of the oligomers with good accuracy. The computed data (generally those by TDDFT method) compare favorably with experimental values establishing exceptional accord, especially for the shorter oligomers.

The effective conjugation lengths (ECL) of **nT**, **nF** and **nP** have been computed upon the least squares fit of some selected theoretical data as 17, 16, and 14 monomer units, respectively. Fits to experimental data produced the ECL of 17, 15 and 13 for **nT**, **nF** and **nP**, respectively. Thereby, accordance of the trends in computed data with those in experimental data have been confirmed.

Using the CIS/6-31G* excited state geometries as inputs, we have computed the emission ($S_1 \rightarrow S_0$) energies at CIS/6-31G*, TDDFT/6-31G*, and TDDFT/6-31+G*. The fluorescence data of **6T**, **6F**, and **6P** have been reproduced with very small errors (~0.02 eV with TDDFT/6-31G*//CIS/6-31G*).

REFERENCES

[1] J. L. Brédas, J. Cornil, D. Beljonne, D. dos Santos, Z. G. Shuai, *Acc. Chem. Res.*, **32**, 267, (1999).

[2] J. Roncali, *Chem. Rev.*, **97**, 173, (1997).

[3] D. R. Baigent, P. J. Hamer, R. H. Friend, S. C. Moratti, A. B. Holmes, *Synth. Met.*, **71**, 2175, (1995).

[4] S. Dähne, *Science*, **199**, 1163, (1978).

[5] (a) M. Kertez, J. Koller, A. Azman, *J. Chem. Phys.*, **67**, 1180, (1977); (b) W. P. Su, J. R. Schrieffer, A. J. Heeger., *Phys. Rev. Lett.*, **42**, 1698, (1979); (c) J. P. Lowe, S. A. Kafafi, *J. Am. Chem. Soc.*, **106**, 5837, (1984); (d) , J. L. Brédas, *J. Chem. Phys.*, **82**, 3808, (1985); (e) Y-S. Lee, M. Kertesz, *J. Chem. Phys.*, **88**, 2609, (1988).

[6] (a) A. Karpfen, *Phys. Scr.*, **T1**, 79, (1982); (b) P. M. Grant, I. P. Batra, *Synth. Met.*, **1**, 193, (1979).

[7] H. Meier, U. Stalmach, H. Kolshorn, *Acta Polym.*, **48**, 379, (1997).

[8] J. Grimme, M. Kreyenschmidt, F. Uckert, K. Müllen, U. Scherf, *Adv. Mater.*, **7**, 292, (1995).

[9] (a) R. E. Martin, T. Mäder, F. Diederich, *Angew. Chem. Int. Ed.*, **38**, 817, (1999); (b) J. L. Brédas, R. Silbey, D. S. Boudreaux, R. R. Chance, *J. Am. Chem. Soc.*, **105**, 6555, (1983); (c) J. Guay, P. Kasai, A. Diaz, R. Wu, J. M. Tour, L. H. Dao, *Chem. Mater.*, **4**, 1097, (1992); (d) G. Zerbi, E. Galbiati, M. C. Gallazi, C. Castiglioni, M. Del Zoppo, R. Schenk, K. Müllen, *J. Chem. Phys.*, **106**, 2509, (1996).

[10] S. A. Jenekhe, *Macromolecules*, **23**, 2848, (1990).

[11] V. Hernandez, C. Castiglioni, M. Del Zopo, G. Zerbi, *Phys. Rev.B*, **50**, 9815, (1994).

[12] D. Delaere, M. T. Nguyen, L. G. Vanquickenborne, *Phys. Chem. Chem. Phys.*, **4**, 1522, (2002).

[13] J. Seixas de Melo, L. M. Silva, L. G. Arnaut, *J. Chem. Phys.*, **111**, 5427, (1999).

[14] (a) G. N. Lewis, M. Calvin, *Chem. Rev.*, **25**, 273, (1939); (b) K. Hirayama, *J. Am. Chem. Soc.*, **77**, 373, (1955); (c) G. Wenz, M. A. Müller, M. Schmidt, G. Wegner, *Macromolecules*, **17**, 837, (1984); (d) R. Schenk, H. Gregorius, K. Meerholz, J. Heinze, K. Müllen, *J. Am. Chem. Soc.*, **113**, 2634, (1991).

[15] W. R. Salaneck, J. L. Brédas, *Solid State Commun.*, **92**, 31, (1994).

[16] H. Shirakawa, E. J. Louis, A. G. MacDiarmid, C. K. Chiang, A. J. Heeger, *J.*

Chem. Soc., Chem. Comm., **16**, 578, (1977).

[17] C. K. Chiang, C. R. Fincher, Y. W. Park, A. J. Heeger, H. Shirakawa, E. J. Louis, S. C. Gua, A. G. MacDiarmid, *Phys. Rev. Lett.*, **39**, 1098, (1977).

[18] C. K. Chiang, Y. W. Park, A. J. Heeger, H. Shirakawa, E. J. Louis, A. G. MacDiarmid, *J. Chem. Phys.*, **69**, 5098, (1978).

[19] (a) H. Shirakawa, *Angew. Chem., Int. Ed. Engl.*, **40**, 2575, (2001); (b) A. G. MacDiarmid, *Angew. Chem., Int. Ed. Engl.*, **40**, 2581, (2001); (c) A. J. Heeger, *Angew. Chem., Int. Ed. Engl.*, **40**, 2591, (2001).

[20] R. H. Friend, G. J. Denton, J. J. M. Halls, N. T. Harrison, A. B. Holmes, A. Kökhler, A. Lux, S. C. Moratti, K. Pichler, N. Tessler, K. Towns, *Synt. Met.*, **84**, 463, (1997).

[21] (a) J. L. Brédas, C. Adant, P. Tackx, A. Persoons, *Chem. Rev.*, **94**, 243, (1994); (b) B. Kirtman, B. Champagne, *Int. Rev. Phys. Chem.*, **16**, 389, (1997).

[22] U. Scherf, S. Riechel, U. Lemmer, R. F. Mahrt, *Cur. Opin. Solid State Mat. Sci.*, **5**, 143, (2001).

[23] (a) K. Gurunathan, A. V. Murugan, R. Marimuthu, U. P. Mulik, D. P. Amalnerkar, *Mat. Chem. Phys.*, **61**, 173, (1999); (b) Y. Shirota, *J. Mater. Chem.*, **10**, 1, (2000).

[24] (a) A. Kraft, A. C. Grimsdale, A. B. Holmes, *Angew. Chem. Int. Ed.*, **37**, 402, (1998); (b) R. H. Friend, R. W. Gymer, A. B. Holmes, J. H. Burroughes, R. N. Marks, C. Taliani, D. D. C. Bradley, D. A. Dos Santos, J. L. Brédas, M. Lögdlund, W. R. Salaneck, *Nature*, **397**, 121, (1999); (c) L. Dai, B. Winkler, L. Dong, L. Tong, A. W. H. Mau, *Adv. Mater.*, **13**, 915, (2001); (d) S. Torgova, A. Strigazzi, *Mol. Cryst. Liq. Cryst.*, 375, **61**, (2002).

[25] (a) J. Alper, *Science*, **246**, 208, (1989); (b) S. Roth, W. Graupner, P. McNeillis, *Acta Phys. Polon. A*, **87**, 699, (1995).

[26] F. Garnier, *Chem. Phys.*, **227**, 253, (1998).

[27] F. Hide, M. A. Diaz-Garcia, B. Schwartz, M. R. Andersson, Q. Pei, A. J. Heeger, *Science*, **273**, 1833, (1996).

[28] (a) M. Granström, K. Petrisch, A. C. Arias, A. Lux, M. Andersson, R. H. Friend, *Nature*, **395**, 257, (1998); (b) L. Ding, M. Jonforsen, L. S. Roman, M. R. Andersson, O. Inganäs, *Synt. Met.*, **110**, 133, (2000); (c) N. S. Sariciftci, *Cur. Opin. Solid State Mat. Sci.*, **4**, 373, (1999).

[29] F. Hide, M. A. Diaz-Garcia, B. J. Schwartz, A. J. Heeger, *Acc. Chem. Res.*, **30**, 430, (1997).

[30] C. J. Brabec, N. S. Sariciftci, J. C. Hummelen, *Adv. Funct. Mater.*, **11**, 15, (2001).

[31] (a) R. J. Mortimer, *Electrochim. Acta*, **44**, 2971, (1999); (b) J. Kalinowski, *J. Phys. D: Appl. Phys.*, **32,** R179, (1999); (c) G. Sönmez, C. K. F. Shen, Y.

Rubin, F. Wudl, *Angew. Chem. Int. Ed.*, **43**, 1498, (2004).

[32] K. Müllen, G. Egner, *Electronic Materials: The Oligomer Approach*, Eds.; Wiley-VCH: Weinheim, 1998.

[33] J. L. Reddinger, J. R. Reynolds, *Adv. Polym. Sci.*, **145**, 57, (1999).

[34] J. M. Tour, *Chem. Rev.*, **96**, 537, (1996).

[35] (a) J. Cornil, D. Beljonne, J. L. Brédas, *J. Chem. Phys.*, **103**, 834, (1995); (b) J. Cornil, D. Beljonne, J. L. Brédas, *J. Chem. Phys.*, **103**, 842, (1995).

[36] J. Seixas de Melo, F. Elisei, C. Gartner, G. G. Aloisi, R. S. Becker, *J. Phys. Chem. A*, **104**, 6907, (2000).

[37] U. Salzner, P. G. Pickup, R. A. Poirier, J. B. Lagowski, *J. Phys. Chem. A*, **102**, 2572, (1998).

[38] P. M. Lahti, J. Obrzut, F. E. Karasz, *Macromolecules*, **20**, 2023, (1987).

[39] P. Bäuerle, U. Mitschke, G. Grüner, G. Rimmel., *Pure Appl. Chem.*, **71**, 2153, (1999).

[40] C. X. Cui, M. Kertesz, Y. Jiang, *J. Phys. Chem.*, **94**, 5172, (1990).

[41] R. E. Martin, F. Diederich, *Angew. Chem. Int. Ed.*, **38**, 1350, (1999).

[42] L. A. Bumm, J. J. Arnold, M. T. Cygan, T. D. Dunbar, T. P. Burgin, L. Jones II, D. L. Allara, J. M. Tour, P. S. Weiss, *Science*, **271**, 1705, (1996).

[43] R. Telesca, H. Bolink, S. Yunoki, G. Hadziioannou, P. Th. Can Duijnen, J. G. Snijders, H. T. Jonkman, G. A. Sawatzky, *Phys. Rev. B*, **63**, 155112, (2001).

[44] M. J. Bielefeld, D. D. Fitts, *J. Am. Chem. Soc.*, **88**, 4804, (1966).

[45] S.-Y. Hong, D. S. Marynick, *Macromolecules*, **25**, 4652, (1992).

[46] J. L. Bredas, B. Themans, J. G. Fripiat, J. M. Andre, R. R. Chance, R. R., *Phys.*

Rev. B, **29**, 6761, (1984).

[47] J. W. Mintmire, C. T. White, M. L. Elert, *Synth. Met.*, **16**, 235, (1986).

[48] S. Y. Hong, S. J. Kwon, S. C. Kim, *J. Chem. Phys.*, **103**, 1871, (1995).

[49] J. Kürti, P. R. Surjan, M. Kertesz, G. Frapper, *Synth. Met.*, **55-57**, 4338, (1993).

[50] U. Salzner, J. B. Lagowski, P. G. Pickup, R. A. Poirier, *Synth. Met.*, **96**, 177, (1998).

[51] T. Jürimäe, M. Strandberg, M. Karelson and J.-L. Calais, *Int. J. Quantum Chem.*, **54**, 369, (1995).

[52] A. Hinchliffe, J. Humberto, M. Soscún, *J. Mol. Struct. (THEOCHEM)*, **331**, 109, (1995).

[53] J. L. Brédas, R. R. Chance, R. Silbey, *Phys. Rev. B*, **26**, 5843, (1982).

[54] H. G. Villar, P. Otto, M. Dupuis, *Synt. Met.*, **59**, 97, (1993).

[55] G. R. Hutchison, Y.-J. Zhao, B. Delley, A. J. Freeman, M. A. Ratner, T. J. Marks, *Phys. Rev. B*, **68**, 035204, (2003).

[56] J. W. Verhoeven, Glossary of terms used in photochemistry, *Pure Appl. Chem.*, **68**, 2250, (1996).

[57] J.-M. Nunzi, N. Pfeffer, F. Charra, *Chem. Phys. Lett.*, **215**, 114, (1993).

[58] (a) S. Mukamel, S. Tretiak, T. Wagersreiter, V. Chernyak, *Science*, **277**, 781, (1997); (b) S. Tretiak, A. Saxena, R.L. Martin, A.R. Bishop, *J. Phys. Chem.*, **104**, 7029, (2000).

[59] J. L. Brédas, *Adv. Mat.*, **7**, 263, (1995).

[60] G. R. Hutchison, M. A. Ratner, T. J. Marks, *J. Phys. Chem. A*, **106**, 10596, (2002).

[61] P. C. Mishra, K. Jug, *Theoret. Chim. Acta*, **61**, 559, (1982).

[62] T. Cvitas, J. M. Hollas, G. H. Kirby, *Mol. Phys.*, **19**, 305, (1970).

[63] S. Tretiak, A. Saxena, R. L. Martin, A. R. Bishop, *Chem. Phys. Lett.*, **331**, 561, (2000).

[64] A. Pogantsch, G. Heimel, E. Zojer, *J. Chem. Phys.*, **117**, 5921, (2002).

[65] B. E. Kohler, *Chem. Rev.*, **93**, 41, (1993).

[66] D. Mukhopadhyay, G. W. Hayden, Z. G. Soos, *Phys. Rev. B*, **51**, 15, (1995).

[67] (a) R. E. Stratmann, G. E. Scuseria, M.J. Frisch, *J. Chem. Phys.*, **109**, 8218, (1998); (b) R. Bauernschmitt, R. Ahlrichs, F. H. Hennrich, M. M. Kappes, *J. Am. Chem. Soc.*, **120**, 5052, (1998); (c) M. E. Casida, C. Jamorski, K. C. Casida, D. R. Salahub, *J. Chem. Phys.*, **108**, 4439, (1998).

[68] J. Roncali, *Chem. Rev.*, **92**, 711, (1992).

[69] R. D. McCullough, *Adv. Mater.*, **10**, 93, (1998).

[70] A. O. Patil, A. J. Heeger, F. Wudi, *Chem. Rev.*, **88**, 183, (1988).

[71] G. Tourillon, F. Garnier, *J. Electroanal. Chem.*, **135**, 173, (1982).

[72] P. N. Prasad, J. Swiatkiewicz, J. Pfleger, *Mol. Cryst. Liq. Cryst.*, **160**, 53, (1988)

[73] T. Sugiyama, T. Wada, H. Sasabe, *Synth. Met.*, **28**, C323, (1989).

[74] A. K. Bakhshi, J. Ladik, M. Seel, *Phys. Rev. B*, **35**, 704, (1987).

[75] F. C. Larvada, M. C. dos Santos, D. S. Galvão, B. Laks, *Phys. Rev. B*, **49**, 979, (1994)

[76] G. Brocks, *J. Chem. Phys.*, **100**, 17327, (1996).

[77] (a) T. C. Chung, J. H. Kaufman, A. J. Heeger, F. Wudl, *Phys. Rev. B*, **30**, 702, (1984); (b) K. Kaneto, K. Yoshino, Y. Inuishi, *Solid State Commun.*, **46**, 389,

(1983); (c) Z. Vardeny, E. Ehrenfreund, J. Shinar, F. Wudl, *Phys. Rev. B*, **35**, 2498, (1987); (d) M. Kobayashi, J. Chen, T-C. Chung, F. Moraes, A. G. Heeger, F. Wudl, *Synth. Met.*, **9**, 77, (1984).

[78] J. L. Brédas, *Synth. Met.*, **17**, 115, (1987).

[79] S. Glenis, G. Horowitz, G. Tourillon, F. Garnier, *Thin Solid Films*, **111**, 93, (1984).

[80] (a) A. Tsumura, H. Koezuka, T. Ando, *Appl. Phys. Lett.*, **49**, 1210, (1986); (b) A. Tsumura, H. Koezuka, T. Ando, *Synth. Met.*, **18**, 699, (1987); (c) A. Tsumura, H. Koezuka, T. Ando, *Synth. Met.*, **25**, 11, (1988).

[81] A. Laforgue, P. Simon, C. Sarrazin, J. F. Fauvarque, *J. Pow. Sourc.*, **80**, 142, (1999).

[82] (a) J. W. Sease, L. Zechmeister, *J. Am. Chem. Soc.*, **69**, 270, (1947); (b) L. Zechmeister, J. W. Sease, *J. Am. Chem. Soc.*, **69**, 273, (1947).

[83] S. Hotta, K. Waragai, *Adv. Mat.*, **5**, 896, (1993).

[84] (a) M. J. Loiacono, E. L. Granstrom, C. D. Frisbie, *J. Phys. Chem. B*, **102**, 1679, (1998); (b) M. Leclerc, K. Faïd, *Adv. Mater.*, **9**, 1087, (1997).

[85] R. S. Becker, J. Seixas de Melo, A. L. Macanita, F. Elisei, *Pure Appl. Chem.*, **67**, 9, (1995).

[86] H. Chosrovian, S. Rentsch, D. Grebner, D. U. Dahm, E. Birckner, H. Naarmann, *Synth. Met.*, **60**, 23, (1993).

[87] D. Grebner, H. Helbig, S. Rentsch, *J. Phys. Chem.*, **99**, 16991, (1995).

[88] D. V. Lap, D. Grebner, S. Rentsch, *J. Phys. Chem. A*, **101**, 107, (1997).

[89] R. S. Becker, J. Seixas de Melo, A. L. Macanita, F. Elisei, *J. Phys. Chem.*, **100**, 18683, (1996).

[90] C. van Pham, A. Burkhardt, R. Shabana et al., *Phosp. Sulf. Silic.*, **46**, 153,

(1989).

[91] P. Garcia, J. M. Pernaut, P. Hapiot, V. Wintgens, P. Valat, F. Garnier, D. Delabouglise, *J. Phys. Chem.*, **97**, 513, (1993).

[92] S. Rentsch, H. Chosrovian, D. Grebner, H. Naarmann, *Synth. Met.*, **57**, 4740, (1993).

[93] P. F. van Hutten, R. E. Gill, J. K. Herrema, G. Hadziioannou, *J. Phys. Chem.*, **99**, 3218, (1995).

[94] M. T. Zhao, B. P. Singh, P. N. Prasad, *J. Chem. Phys.*, **89**, 5535, (1988).

[95] D. Birnbaum, B. E. Kohler, *J. Chem. Phys.*, **95**, 4783, (1991).

[96] D. Birnbaum, B. E. Kohler, *J. Chem. Phys.*, **90**, 3506, (1989).

[97] D. Birnbaum, D. Fichou, B. E. Kohler, *J. Chem. Phys.*, **96**, 165, (1992).

[98] G. Horowitz, S. Romdhane, H. Bouchriha, P. Delannoy, J.-L.Monge, F. Kouki, P. Valat, *Synth. Met.*, **90**, 187, (1997).

[99] W. Gebauer, M. Sokolowski, E. Umbach, *Chem. Phys.*, **227**, 33, (1998).

[100] J. H. Schön, Ch. Kloc, R. A. Laudise, B. Batlogg, *J. Appl. Phys.*, **85**, 2844, (1999).

[101] (a) W. ten Hoeve, H. Wynberg, E. E. Havinga, E. W. Meijer, *J. Am. Chem. Soc.*, **113**, 5887, (1991); (b) E. E. Havinga, I. Rotte, I.; E. W. Meijer, W. ten Hoeve, H. Wynberg, *Synth. Met.*, **41**, 473, (1991); (c) E. E. Havinga, I. Rotte, *Mol. Cryst. Liq. Cryst.*, **218**,1, (1992).

[102] J. M. Tour, R. Wu, *Macromolecules*, **25**, 1901, (1992).

[103] H. Nakanishi, N. Sumi, Y. Aso, T. Otsubo, *J. Org. Chem.*, **63**, 8632, (1998).

[104] S. Kishino, Y. Ueno, K. Ochiai, M. Rikukawa, K. Sanui, T. Kobayashi, H. Kunugita, K. Ema, *Phys. Rev. B*, **58**, R13430, (1998); (b) T. Kobayashi, J.

Hamazaki, H. Kunugita, K. Ema, K. Ochiai, M. Rikukawa, and K. Sanui, *J. Anal. Chem. USSR*, **9**, 55, (2000).

[105] D. Beljonne, Z. Shuai, J. L. Brédas, *J. Chem. Phys.*, **98**, 8819, (1993).

[106] M. A. De Oliveira, H. Duarte, J. Pernaut, W. B. De Almeida, *J. Phys. Chem. A*, **104**, 8256, (2000).

[107] E. Fabiano, F. Della Sala, R. Cingolani, *Phys. Stat. Sol. C*, **1**, 539, (2004).

[108] R. Colditz, D. Grebner, M. Helbig, S. Rentsch, *Chem. Phys.*, **201**, 309, (1995).

[109] N. Periasamy, R. Danieli, G. Ruani, R. Zamboni, C. Taliani, *Phys. Rev. Lett.*, **68**, 919, (1992).

[110] D. Beljonne, J. Cornil, R. H. Friend, R. A. J. Janssen, J. L. Bredas, *J. Am. Chem. Soc.*, **118**, 6453, (1996).

[111] P. Barta, W. Osikowicz, W.R. Salaneck, M. Zagorska, S. Niziol, *Synt. Met.*, **101**, 295, (1999).

[112] A. Forni, M. Sironi, M. Raimondi, D. L. Cooper, J. Gerratt, *J. Phys. Chem. A*, **101**, 4437, (1997).

[113] (a) A. Alberti, L. Favaretto, G. Seconi, *J. Chem. Soc., Perkin Trans. 2,* 931, (1990); (b) D. Jones, M. Guerra, L. Favaretto, A. Modelli, M. Fabrizio, G. Distefano, *J. Phys. Chem.*, **94**, 5761, (1990); (c) G. Barbarella, M. Zambianchi, A. Bongini, L. Antolini, *Adv. Mater.*, **5**, 834, (1993); (d) G. Distefano, M. Da Colle, D. Jones, M. Zambianchi, L. Favaretto, A. Modelli, *J. Phys. Chem.*, **97**, 3504, (1993); (e) J. E. Chadwick, B. E. Kohler *J. Phys. Chem.*, **98**, 3631, (1994); (f) M. Belletête, M. Leclerc, G. Durocher, *J. Phys. Che*m., **98**, 9450, (1994); (g) E. Orti, P. M. Viruela, J. Sanchez-Marin, F. Tomas, *J. Phys. Chem.*, **99**, 4955 (1995); (h) J. C. Horne, G. J. Blanchard, E. LeGoff, *J. Am. Chem. Soc.*, **117**, 955, (1995).

[114] J. C. Horne, G. J. Blanchard, E. LeGoff, *J. Am. Chem. Soc.*, **117**, 9551, (1995).

[115] U. Schoeler, K.-H. Tews, H. Kuhn, *J. Chem. Phys.*, **61**, 5009, (1974).

[116] S. Dunne, L. Nurkkala, R. Steen, *11th Foresight Conference on Molecular Nanotechnology*, 2003.

[117] (a) G. Horowitz, *Adv. Mater.*, **10**, 365, (1998); (b) T. Siegrist, C. Kloc, R. A. Laudise, H. E. Katz, R. C. Haddon, *Adv. Mater.*, **10**, 379, (1998); (b) G. Horowitz, P. Delannoy, *J. Chim. Phys. Phys. Chim. Biol.*, **89**, 1037, (1992); (c) D. Fichou, G. Horowitz, F. Garnier, *Sprin. Ser. Solid-State Sci.*, **107**, 452, (1992); (d) G. Horowitz, D. Fichou, X. Peng, Z. Xu, F. Garnier, *Solid State Commun.*, **72**, 381, (1989); (e) G. Horowitz, X.-Z. Peng, D. Fichou, F. Garnier, *J. Mol. Electron.*, **7**, 85, (1991); (f) F. Garnier, G. Horowitz, X. Peng, D. Fichou, *Adv. Mater.*, **2**, 592, (1990); (g) A. Dodabalapur, L. Torsi, H. E. Katz, *Science*, **268**, 270, (1995); (h) F. Garnier, R. Hailaoui, A. Yassar, P. Srivastava, *Science*, **265**, 1684, (1994); (i) H. E. Katz, *J. Mater. Chem.*, **7**, 369, (1997); (j) F. Garnier, F. Deloffre, G. Horowitz, R. Hajlaoui, *Synth. Met.*, **57**, 4747, (1993); (k) H. Akimichi, K. Waragai, S. Hotta, H. Kano, H. Sakaki, *Appl. Phys. Lett.*, **58**, 1500, (1991); (l) H. E. Katz, L. Torsi, A. Dodabalapur, *Chem. Mater.*, **7**, 2235, (1995).

[118] N. Noma, T. Tsuzuki, Y. Shirota, *Adv. Mater.*, **7**, 647, (1995).

[119] M. Lemaire, W. Buchner, R. Garreau, A. H. Huynh, A. Guy, J. J. Roncali, *Electroanal. Chem.*, **281**, 293, (1990).

[120] D. Fichou, J.-M. Nunzi, F. Charra, N. Pfeffer, *Adv. Mater.*, **6**, 64, (1994).

[121] (a) F. Garnier, G. Horowitz, D. Fichou, *Synth. Met.*, **28**, C705, (1989); (b) D. Fichou, G. Horowitz, Y. Nishikitani, F. Garnier, *Synth. Met.*, **28**, C723, (1989); (c) B. Xu, D. Fichou, G. Horowitz, F. Garnier, *Adv. Mater.*, **3**, 150, (1991); (d) D. Fichou, G. Horowitz, F. Garnier, *Mol. Cryst. Liq. Cryst. Sci. Technol., Sect. A*, **217**, 193, (1992).

[122] K. Yoshino, *Synth. Met.*, **28**, C669, (1989).

[123] T. Wada, L. Wang, D. Fichou, H. Higuchi, J. Ojima, H. Sasabe, *Mol. Cryst. Liq. Cryst. Sci. Technol., Sect. A*, **255**, 149, (1994).

[124] D. M. de Leeuw, E. J. Lous, *Synth. Met.*, **65**, 45, (1994).

[125] D. Fichou, Y. Nishikitani, G. Horowitz, J. Roncali, F. Gamier, *Synth. Met.*, **28**, C729, (1989).

[126] F. Würthner, *Angew. Chem., Int. Ed. Engl.*, **40**, 1037, (2001).

[127] J. H. Burroughes, D. D. C. Bradley, A. R. Brown, R. N. Marks, K. Mackay, R. H. Friend, P. L. Burns, A. B. Holmes, *Nature*, **347**, 539, (1990).

[128] K. Uchiyama, H. Akimichi, S. Hotta, H. Noge, H. Sakaki, *Res. Soc. Symp. Proc.*, **328**, 389, (1994).

[129] J. Paloheimo, H. Stubb, L. Grönberg, *Synth. Met.*, **57**, 4198, (1993).

[130] (a) R. J. Marles, R. L. Compadre, C. M. Compadre et al., *Pestic. Biochem. Physiol.*, **41**, 89, (1991); (b) J. C. Scaiano, A. MacEachern, J. T. Arnason, P. Morand, D. Weir, *Photochem. Photobiol.*, **46**, 193, (1987); (c) J. T. Arnason, B. J. R. Philogène, C. Berg et al., *Photochemistry*, **25**, 1609, (1986).

[131] C. Evans, D. Weir, J. C. Scaino et al., *Photochem. Photobiol.*, **44**, 441, (1986).

[132] J. T. Arnason, G. F. Q. Chan, C. K. Watt, K. Downum, G. H. N. Towers, *Photochem. Photobiol.*, **33**, 821, (1981).

[133] J. Bakker, F. J. Gommers, I. Nieuwenhuis, H. Wynberg, *J. Biol. Chem.*, **254**, 1841, (1979).

[134] D. McLachlan, T. Arnason, J. Lam, *Photochem. Photobiol.*, **39**, 177, (1984).

[135] I. Carrillo, C. Barba, M. J. González-Tejera, I. Hernández-Fuentes, *Macromolecules*, **29**, 5585, (1996); (b) T. Kauffmann, H. Lexy, *Chem. Ber.*, **11**4, 3667, (1981).

[136] M. J. Gonzalez-Tejera, I. Carrillo, I. Hernández-Fuentes, *Synth. Met.*, **73**, 135,

(1995).

[137] S. Glenis, M. Benz, E. Legoff, J. Schindler, C. Kanuewurt, M.G. Kanatzidis, *J. Am. Chem. Soc.*, **115**, 12519, (1993).

[138] V. Hernandez, J. T. Lopez Navarette, J. L. Marcos, *Synth. Met.*, **41-43**, 789, (1991).

[139] D. S. Kumar, Mat. Lett., **41**, 1, (1999).

[140] T. Kauffmann, *Angew. Chem., Int. Ed. Engl.*, **18**, 1, (1979).

[141] (a) A. F. Diaz, K. K. Kanazawa, G. P. Gardini, *J. Chem. Soc., Chem. Commun.*, 635, (1979); (b) A. F. Diaz, J. C. Lacroix, *New J. Chem.*, **12**, 171, (1988); (c) A. F. Diaz, *Chem. Scr.*, **17**, 142, (1981).

[142] A. Dall'Olio, G. Dascola, V. Varacca, B. Vittorio, *C. R. C. R. Seances Acad. Sci., Ser. C*, **267**, 433, (1968).

[143] J. L. Brédas, J. C. Scott, K. Yakushi, G. B. Street, Phys. Rev. B, **30**, 1023, (1984).

[144] A. F. Diaz, J. I. Castillo, *J. Chem. Soc., Chem. Comm.*, **9**, 397, (1980).

[145] K. K. Kanazawa, A. F. Diaz, R.H. Geiss, W. D. Gill, J. F. Kwak, J. A. Logan, J. F. Rabolt, G. B. Street, *J. Chem. Soc., Chem. Commun.*, **19**, 854, (1979).

[146] G. B. Street, T. C. Clarke, M. Krounbi, K. Kanazawa, V. Lee, P. Pfluger, J. C. Scott, G. Weiser, *Mol. Cryst. Liq. Cryst.*, **83**, 1285, (1982).

[147] L. Groenendaal, E. W. Meijer, J. A. J. M. Vekemans, in *Electronic Materials: The Oligomer Approach*, edited by K.Müllen, G. Egner, Wiley-VCH, Weinheim, 1998, p. 235.

[148] J. G. Killian, B. M. Colley, F. Gao, T. O. Poehler, P. C. Searson, *J. Electrochem. Soc.*, **143**, 936, (1996).

[149] W. H. Meyer, *Synt. Met.*, **10**, 255, (1986).

[150] K. Yoshino, K. Kaneto, Y. Inuishi, *Jpn. J. Appl. Phys.*, **22**, L412, (1983).

[151]A. C. Partridge, *Electrochim. Acta*, **40**, 1199, (1995).

[152] G. Zotti, S. Martina, G. Wegner, A.-D. Schlüter, *Adv .Mater.*, **4**, 798, (1992).

[153] J. Ma, S. Li, Y. Jiang, *Macromolecules*, **35**, 1109, (2002).

[154] (a) W. C. Price, A. D. Wallsh, *Proc. R. Soc. London*, **179A**, 20, (1941); (b) W. C. Price, A. D. Wallsh, *Electronic Spectra of Polyatomic Molecules*, G. Herzberg (Ed.), Van Nostrand, New York, (1966); (c) W. M. Flicker, O. A. Mosher, A. Kuppermann, *J. Chem. Phys.*, **64**, 1315, (1976); (d) J. M. Ribo, M. C. Anglada, J. M. Tura, N. Ferrer-Anglada, *Synth. Met.*, **72**, 173, (1995).

[155] S. Hotta, K. Waragai, *Adv. Mater.*, **5**, 12, (1993).

[156] V. Hernández, F.J. Ramirez, G. Zotti, J.T. López Navarrete, *J. Chem. Phys.*, **98**, 769, (1993).

[157] (a) S. N. Yaliraki, R. J. Silbey, *J. Chem. Phys.*, **104**, 1245, (1996); (b) A. Karpfen, C. H. Choi, M. Kertesz, *J. Phys. Chem. A*, **101**, 7426, (1997).

[158] D. Fichou, G. Horowitz, B. Xu, F. Garnier, *Synt. Met.*, **39**, 243, (1990).

[159] J. W. van der Horst, P. A. Bobbert, P. H. L. de Jong, M. A. J. Michels, G. Brocks, P. J. Kelly, *Phys. Rev. B*, **61**, 15817, (2000).

[160] M. Yan, L. J. Rothberg, F. Papadimitrakopoulos, M. E. Galvin, T. M. Miller, Phys. Rev. Lett., **72**, 1140, (1994).

[161] For a review see, e.g., C. J. Cramer, D. G. Truhlar, *Chem. Rev.*, **99**, 2161, (1999).

[162] J. Simons, http://simons.hec.utah.edu/TheoryPage/index.html

[163] E. Schrödinger, *Ann. Physik.*, **79,** 361, (1926).

[164] M. Born, J. R. Oppenheimer, *Ann. Physik.*, **84**, 457, (1927).

[165] J. C. Slater, *Phys. Rev.*, **35**, 210, (1930).

[166] D. R. Hartree, *Proc. Camb. Phil. Soc.*, **24**, 89, (1928).

[167] V. Fock, *Z. Phys.*, **61**, 161, (1930).

[168] I.R. Levine, *Quantum Chemistry*, Prentice Hall, 2000.

[169] F. Jensen, *Introduction to Computational Chemistry*, John Wiley & Sons, 1999.

[170] J. P. Lowe, *Quantum Chemistry*, Academic Press, 1978.

[171] J. C. Slater, *Phys. Rev.*, **36**, 57, (1930).

[172] S. F. Boys, *Proc. Roy. Soc. (London) A*, **200**, 542, (1950).

[173] W. J. Hehre, R. Ditchfield, J. A. Pople, *J. Chem. Phys.*, **56**, 2257, (1972).

[174] J. Harvey, http://www.chm.bris.ac.uk/pt/harvey/elstruct/beyond_hf.html

[175] M. C. Zerner, *Rev. Comput. Chem.*, **2**, 313, (1991)

[176] M. J. S. Dewar, E.G. Zoebisch, E. F. Heally, J. J. P. Steward, *J. Am. Chem. Soc.*, **107**, 3902, (1985).

[177] M. J. S. Dewar, K. M. Dieter, *J. Am. Chem. Soc.*, **108**, 8075, (1986).

[178] J. J. P. Steward, *J. Comp. Aided Mol. Design.*, **4**, 1, (1990).

[179] M. J. S. Dewar, Y. C. Yuan, *Inorg. Chem.*, **29**, 3881, (1990).

[180] M. Kotzian, N. Rösch, M. C. Zerner, *Theoret. Chim. Acta.*, **81**, 201, (1992).

[181] HyperChem Computational Chemistry, Hypercube Inc., 1996.

[182] C. Forber, M. C. Zerner, *J. Am. Chem. Soc.*, **107**, 5884, (1985).

[183] J. Ridley, M. C. Zerner, *Theor. Chim. Acta.*, **32**, 111, (1973).

[184] M. Belletête, S. Beaupré, J. Bouchard, P. Blondin, M. Leclerc, G. Durocher, *J. Phys. Chem. B*, **104**, 9118, (2000).

[185] S. F. Boys, *Proc. Roy. Soc. (London) A*, **201**, 125, (1950).

[186] J. A. Pople, J. S. Binkley, R. Seeger, *Int. J. Quant. Chem. Symp*. **10**, 1, (1976).

[187] J. A. Pople, R. Seeger, R. Krishnan, *Int. J. Quant. Chem. Symp.*, **11**, 149, (1977).

[188] R. Krishnan, H. B. Schlegel, J. A. Pople, *J. Chem. Phys.*, **72**, 4654, (1980).

[189] K. Raghavachari, J. A. Pople, *Int. J. Quant. Chem.*, **20**, 167, (1981).

[190] C. Møller, M. S. Plesset, *Phys. Rev.*, **46**, 618, (1934).

[191] J. Cizek, *J. Chem. Phys.*, **45**, 4256, (1966).

[192] J. Cizek, *Adv. Chem. Phys.,* **14**, 35, *(*1969).

[193] R. J. Bartlett, *J. Phys. Chem.,* **93**, 1697, *(*1989).

[194] J. B. Foreman, M. Head-Gordon, J. A. Pople, M. J. Frisch, *J. Phys. Chem.*, **96**, 135, (1992).

[195] J. F. Stanton, J. Gauss, N. Ishikawa, M. Head-Gordon, *J. Chem. Phys.*, **103**, 4160, (1995).

[196] D. Chackrabory, J. B. Lagowski, *J. Chem. Phys.*, **115**, 184, (2001).

[197] J. B. Lagowski, *J. Mol. Struct. (Theochem)*, **589–590**, 125, (2002).

[198] A. B. J. Parusel. W. Rettig, W. Sudholt, *J. Phys. Chem. A*, **106**, 804, (2002).

[199] S. Tirapattur, M. Belletête, M. Leclerc, G. Durocher, *J. Mol. Struct.*

(Theochem), **625**, 141, (2003).

[200] W. Kohn, *Rev. Mod. Phys.*, **71**, 1253, (1999).

[201] P. Hohenberg, W. Kohn, *Phys. Rev.*, **136**, B864, (1964).

[202] W. Kohn, L. J. Sham, *Phys. Rev.*, **140**, A1133, (1965).

[203] A. D. Becke, *Phys. Rev. A*, **38**, 3098, (1988).

[204] C. Lee, W. Yang, R. G. Parr, *Phys. Rev. B*, **37**, 785, (1988)

[205] J. P. Perdew, Y. Wang, *Phys. Rew. B*, **33**, 8800, (1986)

[206] J. P. Perdew, *Phys. Rev. B*, **33**, 8822, (1986).

[207] J. P. Perdew, Y. Wang, *Phys. Rev. B*, **45**, 13244, (1992).

[208] J. P. Perdew, J. A. Chevary, S. H. Vosko, K. A. Jackson, M. R. Pederson, D. J. Singh, C. Fiolhais, *Phys. Rev. B*, **46**, 6671, (1992).

[209] J. P. Perdew, K. Burke, Y. Wang, *Phys. Rev. B*, **54**, 16533, (1996).

[210] A. D. Becke, *J. Chem. Phys.*, **104**, 1040, (1996).

[211] A. D. Becke, *J. Chem. Phys.*, **98**, 5648, (1993)

[212] C.-P. Hsu, S. Hirata, M. Head-Gordon, *J. Phys. Chem. A*, **105**, 451, (2001).

[213] S. Hirata, T. J. Lee, M. Head-Gordon, *J. Chem. Phys.*, **111**, 8904, (1999).

[214] P. Jørgensen, *Annu. Rev. Phys. Chem.*, **26**, 359, (1975).

[215] T. H. Dunning, V. J. McKoy, *Chem. Phys.*, **47**, 1735, (1967).

[216] E. K. U. Gross, W. Kohn, *Adv. Quantum Chem.*, **21**, 255, (1990).

[217] E. Runge, E. K. U. Gross, *Phys. Rev. Lett.*, **52**, 997, (1984).

[218] R. Bauernschmitt, R. Ahlrichs, *Chem. Phys. Lett.*, **256**, 454, (1996).

[219] F. Furche, R. Ahlrichs, A. Sobanski, F. Vögtle, C. Wachsman, E. Weber, S. Grimme, *J. Am. Chem. Soc.*, **122**, 1717, (2000).

[220] G. Ricciardi, A. Rosa, E. J. Baerends, *J. Phys. Chem. A*, **105**, 5242, (2001).

[221] S. Grimme, M. Parac, *ChemPhysChem*, **3**, 292, (2003).

[222] S. Grimme, M. Parac, *Chem. Phys.*, **292**, 11, (2003).

[223] H. H. Heinze, A. Görling, N. Rösch, *J. Chem. Phys.*, **113**, 2088, (2000).

[224] M. J. Frisch, G. W. Trucks, H. B. Schlegel, G. E. Scuseria, M. A. Robb, J. R. Cheeseman, V. G. Zakrzewski, J. A. Montgomery, Jr., R. E. Stratmann, J. C. Burant, S. Dapprich, J. M. Millam, A. D. Daniels, K. N. Kudin, M. C. Strain, O. Farkas, J. Tomasi, V. Barone, M. Cossi, R. Cammi, B. Mennucci, C. Pomelli, C. Adamo, S. Clifford, J. Ochterski, G. A. Petersson, P. Y. Ayala, Q. Cui, K. Morokuma, D. K. Malick, A. D. Rabuck, K. Raghavachari, J. B. Foresman, J. Cioslowski, J. V. Ortiz, A. G. Baboul, B. B. Stefanov, G. Liu, A. Liashenko, P. Piskorz, I. Komaromi, R. Gomperts, R. L. Martin, D. J. Fox, T. Keith, M. A. Al-Laham, C. Y. Peng, A. Nanayakkara, M. Challacombe, P. M. W. Gill, B. Johnson, W. Chen, M. W. Wong, J. L. Andres, C. Gonzalez, M. Head-Gordon, E. S. Replogle, J. A. Pople, Gaussian 98, Revision A.8, Gaussian, Inc., Pittsburgh PA, 1998.

[225] A. Frisch, M. J. Frisch, GAUSSIAN 98 User's reference, Gaussian, Inc., Pittsburgh, PA, 1998, and references therein.

[226] HyperChem Molecular Modeling System, release 5.0, Hypercube, Inc. 1990-1996

[227] N. L. Alligner, *J. Am. Chem. Soc.*, **99**, 8127, (1977).

[228] M. Pelletier, F. Brisse, *Acta Crystallogr., Sect. C*, **50**, 1942, (1994).

[229] L. Antolini, G. Horowitz, F. Kouki, F. Garnier, *Adv. Mater.*, **10**, 382, (1998).

[230] G. Horowitz, B. Bachet, A. Yassar, P. Lang, F. Demanze, J. L. Fave, F.

Garnier, *Chem. Mater.*, **7**, 1337, (1995).

[231] G. Mao, J. E. Fischer, F. E. Karasz, M. J. Winokur, *J. Chem. Phys.*, **98**, 712, (1993).

[232] (a) P. Vogl, D. K. Campbell, *Phys. Rev. B*, **4**1, 12797, (1990); (b) G. Brocks, P. J. Kelly, R. Car, *Synth. Met.*, **5**7, 4243, (1993); (c) P. G. Dacosta, R. G. Dandrea, E. M. Conwell, *Phys. Rev. B*, **4**7, 1800, (1993).

[233] D. Chackrabory, J. B. Lagowski, *Polymer*, **45**, 1331, (2004).

[234] E. J. P. Malar, F. Neumann, K. Jug, *J. Mol. Struct. (Theochem)*, **336**, 81, (1995).

[235] J. P. Reyftmann, J. Kagan, R. Santus, P. Morliere, *Photochem. Photobiol*, **41**, **1**, (1985).

[236] S. Rentsh, J. P. Yang, W. Paa, E. Birckner, J. Schiedt, R. Weinkauf, *Phys. Chem. Chem. Phys.*, **1**, 1707, (1999).

[237] M. Z. Zgierski, A. Grabowska, *J. Chem. Phys.*, **112**, 6329, (2000).

[238] H. Subramanian, J. B. Lagowski, *Int. J. Quantum Chem.*, **66**, 229, (1998).

[239] In materials in which a vibronic progression of the absorption is resolved, the calculated excitation energy corresponds to the maximum of the envelope of the absorption spectrum rather than to the vibronic 0–0 transition.

[240] E. Zojer, N. Koch, P. Puschnig *et al.*, *Phys. Rev. B*, **61**, 16538, (2000).

[241] F. Della Sala, H. H. Heinze, A. Görling, *Chem. Phys. Lett.*, **339**, 343, (2001).

APPENDIX A

A. Cartesian Coordinates of Ground State Geometries of Studied Structures at AM1 Level

All cartesian coordinates are in angstroms. All electronic energies are in Hartrees.

A.1 Cartesian Coordinates of Ground State Geometries of Thiophene Oligomers (**nT**) at AM1 Level

Table A.1.1 Cartesian coordinates of **1T**(AM1)

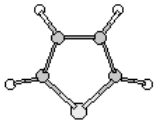

Electronic energy = -93.64978

Atomic symbol	X	Y	Z
C	-0.841666	2.690361	2.378472
C	-0.841693	4.122518	2.378472
C	0.439490	4.627804	2.378472
C	0.439537	2.185123	2.378472
S	1.581702	3.406485	2.378472
H	-1.755886	4.718865	2.378472
H	0.705653	5.683021	2.378472
H	-1.755836	2.093979	2.378472
H	0.705740	1.129917	2.378472

Table A.1.2 Cartesian coordinates of **2T**(AM1)

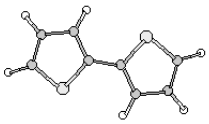

Electronic energy = -254.89972

Atomic symbol	X	Y	Z
S	-1.186767	0.106384	0.000000
C	-2.846143	-0.030420	0.000000
C	-3.463749	1.202358	0.000000
C	-1.208495	1.794155	0.000000
C	-2.513919	2.266020	0.000000
H	-3.357568	-0.991734	0.000000
H	-4.543159	1.366606	0.000000
C	-0.022078	2.581434	0.000000
S	-0.043806	4.269205	0.000000
C	1.615570	4.406009	0.000000
C	1.283346	2.109569	0.000000
C	2.233176	3.173232	0.000000
H	2.126994	5.367323	0.000000
H	1.565247	1.054402	0.000000
H	3.312586	3.008984	0.000000
H	-2.795820	3.321187	0.000000

Table A.1.3 Cartesian coordinates of **3T**(AM1)

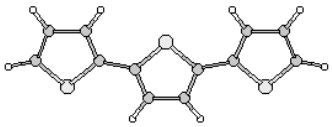

Electronic energy = -454.13405

Atomic symbol	X	Y	Z
S	1.514005	2.993274	-1.493788
C	1.527697	4.674614	-1.493787
C	0.233426	5.181035	-1.493787
C	-0.163937	2.885577	-1.493789
C	-0.741948	4.149499	-1.493789
H	-0.018678	6.244096	-1.493787
C	-0.855771	1.641282	-1.493788
S	-2.539854	1.529763	-1.493789
C	-2.545314	-0.134939	-1.493789
C	-0.282231	0.376814	-1.493787
C	-1.267599	-0.653675	-1.493788
H	-3.463273	-0.720736	-1.493788
H	0.791895	0.178919	-1.493787
H	-1.018982	-1.716860	-1.493787
H	-1.817443	4.341757	-1.493789
C	2.731353	5.434953	-1.493788
S	2.748516	7.122636	-1.493787
C	4.410307	7.221186	-1.493787
C	4.025917	4.933024	-1.493789
C	4.999687	5.974480	-1.493788
H	4.943852	8.170468	-1.493788
H	4.283572	3.871647	-1.493789
H	6.075112	5.785710	-1.493789

Table A.1.4 Cartesian coordinates of **4T**(AM1)

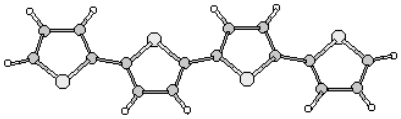

Electronic energy = -678.99664

Atomic symbol	X	Y	Z
S	1.301439	-2.534775	0.249929
C	1.329781	-0.853658	0.249929
C	0.039601	-0.335944	0.249929
C	-0.377164	-2.627875	0.249930
C	-0.944408	-1.358900	0.249930
H	-0.203369	0.729271	0.249929
C	-1.079745	-3.866098	0.249930
S	-2.764631	-3.963225	0.249929
C	-2.784344	-5.627690	0.249929
C	-0.516972	-5.135483	0.249930
C	-1.511091	-6.157444	0.249930
H	-3.707270	-6.205683	0.249929
H	0.555426	-5.342560	0.249930
H	-1.271676	-7.222747	0.249930
H	-2.018262	-1.157546	0.249930
S	2.567745	1.577852	0.249930
C	2.539402	-0.103265	0.249929
C	3.829582	-0.620979	0.249929
C	4.246348	1.670952	0.249930
C	4.813592	0.401976	0.249930
H	4.072552	-1.686194	0.249929
C	4.948929	2.909174	0.249930
S	6.633814	3.006301	0.249930
C	6.653528	4.670766	0.249930
C	4.386156	4.178560	0.249931
C	5.380276	5.200521	0.249930
H	7.576455	5.248759	0.249930
H	3.313758	4.385637	0.249931
H	5.140861	6.265824	0.249931
H	5.887446	0.200623	0.249930

Table A.1.5 Cartesian coordinates of **5T**(AM1)

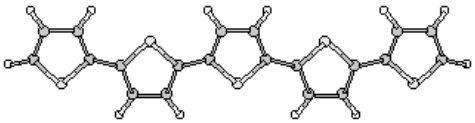

Electronic energy = -923.28922

Atomic symbol	X	Y	Z
S	8.383508	2.270401	-2.346005
C	8.397146	3.951657	-2.346006
C	7.102439	4.458097	-2.346002
C	6.705893	2.162608	-2.346004
C	6.127474	3.426585	-2.346002
H	6.850116	5.521138	-2.346000
C	6.014173	0.918284	-2.346006
S	4.330242	0.806352	-2.346005
C	4.325158	-0.858172	-2.346008
C	6.588113	-0.346119	-2.346009
C	5.603023	-1.376759	-2.346008
H	3.407351	-1.444285	-2.346011
H	7.662291	-0.543783	-2.346013
H	5.851766	-2.439928	-2.346007
H	5.051880	3.618448	-2.346001
C	9.600111	4.712611	-2.346010
S	9.613836	6.393710	-2.346009
C	11.291540	6.501428	-2.346008
C	10.894830	4.205903	-2.346013
C	11.869860	5.237075	-2.346011
H	11.146810	3.142760	-2.346015
H	12.945430	5.044943	-2.346012
S	13.661890	7.852705	-2.346004
C	11.984030	7.745066	-2.346004
C	11.405970	9.009425	-2.346001
C	13.675700	9.533723	-2.346004
C	12.381350	10.040550	-2.346002
H	10.330490	9.201904	-2.345997
C	14.879390	10.293950	-2.346007
S	14.896970	11.981500	-2.346003
C	16.558610	12.079670	-2.346006
S	14.470456	10.026863	-2.346006
C	14.791114	10.365031	-2.346006
C	15.111773	10.703199	-2.346006
C	15.432432	11.041367	-2.346006
C	15.753091	11.379535	-2.346006
H	16.073749	11.717703	-2.346006

Table A.1.6 Cartesian coordinates of **6T**(AM1)

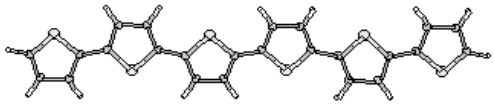

Electronic energy = -1183.17218

Atomic symbol	X	Y	Z
C	-16.452680	-3.473392	0.522712
C	-17.757240	-4.048462	0.522712
C	-18.739270	-3.080206	0.522712
C	-16.498940	-2.085578	0.522712
S	-18.097440	-1.544430	0.522712
H	-17.934420	-5.125872	0.522712
H	-19.811530	-3.270386	0.522712
H	-15.535960	-4.067168	0.522712
C	-14.138500	0.767984	0.522712
C	-15.434060	0.188299	0.522712
C	-15.383560	-1.200842	0.522712
C	-13.136290	-0.195551	0.522712
S	-13.792520	-1.743481	0.522712
H	-16.354280	0.777300	0.522712
H	-13.964640	1.846644	0.522713
C	-9.436062	-0.337341	0.522712
C	-10.731490	-0.916765	0.522712
C	-11.733670	0.046992	0.522712
C	-9.486443	1.052142	0.522713
S	-11.077590	1.594727	0.522713
H	-10.905680	-1.995389	0.522712
H	-8.515948	-0.926545	0.522712
C	-7.125666	3.904919	0.522713
C	-8.421093	3.325494	0.522713
C	-8.370712	1.936011	0.522713
C	-6.123487	2.941162	0.522713
S	-6.779568	1.393426	0.522713
H	-9.341207	3.914697	0.522713
H	-6.951474	4.983543	0.522713
C	-2.423094	2.799858	0.522713
C	-3.718659	2.220171	0.522713
C	-4.720863	3.183706	0.522713
S	-4.064641	4.731637	0.522713
H	-3.892513	1.141511	0.522713
H	-1.502877	2.210858	0.522713
C	-2.473595	4.188999	0.522713
C	-0.099922	7.036622	0.522714

Table A.1.6 (Continue) Cartesian coordinates of **6T**(AM1)

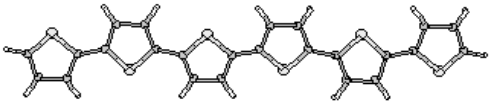

Electronic energy = -1183.17218

Atomic symbol	X	Y	Z
C	-1.404482	6.461550	0.522714
C	-1.358221	5.073736	0.522713
C	0.882113	6.068367	0.522714
S	0.240287	4.532590	0.522713
H	-2.321195	7.055325	0.522714
H	0.077257	8.114032	0.522714
H	1.954375	6.258548	0.522714

A.2 Cartesian Coordinates of Ground State Geometries of Furan Oligomers (**nF**) at AM1 Level

Table A.2.1 Cartesian coordinates of **1F**(AM1)

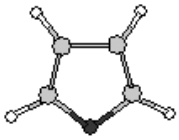

Electronic energy =-102.55747

Atomic symbol	X	Y	Z
C	-0.816293	2.682424	2.378472
C	-0.816368	4.130398	2.378472
C	0.505645	4.524973	2.378472
C	0.505762	2.287987	2.378472
O	1.340079	3.406524	2.378472
H	-1.698882	4.762934	2.378472
H	1.029102	5.475779	2.378472
H	-1.698741	2.049797	2.378472
H	1.029318	1.337236	2.378472

Table A.2.2 Cartesian coordinates of **2F**(AM1)

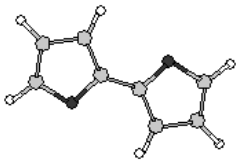

Electronic energy = -276.44765

Atomic symbol	X	Y	Z
O	-1.239572	0.459610	0.000000
C	-2.575049	0.061526	0.000000
C	-3.408678	1.162041	0.000000
C	-1.250613	1.866465	0.000000
C	-2.557486	2.328060	0.000000
H	-2.716969	-1.015336	0.000000
H	-4.494873	1.171142	0.000000
C	0.020028	2.509123	0.000000
O	0.008997	3.915977	0.000000
C	1.344478	4.314051	0.000000
C	1.326897	2.047518	0.000000
C	2.178098	3.213530	0.000000
H	1.486407	5.390912	0.000000
H	1.652140	1.010675	0.000000
H	3.264292	3.204420	0.000000
H	-2.882738	3.364900	0.000000

Table A.2.3 Cartesian coordinates of **3F**(AM1)

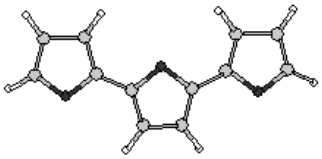

Electronic energy = -491.90642

Atomic symbol	X	Y	Z
H	6.075112	5.785710	-1.493789
O	1.162766	3.370205	-1.493788
C	1.173306	4.775609	-1.493788
C	-0.123964	5.267050	-1.493788
C	-0.192764	2.998975	-1.493788
C	-1.000977	4.126457	-1.493788
H	-0.422906	6.312238	-1.493788
C	-0.460131	1.600529	-1.493788
O	-1.815950	1.224134	-1.493788
C	-1.831117	-0.169061	-1.493788
C	0.343265	0.470813	-1.493787
C	-0.543607	-0.668018	-1.493787
H	-2.827498	-0.601873	-1.493788
H	1.429646	0.443286	-1.493787
H	-0.236297	-1.709938	-1.493787
H	-2.087883	4.146863	-1.493788
C	2.456129	5.393266	-1.493788
O	2.471567	6.800278	-1.493788
C	3.814104	7.172861	-1.493788
C	3.754326	4.907071	-1.493788
C	4.627087	6.056752	-1.493788
H	3.976408	8.246993	-1.493788
H	4.060033	3.864227	-1.493788
H	5.712986	6.027437	-1.493788

Table A.2.4 Cartesian coordinates of **4F**(AM1)

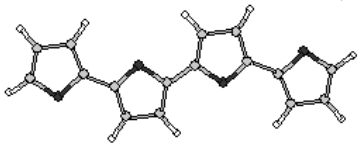

Electronic energy = -735.25497

Atomic symbol	X	Y	Z
O	1.302169	-2.215257	0.205832
C	1.323409	-0.809692	0.205832
C	0.029678	-0.308374	0.205832
C	-0.055966	-2.575855	0.205832
C	-0.855775	-1.442141	0.205832
H	-0.261336	0.739104	0.205832
C	-0.334316	-3.972131	0.205833
O	-1.693163	-4.337688	0.205833
C	-1.719400	-5.730608	0.205833
C	0.460065	-5.108247	0.205833
C	-0.435865	-6.239902	0.205833
H	-2.719233	-6.155541	0.205833
H	1.546242	-5.144563	0.205833
H	-0.136917	-7.284286	0.205833
H	-1.942543	-1.413713	0.205832
O	2.632403	1.202776	0.205832
C	2.611160	-0.202788	0.205832
C	3.904890	-0.704110	0.205832
C	3.990539	1.563372	0.205832
C	4.790345	0.429656	0.205832
H	4.195901	-1.751588	0.205832
C	4.268893	2.959647	0.205832
O	5.627742	3.325198	0.205832
C	5.653985	4.718117	0.205832
C	3.474518	4.095766	0.205832
C	4.370452	5.227417	0.205832
H	6.653820	5.143046	0.205832
H	2.388341	4.132087	0.205832
H	4.071509	6.271802	0.205832
H	5.877112	0.401225	0.205832

Table A.2.5 Cartesian coordinates of **5F**(AM1)

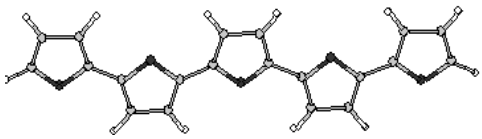

Electronic energy = -999.86206

Atomic symbol	X	Y	Z
H	16.073749	11.717703	-2.346006
O	8.569792	2.598970	-1.926162
C	8.579636	4.004759	-1.926162
C	7.281871	4.495579	-1.926162
C	7.214721	2.227463	-1.926162
C	6.405673	3.354688	-1.926162
H	6.982243	5.540680	-1.926162
C	6.947606	0.828988	-1.926162
O	5.591717	0.452559	-1.926162
C	5.576649	-0.940475	-1.926162
C	7.751071	-0.300737	-1.926162
C	6.864244	-1.439511	-1.926162
H	4.580234	-1.373442	-1.926162
H	8.837517	-0.328394	-1.926162
H	7.171511	-2.481489	-1.926162
H	5.318685	3.374267	-1.926162
C	9.862529	4.621823	-1.926162
O	9.872822	6.027264	-1.926162
C	11.228450	6.398267	-1.926162
C	11.160190	4.130206	-1.926162
C	12.036930	5.270454	-1.926162
H	11.458950	3.084875	-1.926162
H	13.123930	5.250267	-1.926162
O	12.851310	8.167285	-1.926162
C	11.495230	7.796627	-1.926162
C	10.687490	8.924747	-1.926162
C	12.862240	9.572317	-1.926162
C	11.565000	10.064630	-1.926162
H	9.600494	8.945835	-1.926162
C	14.145160	10.189730	-1.926162
O	14.160630	11.596820	-1.926162
C	15.503040	11.969240	-1.926162
C	15.443370	9.703447	-1.926162
C	16.316110	10.853060	-1.926162
H	15.665510	13.043440	-1.926162
H	15.749200	8.660569	-1.926162
H	17.402050	10.823780	-1.926162
H	11.266830	11.110110	-1.926162

Table A.2.6 Cartesian coordinates of **6F**(AM1)

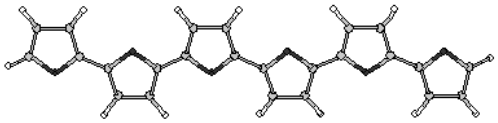

Electronic energy = -1281.48681

Atomic symbol	X	Y	Z
C	-16.250660	-2.268763	0.522712
C	-17.642850	-2.649583	0.522712
C	-18.375110	-1.478780	0.522712
C	-16.217490	-0.882853	0.522712
O	-17.528770	-0.372249	0.522712
H	-18.020850	-3.668047	0.522712
H	-19.432390	-1.228769	0.522712
H	-15.397180	-2.941620	0.522712
C	-13.754180	1.853490	0.522713
C	-15.139080	1.464432	0.522712
C	-15.166070	0.077149	0.522712
C	-13.008700	0.683292	0.522712
O	-13.858400	-0.436735	0.522712
H	-15.997940	2.130984	0.522713
H	-13.368380	2.869955	0.522713
C	-9.481913	-0.373472	0.522712
C	-10.866880	-0.761601	0.522712
C	-11.611730	0.409288	0.522712
C	-9.454013	1.013909	0.522713
O	-10.761960	1.528636	0.522713
H	-11.253640	-1.777690	0.522712
H	-8.623499	-1.040712	0.522712
C	-6.990280	3.749754	0.522713
C	-8.375248	3.361626	0.522713
C	-8.403149	1.974244	0.522713
C	-6.245435	2.578865	0.522713
O	-7.095203	1.459518	0.522713
H	-9.233662	4.028866	0.522713
H	-6.603524	4.765843	0.522713
C	-2.718086	1.523719	0.522713
C	-4.102984	1.134662	0.522713
C	-4.848459	2.304861	0.522713
O	-3.998763	3.424887	0.522713
H	-4.488779	0.118197	0.522712
H	-1.859220	0.857167	0.522713
C	-2.691092	2.911003	0.522713
C	-0.214305	5.637733	0.522714
C	-1.606503	5.256914	0.522714

Table A.2.6 (Continue) Cartesian coordinates of **6F**(AM1)

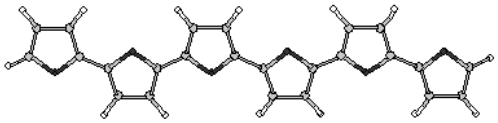

Electronic energy = -1281.48681

Atomic symbol	X	Y	Z
C	-1.639670	3.871004	0.522713
C	0.517952	4.466929	0.522713
O	-0.328388	3.360399	0.522713
H	-2.459976	5.929771	0.522714
H	0.163695	6.656197	0.522714
H	1.575228	4.216918	0.522713

A.3 Cartesian Coordinates of Ground State Geometries of Pyrrole Oligomers (**nP**) at AM1 Level

Table A.3.1 Cartesian coordinates of **1P**(AM1)

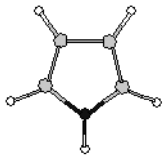

Electronic energy = -99.09285

Atomic symbol	X	Y	Z
C	-0.833884	2.689003	2.378472
C	-0.833884	4.123914	2.378472
C	0.505283	4.538121	2.378472
C	0.505283	2.274795	2.378472
N	1.315561	3.406458	2.378472
H	-1.707417	4.767213	2.378472
H	0.929570	5.541380	2.378472
H	-1.707418	2.045704	2.378472
H	0.929570	1.271536	2.378472
H	2.299839	3.406458	2.378472

Table A.3.2 Cartesian coordinates of **2P**(AM1)

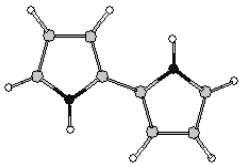

Electronic energy = -268.23726

Atomic symbol	X	Y	Z
N	-1.190243	0.390343	0.000000
C	-2.497586	-0.078346	0.000000
C	-3.369138	1.021383	0.000000
C	-1.214311	1.789041	0.000000
C	-2.562425	2.202956	0.000000
H	-2.715406	-1.146077	0.000000
H	-4.453568	0.982461	0.000000
C	-0.016262	2.586548	0.000000
N	-0.040328	3.985245	0.000000
C	1.267015	4.453934	0.000000
C	1.331853	2.172631	0.000000
C	2.138567	3.354204	0.000000
H	1.484837	5.521665	0.000000
H	1.691843	1.149603	0.000000
H	3.222997	3.393124	0.000000
H	-2.922417	3.225984	0.000000
H	-0.371207	-0.157608	0.000000
H	-0.859364	4.533197	0.000000

Table A.3.3 Cartesian coordinates of **3P**(AM1)

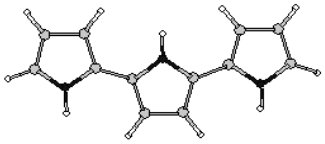

Electronic energy = -477.76375

Atomic symbol	X	Y	Z
N	1.202945	3.359180	-1.493788
C	1.179623	4.755226	-1.493788
C	-0.168075	5.175457	-1.493788
C	-0.111843	2.889267	-1.493788
C	-0.979852	4.002570	-1.493788
H	-0.521856	6.200911	-1.493788
C	-0.432417	1.486346	-1.493788
N	-1.748964	1.012447	-1.493788
C	-1.722825	-0.375864	-1.493788
C	0.433131	0.372802	-1.493788
C	-0.385180	-0.800487	-1.493788
H	-2.643677	-0.958719	-1.493788
H	1.517494	0.399576	-1.493788
H	-0.036772	-1.828229	-1.493788
H	-2.064201	3.972472	-1.493788
C	2.379714	5.549415	-1.493788
N	2.359508	6.948510	-1.493788
C	3.668052	7.413058	-1.493788
C	3.726769	5.131567	-1.493788
C	4.536626	6.310707	-1.493788
H	3.889196	8.480195	-1.493788
H	4.083661	4.107269	-1.493788
H	5.621223	6.346634	-1.493788
H	2.013999	2.797835	-1.493788
H	-2.552058	1.583445	-1.493788
H	1.542226	7.499011	-1.493788

Table A.3.4 Cartesian coordinates of **4P**(AM1)

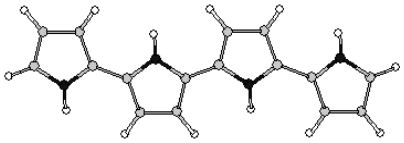

Electronic energy = -714.47316

Atomic symbol	X	Y	Z
N	1.393667	-2.303456	0.198835
C	1.372028	-0.906998	0.198835
C	0.024771	-0.484978	0.198835
C	0.078421	-2.771288	0.198835
C	-0.788300	-1.656687	0.198835
H	-0.327503	0.541179	0.198835
C	-0.244317	-4.173704	0.198835
N	-1.561607	-4.645606	0.198835
C	-1.537546	-6.033833	0.198835
C	0.619569	-5.288607	0.198835
C	-0.200482	-6.460581	0.198835
H	-2.459281	-6.615375	0.198835
H	1.703971	-5.263516	0.198835
H	0.146235	-7.488905	0.198835
H	-1.872728	-1.685445	0.198835
N	2.551285	1.282162	0.198835
C	2.572924	-0.114297	0.198835
C	3.920181	-0.536317	0.198835
C	3.866532	1.749993	0.198835
C	4.733253	0.635392	0.198835
H	4.272455	-1.562473	0.198835
C	4.189269	3.152410	0.198836
N	5.506559	3.624310	0.198836
C	5.482498	5.012537	0.198836
C	3.325383	4.267313	0.198836
C	4.145435	5.439287	0.198836
H	6.404233	5.594080	0.198836
H	2.240982	4.242222	0.198836
H	3.798717	6.467611	0.198836
H	5.817680	0.664150	0.198835
H	2.203812	-2.866022	0.198835
H	-2.363860	-4.073321	0.198835
H	1.741140	1.844728	0.198836
H	6.308812	3.052027	0.198835

Table A.3.5 Cartesian coordinates of **5P**(AM1)

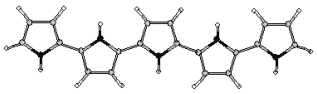

Electronic energy = -971.87822

Atomic symbol	X	Y	Z
N	8.694102	2.417078	-1.926162
C	8.670220	3.813554	-1.926162
C	7.322269	4.233409	-1.926162
C	7.379712	1.947204	-1.926162
C	6.511109	3.060441	-1.926162
H	6.968298	5.258978	-1.926162
C	7.059287	0.544256	-1.926162
N	5.742799	0.070049	-1.926162
C	5.769333	-1.318090	-1.926162
C	7.925146	-0.569132	-1.926162
C	7.107171	-1.742515	-1.926162
H	4.848636	-1.901304	-1.926162
H	9.009523	-0.542182	-1.926162
H	7.455687	-2.770243	-1.926162
H	5.426733	3.029858	-1.926162
C	9.869884	4.608102	-1.926162
N	9.846131	6.004261	-1.926162
C	11.161180	6.473810	-1.926162
C	11.217890	4.187743	-1.926162
C	12.029420	5.360265	-1.926162
H	11.571460	3.161994	-1.926162
H	13.113970	5.390659	-1.926162
N	12.797630	8.346000	-1.926162
C	11.482240	7.876459	-1.926162
C	10.614490	8.990130	-1.926162
C	12.774410	9.741658	-1.926162
C	11.426560	10.162470	-1.926162
H	9.529967	8.960173	-1.926162
C	13.974570	10.535720	-1.926162
N	13.954670	11.934870	-1.926162
C	15.263190	12.398990	-1.926162
C	15.321590	10.117530	-1.926162
C	16.131650	11.296390	-1.926162
H	15.484730	13.466110	-1.926162
H	15.678330	9.093156	-1.926162
H	17.216280	11.332210	-1.926162
H	11.073230	11.188120	-1.926162
H	9.505230	1.855843	-1.926162
H	4.939534	0.640912	-1.926162
H	9.035169	6.565545	-1.926162
H	13.608600	7.784544	-1.926162
H	13.137460	12.485570	-1.926162

Table A.3.6 Cartesian coordinates of **6P**(AM1)

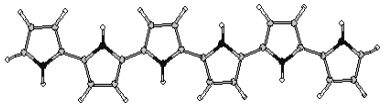

Electronic energy = -1245.86490

Atomic symbol	X	Y	Z
C	-16.477640	-2.316815	0.522713
C	-17.855400	-2.701034	0.522713
C	-18.616980	-1.522050	0.522713
C	-16.436640	-0.906960	0.522713
N	-17.753810	-0.434623	0.522713
H	-18.240880	-3.715481	0.522713
H	-19.698310	-1.385757	0.522713
H	-15.624190	-2.986315	0.522713
C	-13.885400	1.770738	0.522713
C	-15.257640	1.382508	0.522713
C	-15.296410	-0.029003	0.522713
C	-13.113120	0.588858	0.522713
N	-13.983680	-0.503360	0.522713
H	-16.113390	2.049222	0.522713
H	-13.505570	2.787036	0.522713
C	-9.537745	-0.356239	0.522713
C	-10.909890	-0.744139	0.522713
C	-11.682110	0.438112	0.522713
C	-9.498723	1.055260	0.522713
N	-10.811950	1.530044	0.522713
H	-11.290090	-1.760320	0.522713
H	-8.681897	-1.023089	0.522713
C	-6.947265	3.732293	0.522713
C	-8.319412	3.344393	0.522713
C	-8.358437	1.932894	0.522713
C	-6.175053	2.550041	0.522713
N	-7.045210	1.458109	0.522713
H	-9.175261	4.011242	0.522713
H	-6.567072	4.748475	0.522713
C	-2.599521	1.605646	0.522712
C	-3.971758	1.217417	0.522713
C	-4.744040	2.399297	0.522713
N	-3.873477	3.491513	0.522713
H	-4.351586	0.201118	0.522712
H	-1.743766	0.938933	0.522712
C	-2.560745	3.017156	0.522713
C	-0.001754	5.689189	0.522713
C	-1.379519	5.304969	0.522713
C	-1.420514	3.895115	0.522713
C	0.759822	4.510205	0.522713
N	-0.103350	3.422778	0.522713
H	-2.232964	5.974470	0.522713

Table A.3.6 (Continue) Cartesian coordinates of **6P**(AM1)

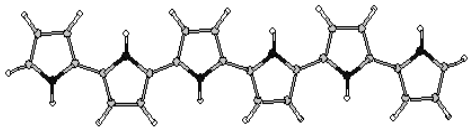

Electronic energy = -1245.86490

Atomic symbol	X	Y	Z
H	0.383721	6.703636	0.522713
H	1.841150	4.373913	0.522713
H	-18.009900	0.516988	0.522713
H	-13.715420	-1.452540	0.522713
H	-11.080190	2.479171	0.522713
H	-6.776968	0.508983	0.522713
H	-4.141740	4.440693	0.522713
H	0.152746	2.471168	0.522712

APPENDIX B

B. Cartesian Coordinates of Ground State Geometries of Studied Structures at HF/6-31G* Level

All cartesian coordinates are in angstroms. All electronic energies are in Hartrees.

B.1 Cartesian Coordinates of Ground State Geometries of Thiophene Oligomers (**nT**) at HF/6-31G* Level

Table B.1.1 Cartesian coordinates of **1T**(RHF)

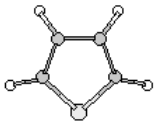

Electronic energy = -551.29035

Atom symbol	X	Y	Z
C	-1.258076	-0.718490	0.000000
C	-1.258104	0.718442	0.000000
C	-0.015659	1.234024	0.000000
C	-0.015612	-1.234024	0.000000
S	1.190836	0.000023	0.000000
H	-2.150318	1.315432	0.000000
H	0.265912	2.267225	0.000000
H	-2.150268	-1.315513	0.000000
H	0.265998	-2.267215	0.000000

Table B.1.2 Cartesian coordinates of **2T**(RHF)

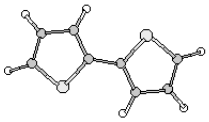

Electronic energy = -1101.42989

Atom symbol	X	Y	Z
S	-0.576023	-2.133791	0.000000
C	-2.299877	-2.223972	0.000000
C	-2.863683	-1.004513	0.000000
C	-0.617194	-0.393206	0.000000
C	-1.894139	0.051282	0.000000
H	-2.788807	-3.176633	0.000000
H	-3.923803	-0.836353	0.000000
C	0.617194	0.393206	0.000000
S	0.576023	2.133791	0.000000
C	2.299877	2.223972	0.000000
C	1.894139	-0.051282	0.000000
C	2.863683	1.004513	0.000000
H	2.788807	3.176633	0.000000
H	2.159871	-1.091547	0.000000
H	3.923803	0.836353	0.000000
H	-2.159871	1.091547	0.000000

Table B.1.3 Cartesian coordinates of **3T**(RHF)

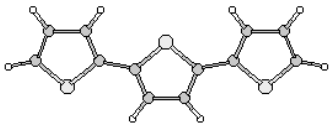

Electronic energy = -1651.56988

Atom symbol	X	Y	Z
S	0.697292	-0.659328	0.000000
C	0.679245	1.082281	0.000000
C	-0.591111	1.542246	0.000000
C	-1.042600	-0.738708	0.000000
C	-1.572890	0.503937	0.000000
H	-0.844839	2.585350	0.000000
C	-1.737829	-2.024902	0.000000
S	-3.477438	-2.108004	-0.000001
C	-3.443200	-3.833494	0.000000
C	-1.202919	-3.267287	0.000000
C	-2.186610	-4.309284	0.000000
H	-4.358368	-4.389384	-0.000001
H	-0.146313	-3.457713	0.000001
H	-1.944263	-5.354866	0.000001
H	-2.628551	0.698932	0.000001
C	1.924545	1.848351	0.000000
S	1.910231	3.589885	0.000000
C	3.634934	3.652199	0.000000
C	3.194900	1.383759	0.000000
C	4.180255	2.424184	0.000000
H	4.138774	4.597022	0.000000
H	3.444119	0.339456	0.000000
H	5.237754	2.240689	0.000000

Table B.1.4 Cartesian coordinates of **4T**(RHF)

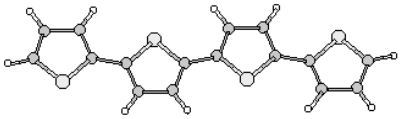

Electronic energy = -2201.70988

Atom symbol	X	Y	Z
S	1.317698	-2.598660	0.249930
C	1.310504	-0.856830	0.249929
C	0.042661	-0.388754	0.249929
C	-0.422542	-2.666639	0.249929
C	-0.945100	-1.420586	0.249929
H	-0.205372	0.655732	0.249929
C	-1.125589	-3.947955	0.249929
S	-2.865664	-4.020333	0.249929
C	-2.842377	-5.745657	0.249929
C	-0.598462	-5.193538	0.249930
C	-1.588722	-6.229257	0.249930
H	-3.761074	-6.295778	0.249929
H	0.456882	-5.391079	0.249931
H	-1.352314	-7.276158	0.249930
H	-1.999434	-1.218602	0.249929
S	2.551486	1.641737	0.249930
C	2.558680	-0.100094	0.249929
C	3.826523	-0.568169	0.249929
C	4.291726	1.709716	0.249930
C	4.814284	0.463662	0.249929
H	4.074556	-1.612655	0.249929
C	4.994773	2.991031	0.249930
S	6.734848	3.063410	0.249929
C	6.711561	4.788734	0.249930
C	4.467646	4.236614	0.249931
C	5.457906	5.272333	0.249931
H	7.630258	5.338854	0.249930
H	3.412301	4.434156	0.249932
H	5.221498	6.319234	0.249931
H	5.868618	0.261678	0.249929

Table B.1.5 Cartesian coordinates of **5T**(RHF)

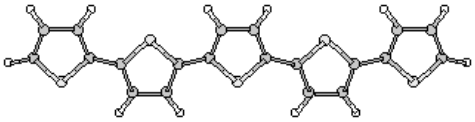

Electronic energy = -2751.84986

Atom symbol	X	Y	Z
S	-1.975088	-3.521250	-0.000001
C	-1.993222	-1.779506	0.000000
C	-3.263987	-1.319315	0.000001
C	-3.714803	-3.600019	-0.000001
C	-4.245223	-2.357236	0.000001
H	-3.518633	-0.276413	0.000002
C	-4.409840	-4.885691	-0.000001
S	-6.149399	-4.968917	0.000001
C	-6.115267	-6.694014	-0.000001
C	-3.874886	-6.127938	-0.000004
C	-4.858616	-7.169815	-0.000004
H	-7.030509	-7.249863	-0.000001
H	-2.818325	-6.318886	-0.000006
H	-4.615701	-8.215218	-0.000005
H	-5.300787	-2.161874	0.000002
C	-0.749990	-1.014943	-0.000001
S	-0.768549	0.726706	0.000001
C	0.971412	0.805576	0.000000
C	0.520950	-1.475209	-0.000002
C	1.502034	-0.437635	-0.000002
H	0.775354	-2.518125	-0.000004
H	2.557545	-0.633318	-0.000003
S	3.405285	2.168918	-0.000001
C	1.665253	2.089619	0.000001
C	1.134716	3.332660	0.000004
C	3.386640	3.910315	0.000001
C	2.116139	4.370405	0.000003
H	0.079206	3.528585	0.000005
C	4.631431	4.676164	0.000000
S	4.617244	6.417655	0.000008
C	6.341550	6.480050	0.000002
C	5.901651	4.211518	-0.000007
C	6.886883	5.251974	-0.000005
H	6.845346	7.424945	0.000004
H	6.151386	3.167289	-0.000014
H	7.944235	5.067902	-0.000010
H	1.862051	5.413391	0.000005

Table B.1.6. Cartesian coordinates of **6T**(RHF)

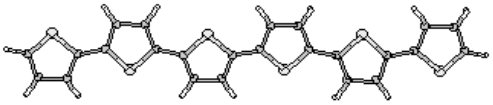

Electronic energy = -3301.98983

Atom symbol	X	Y	Z
C	-7.690962	-5.020152	0.000000
C	-8.997832	-5.607759	0.000000
C	-9.977786	-4.688380	0.000000
C	-7.711377	-3.667774	0.000000
S	-9.351026	-3.080821	0.000000
H	-9.172267	-6.666739	0.000000
H	-11.035885	-4.852881	0.000000
H	-6.787242	-5.599870	0.000000
C	-5.291257	-0.808626	0.000000
C	-6.594314	-1.393489	0.000000
C	-6.578285	-2.744657	0.000000
C	-4.292315	-1.718975	0.000000
S	-4.940232	-3.335800	0.000000
H	-7.495434	-0.810097	0.000000
H	-5.128642	0.252531	0.000000
C	-0.549587	-1.812605	0.000000
C	-1.852304	-2.397231	0.000000
C	-2.851411	-1.486702	0.000000
C	-0.565658	-0.460950	0.000000
S	-2.204020	0.130188	0.000000
H	-2.015161	-3.458284	0.000000
H	0.351323	-2.396362	0.000000
C	1.852304	2.397231	0.000000
C	0.549587	1.812605	0.000000
C	0.565658	0.460950	0.000000
C	2.851411	1.486702	0.000000
S	2.204020	-0.130188	0.000000
H	-0.351323	2.396362	0.000000
H	2.015161	3.458284	0.000000
C	6.594314	1.393489	0.000000
C	5.291257	0.808626	0.000000
C	4.292315	1.718975	0.000000
S	4.940232	3.335800	0.000000
H	5.128642	-0.252531	0.000000
H	7.495434	0.810097	0.000000
C	6.578285	2.744657	0.000000
C	8.997832	5.607759	0.000000

Table B.1.6 (Continue) Cartesian coordinates of **6T**(RHF)

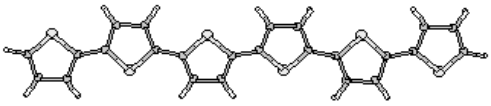

Electronic energy = -3301.98983

Atom symbol	X	Y	Z
C	7.690962	5.020152	0.000000
C	7.711377	3.667774	0.000000
C	9.977786	4.688380	0.000000
S	9.351026	3.080821	0.000000
H	6.787242	5.599870	0.000000
H	9.172267	6.666739	0.000001
H	11.035885	4.852881	0.000000

B.2 Cartesian Coordinates of Ground State Geometries of Furan Oligomers (**nF**) at HF/6-31G* Level

Table B.2.1 Cartesian coordinates of **1F**(RHF)

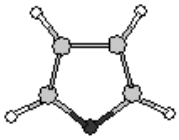

Electronic energy = -228.62521

Atom symbol	X	Y	Z
C	-0.945641	-0.720536	0.000000
C	-0.945716	0.720438	0.000000
C	0.343849	1.081099	0.000000
C	0.343962	-1.081063	0.000000
O	1.142020	0.000059	0.000000
H	-1.793481	1.373527	0.000000
H	0.835862	2.029044	0.000000
H	-1.793338	-1.373714	0.000000
H	0.836073	-2.028957	0.000000

Table B.2.2 Cartesian coordinates of **2F**(RHF)

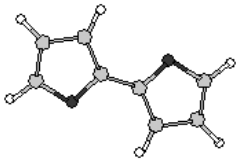

Electronic energy = -456.10851

Atom symbol	X	Y	Z
O	-0.641869	-1.673762	0.000000
C	-1.925792	-2.076586	0.000000
C	-2.752319	-1.023326	0.000000
C	-0.645923	-0.328082	0.000000
C	-1.906515	0.139463	0.000000
H	-2.085859	-3.132206	0.000000
H	-3.821945	-1.049688	0.000000
C	0.645923	0.328082	0.000000
O	0.641868	1.673762	0.000000
C	1.925792	2.076586	0.000000
C	1.906515	-0.139463	0.000000
C	2.752319	1.023326	0.000000
H	2.085859	3.132206	0.000000
H	2.201805	-1.167096	0.000000
H	3.821945	1.049688	0.000000
H	-2.201805	1.167096	0.000000

Table B.2.3 Cartesian coordinates of **3F**(RHF)

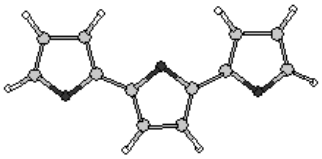

Electronic energy = -683.59215

Atom symbol	X	Y	Z
O	0.188578	-0.144999	0.000000
C	0.217997	1.202180	0.000000
C	-1.032675	1.698200	0.000000
C	-1.105827	-0.519525	0.000000
C	-1.906501	0.561742	0.000000
H	-1.303613	2.732607	0.000000
C	-1.372795	-1.941409	0.000000
O	-2.665907	-2.314157	0.000000
C	-2.693560	-3.659306	0.000000
C	-0.571227	-3.021760	0.000000
C	-1.450994	-4.158686	0.000000
H	-3.662328	-4.108438	0.000000
H	0.498077	-3.019004	0.000000
H	-1.176839	-5.193041	0.000000
H	-2.975795	0.557843	0.000000
C	1.523573	1.825475	0.000000
O	1.551605	3.170947	0.000000
C	2.844503	3.543245	0.000000
C	2.773590	1.328356	0.000000
C	3.646342	2.470677	0.000000
H	3.029681	4.594883	0.000000
H	3.045635	0.294233	0.000000
H	4.716413	2.471452	0.000000

Table B.2.4 Cartesian coordinates of **4F**(RHF)

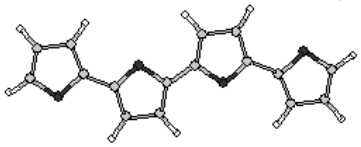

Electronic energy = -911.07580

Atom symbol	X	Y	Z
O	1.269772	-2.157587	0.205832
C	1.312202	-0.810644	0.205832
C	0.065773	-0.302714	0.205832
C	-0.028113	-2.519487	0.205832
C	-0.818453	-1.430402	0.205832
H	-0.195732	0.734091	0.205832
C	-0.308833	-3.938486	0.205832
O	-1.605522	-4.298441	0.205832
C	-1.646108	-5.643235	0.205832
C	0.482239	-5.026578	0.205832
C	-0.408469	-6.154730	0.205833
H	-2.619288	-6.082623	0.205833
H	1.551517	-5.034135	0.205832
H	-0.144625	-7.191756	0.205833
H	-1.887712	-1.424190	0.205833
O	2.664806	1.145103	0.205832
C	2.622376	-0.201841	0.205832
C	3.868804	-0.709770	0.205832
C	3.962690	1.507003	0.205832
C	4.753030	0.417917	0.205832
H	4.130310	-1.746575	0.205832
C	4.243410	2.926001	0.205832
O	5.540099	3.285957	0.205832
C	5.580685	4.630750	0.205832
C	3.452338	4.014094	0.205832
C	4.343046	5.142245	0.205833
H	6.553866	5.070138	0.205832
H	2.383061	4.021651	0.205832
H	4.079203	6.179271	0.205833
H	5.822289	0.411705	0.205832

Table B.2.5 Cartesian coordinates of **5F**(RHF)

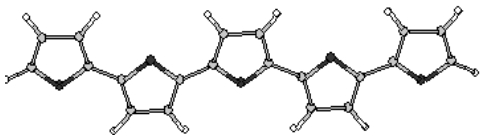

Electronic energy = -1138.55944

Atom symbol	X	Y	Z
O	8.555707	2.676420	-1.926162
C	8.584609	4.023632	-1.926162
C	7.333230	4.519468	-1.926162
C	7.261617	2.301943	-1.926162
C	6.460230	3.383096	-1.926162
H	7.061230	5.553484	-1.926162
C	6.994467	0.880140	-1.926162
O	5.701325	0.508092	-1.926162
C	5.673714	-0.836862	-1.926162
C	7.796074	-0.200274	-1.926162
C	6.916139	-1.336835	-1.926162
H	4.705099	-1.286044	-1.926162
H	8.865285	-0.197986	-1.926162
H	7.190075	-2.371149	-1.926162
H	5.391066	3.378935	-1.926162
C	9.888658	4.645512	-1.926162
O	9.917945	5.992568	-1.926162
C	11.212269	6.366926	-1.926162
C	11.140087	4.149248	-1.926162
C	12.013366	5.284986	-1.926162
H	11.411618	3.115142	-1.926162
H	13.082521	5.288227	-1.926162
O	12.772844	8.160996	-1.926162
C	11.478271	7.786970	-1.926162
C	10.677600	8.868971	-1.926162
C	12.802306	9.507857	-1.926162
C	11.551564	10.004603	-1.926162
H	9.608412	8.866208	-1.926162
C	14.107761	10.131298	-1.926162
O	14.135119	11.476619	-1.926162
C	15.427841	11.848817	-1.926162
C	15.357846	9.634149	-1.926162
C	16.230209	10.776531	-1.926162
H	15.613114	12.900318	-1.926162
H	15.630312	8.600235	-1.926162
H	17.300184	10.777502	-1.926162
H	11.280920	11.038954	-1.926162

Table B.2.6 Cartesian coordinates of **6F**(RHF)

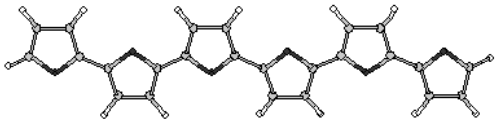

Electronic energy = -1366.04308

Atom symbol	X	Y	Z
C	-16.131618	-2.202473	0.522712
C	-17.517218	-2.584638	0.522712
C	-18.211895	-1.439598	0.522712
C	-16.125565	-0.857153	0.522712
O	-17.383573	-0.379636	0.522712
H	-17.918041	-3.576681	0.522711
H	-19.256430	-1.218509	0.522712
H	-15.274482	-2.841616	0.522712
C	-13.672863	1.852695	0.522713
C	-15.052779	1.466475	0.522713
C	-15.059390	0.120669	0.522712
C	-12.968492	0.705654	0.522712
O	-13.799170	-0.355372	0.522712
H	-15.911040	2.104026	0.522713
H	-13.270754	2.843376	0.522713
C	-9.468209	-0.340623	0.522712
C	-10.847976	-0.725934	0.522712
C	-11.551964	0.421663	0.522712
C	-9.460659	1.005621	0.522713
O	-10.720994	1.482180	0.522713
H	-11.250667	-1.716328	0.522712
H	-8.610660	-0.979132	0.522712
C	-7.009184	3.714086	0.522713
C	-8.388952	3.328775	0.522713
C	-8.396502	1.982531	0.522713
C	-6.305197	2.566489	0.522713
O	-7.136166	1.505972	0.522713
H	-9.246501	3.967284	0.522713
H	-6.606494	4.704480	0.522713
C	-2.804382	1.521676	0.522713
C	-4.184298	1.135457	0.522713
C	-4.888669	2.282498	0.522713
O	-4.057991	3.343523	0.522713
H	-4.586407	0.144776	0.522713
H	-1.946121	0.884125	0.522713
C	-2.797770	2.867483	0.522713
C	-0.339943	5.572790	0.522713

Table B.2.6 (Continue) Cartesian coordinates of **6F**(RHF)

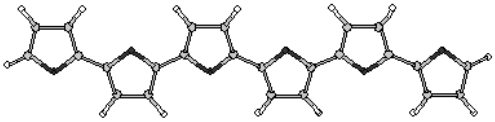

Electronic energy = -1366.04308

Atom symbol	X	Y	Z
C	-1.725543	5.190625	0.522713
C	-1.731596	3.845305	0.522713
C	0.354735	4.427750	0.522713
O	-0.473588	3.367788	0.522713
H	-2.582679	5.829767	0.522713
H	0.060880	6.564833	0.522714
H	1.399269	4.206660	0.522713

B.3 Cartesian Coordinates of Ground State Geometries of Pyrrole Oligomers (**nP**) at HF/6-31G* Level

Table B.3.1 Cartesian coordinates of **1P**(RHF)

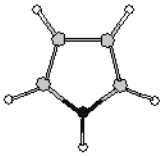

Electronic energy = -208.80785

Atom symbol	X	Y	Z
C	-0.809503	2.693208	2.378472
C	-0.809502	4.119709	2.378472
C	0.488220	4.519198	2.378472
C	0.488219	2.293719	2.378472
N	1.275014	3.406458	2.378472
H	-1.665995	4.762973	2.378472
H	0.917283	5.499448	2.378472
H	-1.665996	2.049944	2.378472
H	0.917282	1.313468	2.378472
H	2.267480	3.406458	2.378472

Table B.3.2 Cartesian coordinates of **2P**(RHF)

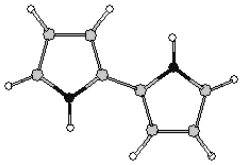

Electronic energy = -416.47073

Atom symbol	X	Y	Z
N	-0.602886	-1.752571	0.000000
C	-1.879142	-2.231630	0.000000
C	-2.726787	-1.172587	0.000000
C	-0.617438	-0.387988	0.000000
C	-1.925409	0.004146	0.000000
H	-2.073140	-3.283511	0.000000
H	-3.796534	-1.219496	0.000000
C	0.617438	0.387988	0.000000
N	0.602886	1.752571	0.000000
C	1.879142	2.231630	0.000000
C	1.925409	-0.004146	0.000000
C	2.726787	1.172587	0.000000
H	2.073140	3.283511	0.000000
H	2.286209	-1.013306	0.000000
H	3.796534	1.219496	0.000000
H	-2.286209	1.013306	0.000000
H	0.217019	-2.311741	0.000000
H	-0.217019	2.311741	0.000000

Table B.3.3 Cartesian coordinates of **3P**(RHF)

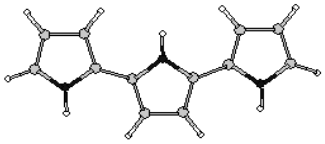

Electronic energy = -624.13378

Atom symbol	X	Y	Z
N	0.219520	-0.151935	0.000000
C	0.217715	1.213307	0.000000
C	-1.086369	1.615554	0.000000
C	-1.058860	-0.631132	0.000000
C	-1.894674	0.447688	0.000000
H	-1.441721	2.626356	0.000000
C	-1.335907	-2.061361	0.000000
N	-2.613583	-2.542132	0.000000
C	-2.597279	-3.905028	0.000000
C	-0.496578	-3.138643	0.000000
C	-1.302981	-4.311487	0.000000
H	-3.507255	-4.467113	0.000000
H	0.574633	-3.109416	0.000000
H	-0.959178	-5.325475	0.000000
H	-2.965862	0.424224	0.000000
C	1.458696	1.976377	0.000000
N	1.458610	3.341513	0.000000
C	2.739902	3.806316	0.000000
C	2.762577	1.570297	0.000000
C	3.576211	2.738137	0.000000
H	2.945437	4.855959	0.000000
H	3.112543	0.557444	0.000000
H	4.646313	2.773532	0.000000
H	1.035521	-0.716706	0.000000
H	-3.432251	-1.981215	0.000000
H	0.645276	3.910138	0.000000

Table B.3.4 Cartesian coordinates of **4P**(RHF)

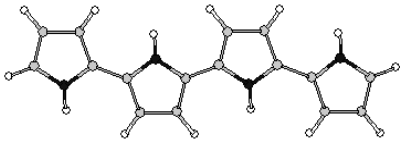

Electronic energy = -831.79689

Atom symbol	X	Y	Z
N	1.347457	-2.255175	0.198835
C	1.351479	-0.889608	0.198835
C	0.048789	-0.481601	0.198835
C	0.067277	-2.728532	0.198835
C	-0.764251	-1.645936	0.198835
H	-0.302111	0.530820	0.198835
C	-0.215996	-4.157304	0.198835
N	-1.495565	-4.632475	0.198835
C	-1.485228	-5.995181	0.198835
C	0.618865	-5.238335	0.198835
C	-0.192650	-6.407746	0.198835
H	-2.397825	-6.553264	0.198835
H	1.690310	-5.213844	0.198835
H	0.146588	-7.423432	0.198835
H	-1.835598	-1.664966	0.198835
N	2.597495	1.233881	0.198835
C	2.593474	-0.131687	0.198835
C	3.896164	-0.539693	0.198835
C	3.877676	1.707238	0.198835
C	4.709203	0.624642	0.198835
H	4.247063	-1.552114	0.198835
C	4.160948	3.136009	0.198835
N	5.440517	3.611181	0.198835
C	5.430180	4.973886	0.198836
C	3.326087	4.217040	0.198836
C	4.137603	5.386451	0.198836
H	6.342778	5.531969	0.198835
H	2.254642	4.192550	0.198836
H	3.798364	6.402137	0.198836
H	5.780550	0.643671	0.198835
H	2.160524	-2.824151	0.198835
H	-2.311964	-4.068153	0.198835
H	1.784428	1.802856	0.198836
H	6.256916	3.046858	0.198835

Table B.3.5 Cartesian coordinates of **5P**(RHF)

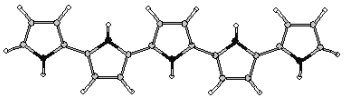

Electronic energy = -1039.45998

Atom symbol	X	Y	Z
N	8.656811	2.478741	-1.926162
C	8.654746	3.844330	-1.926162
C	7.350213	4.246469	-1.926162
C	7.378881	1.999708	-1.926162
C	6.542434	3.078601	-1.926162
H	6.994776	5.257302	-1.926162
C	7.101903	0.569735	-1.926162
N	5.824478	0.088793	-1.926162
C	5.841011	-1.273801	-1.926162
C	7.941625	-0.507495	-1.926162
C	7.135443	-1.680525	-1.926162
H	4.930990	-1.836028	-1.926162
H	9.012930	-0.478181	-1.926162
H	7.479272	-2.694638	-1.926162
H	5.471214	3.054676	-1.926162
C	9.893114	4.607900	-1.926162
N	9.890901	5.973275	-1.926162
C	11.169549	6.452141	-1.926162
C	11.197770	4.205495	-1.926162
C	12.005714	5.372842	-1.926162
H	11.552977	3.194645	-1.926162
H	13.076896	5.396459	-1.926162
N	12.726779	8.359180	-1.926162
C	11.447983	7.880101	-1.926162
C	10.612111	8.959379	-1.926162
C	12.724975	9.723942	-1.926162
C	11.420600	10.126755	-1.926162
H	9.540863	8.935982	-1.926162
C	13.965740	10.486859	-1.926162
N	13.965902	11.851820	-1.926162
C	15.246991	12.316304	-1.926162
C	15.269713	10.080396	-1.926162
C	16.083597	11.248096	-1.926162
H	15.452642	13.366040	-1.926162
H	15.619632	9.067425	-1.926162
H	17.153825	11.283512	-1.926162
H	11.065667	11.137747	-1.926162
H	9.472382	1.913320	-1.926162
H	5.005500	0.649375	-1.926162
H	9.074930	6.538025	-1.926162
H	13.543237	7.795042	-1.926162
H	13.152772	12.420852	-1.926162

Table B.3.6 Cartesian coordinates of **6P**(RHF)

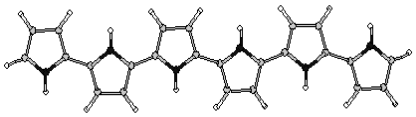

Electronic energy = -1247.12307

Atom symbol	X	Y	Z
C	-16.415100	-2.270481	0.522713
C	-17.784066	-2.660136	0.522713
C	-18.521926	-1.521468	0.522713
C	-16.375165	-0.905213	0.522713
N	-17.665898	-0.461234	0.522713
H	-18.165780	-3.660593	0.522713
H	-19.581443	-1.374374	0.522713
H	-15.571118	-2.930961	0.522712
C	-13.839593	1.768856	0.522713
C	-15.206481	1.384228	0.522713
C	-15.250011	0.019739	0.522713
C	-13.091046	0.627299	0.522713
N	-13.960154	-0.426067	0.522713
H	-16.046938	2.048814	0.522713
H	-13.468935	2.774196	0.522713
C	-9.535062	-0.331716	0.522712
C	-10.901694	-0.715883	0.522712
C	-11.650198	0.426048	0.522713
C	-9.491052	1.032900	0.522713
N	-10.781450	1.479245	0.522713
H	-11.272600	-1.721055	0.522712
H	-8.694821	-0.996542	0.522712
C	-6.955463	3.704037	0.522713
C	-8.322096	3.319871	0.522713
C	-8.366106	1.955255	0.522713
C	-6.206960	2.562106	0.522713
N	-7.075708	1.508910	0.522713
H	-9.162337	3.984696	0.522713
H	-6.584558	4.709210	0.522713
C	-2.650677	1.603926	0.522713
C	-4.017565	1.219299	0.522712
C	-4.766112	2.360856	0.522713
N	-3.897004	3.414222	0.522713
H	-4.388223	0.213958	0.522712
H	-1.810219	0.939340	0.522712
C	-2.607147	2.968415	0.522713
C	-0.073092	5.648290	0.522713
C	-1.442058	5.258635	0.522713
C	-1.481993	3.893367	0.522713
C	0.664768	4.509622	0.522713
N	-0.191260	3.449388	0.522713
H	-2.286040	5.919115	0.522713

Table B.3.6 (Continue) Cartesian coordinates of **6P**(RHF)

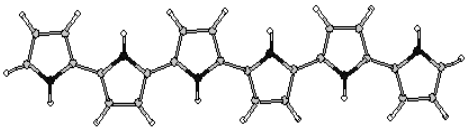

Electronic energy = -1247.12307

Atom symbol	X	Y	Z
H	0.308622	6.648747	0.522713
H	1.724285	4.362528	0.522713
H	-17.939411	0.492800	0.522713
H	-13.692459	-1.381678	0.522712
H	-11.050074	2.434560	0.522713
H	-6.807084	0.553594	0.522712
H	-4.164699	4.369832	0.522713
H	0.082254	2.495354	0.522713

APPENDIX C

C. Cartesian Coordinates of Ground State Geometries of Studied Structures at B3LYP/6-31G* Level

All cartesian coordinates are in angstroms. All electronic energies are in Hartrees.

C.1 Cartesian Coordinates of Ground State Geometries of Thiophene Oligomers (**nT**) at B3LYP/6-31G* Level

Table C.1.1 Cartesian coordinates of **1T**(DFT)

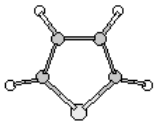

Electronic energy = -553.00263

Atom symbol	X	Y	Z
C	-0.847061	2.691541	2.378472
C	-0.847088	4.121338	2.378472
C	0.413934	4.650222	2.378472
C	0.413981	2.162705	2.378472
S	1.625216	3.406486	2.378472
H	-1.747304	4.726617	2.378472
H	0.706265	5.691638	2.378472
H	-1.747254	2.086227	2.378472
H	0.706352	1.121300	2.378472

Table C.1.2 Cartesian coordinates of **2T**(DFT)

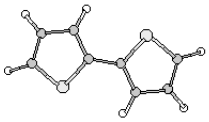

Electronic energy = -1104.81654

Atom symbol	X	Y	Z
S	-0.573260	-2.142706	0.000000
C	-2.306701	-2.238384	0.000000
C	-2.878958	-0.996724	0.000000
C	-0.613767	-0.386449	0.000000
C	-1.919400	0.055403	0.000000
H	-2.792123	-3.204874	0.000000
H	-3.950997	-0.832320	0.000000
C	0.613767	0.386449	0.000000
S	0.573260	2.142706	0.000000
C	2.306701	2.238384	0.000000
C	1.919400	-0.055403	0.000000
C	2.878958	0.996724	0.000000
H	2.792123	3.204875	0.000000
H	2.185354	-1.107309	0.000000
H	3.950997	0.832321	0.000000
H	-2.185354	1.107309	0.000000

Table C.1.3 Cartesian coordinates of **3T**(DFT)

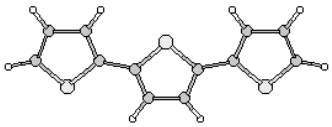

Electronic energy = -1656.63160

Atom symbol	X	Y	Z
S	-0.456664	-0.482958	-0.702945
C	0.750798	0.794029	-0.687339
C	1.067483	1.128948	0.612700
C	-0.513486	-0.543052	1.052636
C	0.360599	0.381362	1.585552
H	1.792610	1.895828	0.864044
C	-1.390388	-1.470446	1.733781
S	-1.448939	-1.532368	3.489932
C	-2.641203	-2.793282	3.459952
C	-2.264274	-2.394651	1.199575
C	-2.972729	-3.143898	2.180369
H	-3.021815	-3.195810	4.388866
H	-2.395287	-2.533207	0.131477
H	-3.699377	-3.912386	1.940279
H	0.492462	0.520817	2.653378
C	1.267087	1.340045	-1.923580
S	2.475036	2.617548	-1.910454
C	2.521148	2.666315	-3.644753
C	0.949507	1.004179	-3.223404
C	1.661926	1.757620	-4.198094
H	3.179645	3.362728	-4.145918
H	0.224145	0.237051	-3.473527
H	1.537868	1.626418	-5.267500

Table C.1.4 Cartesian coordinates of **4T**(DFT)

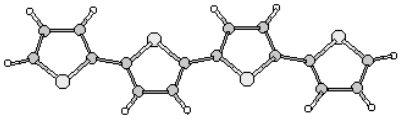

Electronic energy = -2208.44680

Atom symbol	X	Y	Z
S	1.319985	-2.608152	0.249929
C	1.316068	-0.849361	0.249927
C	0.017316	-0.379951	0.249925
C	-0.436238	-2.678532	0.249927
C	-0.960894	-1.402061	0.249925
H	-0.226003	0.677366	0.249923
C	-1.125747	-3.949738	0.249929
S	-2.882419	-4.024178	0.249927
C	-2.862586	-5.760311	0.249932
C	-0.599080	-5.225172	0.249932
C	-1.585768	-6.250249	0.249934
H	-3.794972	-6.308438	0.249933
H	0.468124	-5.420826	0.249934
H	-1.353345	-7.309688	0.249937
H	-2.027843	-1.205169	0.249924
S	2.549203	1.651225	0.249929
C	2.553123	-0.107567	0.249927
C	3.851875	-0.576975	0.249926
C	4.305426	1.721607	0.249929
C	4.830084	0.445137	0.249927
H	4.095194	-1.634291	0.249925
C	4.994932	2.992814	0.249930
S	6.751604	3.067261	0.249925
C	6.731763	4.803395	0.249930
C	4.468260	4.268247	0.249935
C	5.454944	5.293327	0.249935
H	7.664148	5.351525	0.249929
H	3.401055	4.463895	0.249939
H	5.222516	6.352766	0.249939
H	5.897033	0.248246	0.249927

Table C.1.5 Cartesian coordinates of **5T**(DFT)

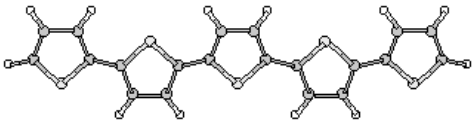

Electronic energy = -2760.26207

Atom symbol	X	Y	Z
S	-1.974754	-3.535279	-0.000001
C	-1.988897	-1.776469	-0.000001
C	-3.290667	-1.314621	-0.000003
C	-3.730502	-3.615763	-0.000003
C	-4.262638	-2.342201	-0.000004
H	-3.541130	-0.259008	-0.000004
C	-4.412993	-4.890382	-0.000003
S	-6.169334	-4.973984	-0.000006
C	-6.140886	-6.709355	-0.000005
C	-3.879946	-6.163153	-0.000002
C	-4.861700	-7.193096	-0.000002
H	-7.070498	-7.262208	-0.000006
H	-2.811972	-6.354580	0.000000
H	-4.623277	-8.251110	-0.000001
H	-5.330501	-2.150477	-0.000006
C	-0.757326	-1.027268	0.000000
S	-0.773549	0.731428	0.000003
C	0.983302	0.813594	0.000004
C	0.545223	-1.488267	0.000000
C	1.516429	-0.461134	0.000003
H	0.795906	-2.543824	-0.000001
H	2.584354	-0.652388	0.000004
S	3.419304	2.169369	0.000000
C	1.662454	2.085137	0.000006
C	1.128535	3.359044	0.000010
C	3.401482	3.926871	0.000004
C	2.100156	4.386956	0.000009
H	0.060569	3.550088	0.000014
C	4.635941	4.679573	0.000000
S	4.621190	6.437841	0.000011
C	6.355436	6.506487	-0.000002
C	5.936531	4.218540	-0.000012
C	6.909958	5.256356	-0.000013
H	6.855436	7.465562	-0.000001
H	6.187386	3.162943	-0.000021
H	7.979650	5.077475	-0.000021
H	1.849017	5.442426	0.000012

Table C.1.6 Cartesian coordinates of **6T**(DFT)

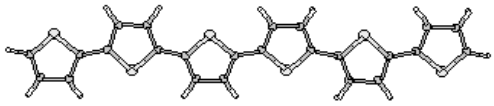

Electronic energy = -3312.07733

Atom symbol	X	Y	Z
C	-7.711431	-5.053197	-0.000012
C	-9.011438	-5.631546	-0.000017
C	-10.009939	-4.697006	-0.000019
C	-7.719531	-3.673320	-0.000009
S	-9.375314	-3.081610	-0.000013
H	-9.194027	-6.700608	-0.000020
H	-11.080051	-4.854112	-0.000022
H	-6.796842	-5.636919	-0.000011
C	-5.319608	-0.794809	0.000003
C	-6.609709	-1.374524	-0.000002
C	-6.602934	-2.754839	-0.000005
C	-4.291949	-1.717878	0.000004
S	-4.949027	-3.349430	-0.000002
H	-7.524030	-0.790505	-0.000003
H	-5.149007	0.276620	0.000006
C	-0.550348	-1.839469	0.000012
C	-1.839714	-2.418022	0.000009
C	-2.867969	-1.494715	0.000009
C	-0.556543	-0.457419	0.000014
S	-2.212009	0.137142	0.000013
H	-2.010873	-3.489343	0.000007
H	0.363799	-2.423728	0.000013
C	1.839718	2.418021	0.000014
C	0.550348	1.839475	0.000016
C	0.556537	0.457425	0.000016
C	2.867969	1.494710	0.000013
S	2.212000	-0.137144	0.000014
H	-0.363795	2.423741	0.000017
H	2.010881	3.489342	0.000013
C	6.609712	1.374526	0.000002
C	5.319613	0.794806	0.000008
C	4.291950	1.717872	0.000010
S	4.949025	3.349425	0.000005
H	5.149017	-0.276623	0.000010
H	7.524035	0.790509	-0.000001
C	6.602934	2.754841	-0.000001
C	9.011444	5.631548	-0.000020

Table C.1.6 (Continue) Cartesian coordinates of **6T**(DFT)

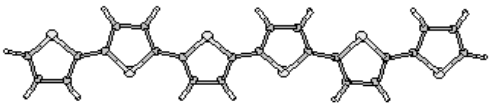

Electronic energy = -3312.07733

Atom symbol	X	Y	Z
C	7.711436	5.053202	-0.000012
C	7.719532	3.673324	-0.000008
C	10.009943	4.697006	-0.000022
S	9.375314	3.081612	-0.000015
H	6.796850	5.636927	-0.000010
H	9.194035	6.700609	-0.000024
H	11.080056	4.854110	-0.000027

C.2 Cartesian Coordinates of Ground State Geometries of Furan Oligomers (**nF**) at B3LYP/6-31G* Level

Table C.2.1 Cartesian coordinates of **1F**(DFT)

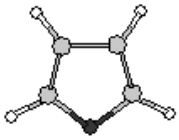

Electronic energy = -230.02058

Atom symbol	X	Y	Z
C	-0.959900	-0.717964	0.000000
C	-0.960012	0.717920	0.000000
C	0.347298	1.094948	0.000000
C	0.347445	-1.094948	0.000000
O	1.161165	0.000046	0.000000
H	-1.819106	1.374299	0.000000
H	0.849735	2.050216	0.000000
H	-1.818911	-1.374448	0.000000
H	0.849979	-2.050169	0.000000

Table C.2.2 Cartesian coordinates of **2F**(DFT)

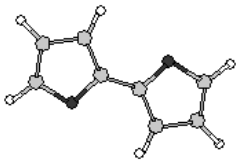

Electronic energy = -458.85992

Atom symbol	X	Y	Z
O	-0.635760	-1.694660	0.000000
C	-1.940314	-2.097540	0.000000
C	-2.772261	-1.019719	0.000000
C	-0.641312	-0.325347	0.000000
C	-1.931388	0.137538	0.000000
H	-2.097588	-3.165058	0.000000
H	-3.853144	-1.041738	0.000000
C	0.641312	0.325347	0.000000
O	0.635760	1.694660	0.000000
C	1.940314	2.097540	0.000000
C	1.931388	-0.137538	0.000000
C	2.772261	1.019719	0.000000
H	2.097589	3.165058	0.000000
H	2.233738	-1.174556	0.000000
H	3.853144	1.041738	0.000000
H	-2.233738	1.174556	0.000000

Table C.2.3 Cartesian coordinates of **3F**(DFT)

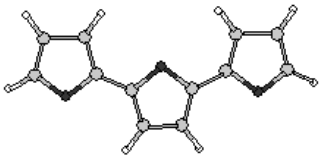

Electronic energy = -687.70015

Atom symbol	X	Y	Z
O	0.205363	-0.157904	0.000000
C	0.231853	1.212523	0.000000
C	-1.049687	1.704726	0.000000
C	-1.112263	-0.535573	0.000000
C	-1.917179	0.576506	0.000000
H	-1.326414	2.748925	0.000000
C	-1.379391	-1.945636	0.000000
O	-2.696897	-2.321197	0.000000
C	-2.720956	-3.686033	0.000000
C	-0.576051	-3.057510	0.000000
C	-1.454169	-4.186014	0.000000
H	-3.702609	-4.133992	0.000000
H	0.504093	-3.060720	0.000000
H	-1.175003	-5.230413	0.000000
H	-2.997424	0.575687	0.000000
C	1.525964	1.832936	0.000000
O	1.550448	3.202705	0.000000
C	2.863294	3.576588	0.000000
C	2.806901	1.342203	0.000000
C	3.671937	2.480765	0.000000
H	3.044028	4.640376	0.000000
H	3.087496	0.299136	0.000000
H	4.753002	2.479279	0.000000

Table C.2.4 Cartesian coordinates of **4F**(DFT)

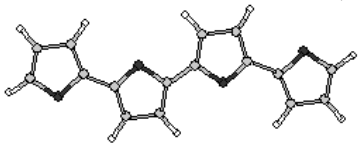

Electronic energy = -916.54058

Atom symbol	X	Y	Z
O	1.279830	-2.180482	0.205840
C	1.319106	-0.809716	0.205824
C	0.040383	-0.306246	0.205807
C	-0.041018	-2.545955	0.205829
C	-0.836100	-1.426051	0.205809
H	-0.227219	0.740301	0.205792
C	-0.321352	-3.952863	0.205839
O	-1.642196	-4.316439	0.205849
C	-1.678563	-5.680956	0.205854
C	0.471955	-5.072204	0.205837
C	-0.416264	-6.192392	0.205848
H	-2.664198	-6.120095	0.205863
H	1.552035	-5.085028	0.205830
H	-0.146926	-7.239384	0.205851
H	-1.916321	-1.417679	0.205797
O	2.654744	1.168000	0.205837
C	2.615466	-0.202766	0.205825
C	3.894189	-0.706238	0.205813
C	3.975593	1.533471	0.205831
C	4.770674	0.413565	0.205817
H	4.161788	-1.752786	0.205802
C	4.255930	2.940379	0.205839
O	5.576775	3.303952	0.205839
C	5.613145	4.668469	0.205846
C	3.462625	4.059721	0.205846
C	4.350847	5.179907	0.205850
H	6.598781	5.107606	0.205846
H	2.382545	4.072547	0.205848
H	4.081512	6.226900	0.205855
H	5.850895	0.405192	0.205809

Table C.2.5 Cartesian coordinates of **5F**(DFT)

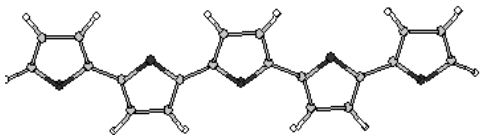

Electronic energy = -1145.38100

Atom symbol	X	Y	Z
O	8.557795	2.644654	-1.926163
C	8.584387	4.015775	-1.926164
C	7.300857	4.507531	-1.926165
C	7.240487	2.267245	-1.926163
C	6.434913	3.379831	-1.926164
H	7.023294	5.551490	-1.926166
C	6.972799	0.857866	-1.926162
O	5.655126	0.482946	-1.926162
C	5.630535	-0.881648	-1.926160
C	7.775791	-0.254553	-1.926160
C	6.897216	-1.382348	-1.926159
H	4.648760	-1.329383	-1.926160
H	8.855950	-0.258362	-1.926160
H	7.175857	-2.426889	-1.926157
H	5.354665	3.378413	-1.926165
C	9.874591	4.634671	-1.926164
O	9.901178	6.005526	-1.926163
C	11.219171	6.383362	-1.926163
C	11.158421	4.142565	-1.926164
C	12.024588	5.269041	-1.926164
H	11.435358	3.098444	-1.926165
H	13.104810	5.269533	-1.926164
O	12.803975	8.167189	-1.926162
C	11.485730	7.789275	-1.926162
C	10.680728	8.903395	-1.926161
C	12.830326	9.537274	-1.926161
C	11.548132	10.029975	-1.926160
H	9.600503	8.903543	-1.926160
C	14.123617	10.158097	-1.926161
O	14.147593	11.527910	-1.926159
C	15.460126	11.902016	-1.926160
C	15.404928	9.667694	-1.926163
C	16.269305	10.806392	-1.926162
H	15.640790	12.965836	-1.926159
H	15.685901	8.624709	-1.926164
H	17.350364	10.805327	-1.926163
H	11.272070	11.074354	-1.926159

Table C.2.6 Cartesian coordinates of **6F**(DFT)

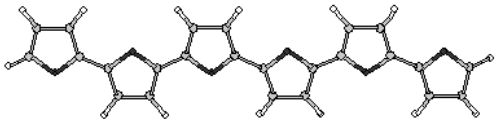

Electronic energy = -1374.22135

Atom symbol	X	Y	Z
C	-16.190866	-2.239714	0.522713
C	-17.570156	-2.616147	0.522711
C	-18.283915	-1.456335	0.522709
C	-16.166745	-0.868271	0.522711
O	-17.446461	-0.378795	0.522709
H	-17.972233	-3.619621	0.522712
H	-19.338016	-1.225749	0.522707
H	-15.328901	-2.890606	0.522714
C	-13.717785	1.858061	0.522712
C	-15.086730	1.473859	0.522710
C	-15.108480	0.100648	0.522711
C	-12.984600	0.695643	0.522713
O	-13.827541	-0.386139	0.522713
H	-15.952172	2.120269	0.522709
H	-13.315392	2.860519	0.522711
C	-9.479650	-0.363565	0.522715
C	-10.847956	-0.746151	0.522715
C	-11.580925	0.417052	0.522714
C	-9.456254	1.011123	0.522715
O	-10.738059	1.498404	0.522714
H	-11.251269	-1.748226	0.522715
H	-8.614996	-1.011009	0.522716
C	-7.009210	3.734325	0.522716
C	-8.377517	3.351740	0.522716
C	-8.400915	1.977053	0.522715
C	-6.276243	2.571121	0.522714
O	-7.119111	1.489771	0.522714
H	-9.242170	3.999186	0.522717
H	-6.605897	4.736400	0.522716
C	-2.770445	1.514291	0.522711
C	-4.139393	1.130100	0.522712
C	-4.872569	2.292523	0.522713
O	-4.029619	3.374299	0.522714
H	-4.541794	0.127645	0.522711
H	-1.905008	0.867873	0.522709
C	-2.748683	2.887501	0.522712
C	-0.286981	5.604272	0.522713

Table C.2.6 (Continue) Cartesian coordinates of **6F**(DFT)

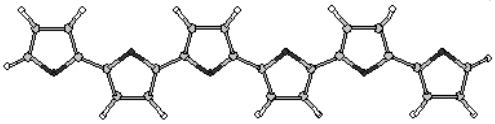

Electronic energy = -1374.22135

Atom symbol	X	Y	Z
C	-1.666274	5.227853	0.522714
C	-1.690410	3.856410	0.522712
C	0.426766	4.444453	0.522710
O	-0.410698	3.366922	0.522709
H	-2.528233	5.878753	0.522716
H	0.115106	6.607742	0.522714
H	1.480865	4.213856	0.522708

C.3 Cartesian Coordinates of Ground State Geometries of Pyrrole Oligomers (**nP**) at B3LYP/6-31G* Level

Table C.3.1 Cartesian coordinates of **1P**(DFT)

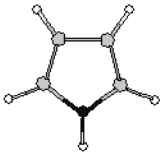

Electronic energy = -210.16589

Atom symbol	X	Y	Z
C	-0.821753	2.693697	2.378472
C	-0.821753	4.119219	2.378472
C	0.493265	4.531977	2.378472
C	0.493265	2.280939	2.378472
N	1.284053	3.406458	2.378472
H	-1.687804	4.767385	2.378472
H	0.929493	5.520576	2.378472
H	-1.687804	2.045532	2.378472
H	0.929492	1.292340	2.378472
H	2.292049	3.406458	2.378472

Table C.3.2 Cartesian coordinates of **2P**(DFT)

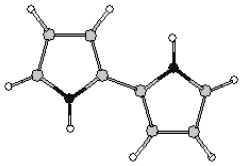

Electronic energy = -419.14800

Atom symbol	X	Y	Z
N	-0.605000	-1.764249	0.000000
C	-1.890822	-2.251099	0.000000
C	-2.747002	-1.170934	0.000000
C	-0.613668	-0.384540	0.000000
C	-1.948563	0.004191	0.000000
H	-2.085440	-3.313951	0.000000
H	-3.827903	-1.219439	0.000000
C	0.613668	0.384540	0.000000
N	0.605000	1.764249	0.000000
C	1.890822	2.251099	0.000000
C	1.948563	-0.004192	0.000000
C	2.747002	1.170934	0.000000
H	2.085440	3.313951	0.000000
H	2.312963	-1.023871	0.000000
H	3.827903	1.219438	0.000000
H	-2.312963	1.023871	0.000000
H	0.230538	-2.327999	0.000000
H	-0.230538	2.327999	0.000000

Table C.3.3 Cartesian coordinates of **3P**(DFT)

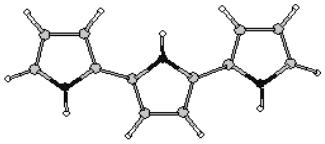

Electronic energy = -628.13065

Atom symbol	X	Y	Z
N	0.223521	-0.154703	0.000000
C	0.227777	1.225011	0.000000
C	-1.103880	1.624958	0.000000
C	-1.066270	-0.644672	0.000000
C	-1.909643	0.460764	0.000000
H	-1.462475	2.646110	0.000000
C	-1.340978	-2.063905	0.000000
N	-2.631409	-2.554934	0.000000
C	-2.619794	-3.929699	0.000000
C	-0.496083	-3.168130	0.000000
C	-1.303157	-4.337065	0.000000
H	-3.540418	-4.494762	0.000000
H	0.585939	-3.140102	0.000000
H	-0.956433	-5.361414	0.000000
H	-2.991661	0.436690	0.000000
C	1.459290	1.982019	0.000000
N	1.464312	3.362705	0.000000
C	2.755061	3.836077	0.000000
C	2.790350	1.580221	0.000000
C	3.600088	2.747312	0.000000
H	2.959633	4.896736	0.000000
H	3.145246	0.557672	0.000000
H	4.680915	2.783622	0.000000
H	1.052315	-0.728329	0.000000
H	-3.459611	-1.980552	0.000000
H	0.635019	3.935510	0.000000

Table C.3.4. Cartesian coordinates of **4P**(DFT)

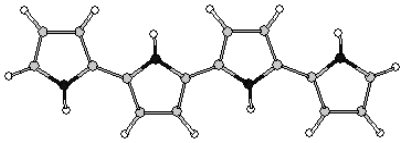

Electronic energy = -837.11346

Atom symbol	X	Y	Z
N	1.347575	-2.267555	0.198835
C	1.357238	-0.887257	0.198834
C	0.026013	-0.481996	0.198834
C	0.056144	-2.751978	0.198835
C	-0.783551	-1.642889	0.198834
H	-0.328563	0.540505	0.198833
C	-0.225243	-4.169628	0.198835
N	-1.517735	-4.654956	0.198836
C	-1.512282	-6.029364	0.198837
C	0.615208	-5.277702	0.198836
C	-0.197212	-6.443179	0.198837
H	-2.435432	-6.590337	0.198837
H	1.697390	-5.254490	0.198837
H	0.144644	-7.469182	0.198838
H	-1.865635	-1.663316	0.198834
N	2.597375	1.246263	0.198835
C	2.587710	-0.134036	0.198834
C	3.918935	-0.539299	0.198833
C	3.888806	1.730684	0.198835
C	4.728500	0.621594	0.198834
H	4.273509	-1.561800	0.198833
C	4.170195	3.148333	0.198836
N	5.462689	3.633660	0.198836
C	5.457238	5.008068	0.198837
C	3.329746	4.256409	0.198836
C	4.142169	5.421885	0.198837
H	6.380389	5.569039	0.198837
H	2.247564	4.233199	0.198836
H	3.800314	6.447888	0.198838
H	5.810585	0.642020	0.198834
H	2.173629	-2.845433	0.198835
H	-2.343714	-4.076950	0.198835
H	1.771321	1.824141	0.198836
H	6.288667	3.055652	0.198835

Table C.3.5 Cartesian coordinates of **5P**(DFT)

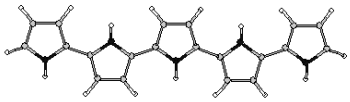

Electronic energy = -1046.09624

Atom symbol	X	Y	Z
N	8.651124	2.457480	-1.926163
C	8.655962	3.837889	-1.926165
C	7.323176	4.238380	-1.926165
C	7.361492	1.968586	-1.926163
C	6.517818	3.074760	-1.926164
H	6.964884	5.259595	-1.926166
C	7.084821	0.550015	-1.926161
N	5.793882	0.060555	-1.926161
C	5.803749	-1.313768	-1.926159
C	7.928815	-0.555342	-1.926160
C	7.120146	-1.723379	-1.926158
H	4.882397	-1.877675	-1.926159
H	9.010913	-0.528723	-1.926159
H	7.465302	-2.748264	-1.926156
H	5.435823	3.050490	-1.926164
C	9.883168	4.595848	-1.926165
N	9.886969	5.975966	-1.926164
C	11.177216	6.465804	-1.926164
C	11.216439	4.195887	-1.926165
C	12.021389	5.359102	-1.926165
H	11.574945	3.174785	-1.926166
H	13.103287	5.383848	-1.926165
N	12.744530	8.372161	-1.926163
C	11.454342	7.881356	-1.926163
C	10.609934	8.987490	-1.926162
C	12.747789	9.751363	-1.926162
C	11.415224	10.151166	-1.926161
H	9.528002	8.962591	-1.926161
C	13.978100	10.509774	-1.926161
N	13.981735	11.890395	-1.926159
C	15.271534	12.365118	-1.926159
C	15.309922	10.109148	-1.926163
C	16.118408	11.277284	-1.926162
H	15.474786	13.426042	-1.926157
H	15.666491	9.087111	-1.926165
H	17.199179	11.315146	-1.926163
H	11.056342	11.172225	-1.926160
H	9.479168	1.882400	-1.926162
H	4.965993	0.635849	-1.926162
H	9.058098	6.549702	-1.926164
H	13.574319	7.799604	-1.926164
H	13.151877	12.462832	-1.926157

Table C.3.6 Cartesian coordinates of **6P**(DFT)

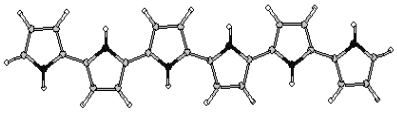

Electronic energy = -1255.07893

Atom symbol	X	Y	Z
C	-16.461518	-2.303469	0.522714
C	-17.828455	-2.690232	0.522714
C	-18.583533	-1.536795	0.522714
C	-16.409370	-0.913734	0.522713
N	-17.716814	-0.470175	0.522713
H	-18.214193	-3.700531	0.522715
H	-19.653121	-1.385670	0.522714
H	-15.609852	-2.971544	0.522714
C	-13.876730	1.778641	0.522712
C	-15.238825	1.394763	0.522712
C	-15.293318	0.004594	0.522712
C	-13.104623	0.620858	0.522712
N	-13.987830	-0.440019	0.522712
H	-16.088157	2.065526	0.522712
H	-13.501833	2.793879	0.522711
C	-9.542456	-0.353490	0.522711
C	-10.904171	-0.735994	0.522711
C	-11.675984	0.422475	0.522712
C	-9.486600	1.037441	0.522712
N	-10.792937	1.482988	0.522712
H	-11.279844	-1.750901	0.522711
H	-8.693556	-1.024695	0.522711
C	-6.952988	3.724157	0.522713
C	-8.314703	3.341654	0.522713
C	-8.370561	1.950724	0.522712
C	-6.181177	2.565686	0.522713
N	-7.064224	1.505175	0.522712
H	-9.163603	4.012860	0.522713
H	-6.577315	4.739064	0.522714
C	-2.618338	1.593391	0.522712
C	-3.980434	1.209516	0.522712
C	-4.752538	2.367301	0.522713
N	-3.869328	3.428176	0.522713
H	-4.355334	0.194279	0.522711
H	-1.769008	0.922625	0.522711
C	-2.563840	2.983559	0.522713
C	-0.028695	5.678376	0.522714
C	-1.395632	5.291618	0.522714
C	-1.447786	3.901883	0.522713
C	0.726380	4.524936	0.522713
N	-0.140343	3.458319	0.522713
H	-2.247296	5.959697	0.522714

Table C.3.6 (Continue) Cartesian coordinates of **6P**(DFT)

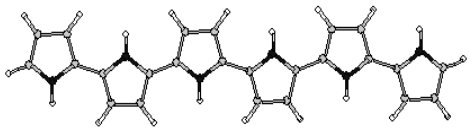

Electronic energy = -1255.07893

Atom symbol	X	Y	Z
H	0.357047	6.688673	0.522714
H	1.795967	4.373808	0.522713
H	-17.989853	0.500312	0.522712
H	-13.715818	-1.410779	0.522713
H	-11.065742	2.453458	0.522712
H	-6.791421	0.534704	0.522712
H	-4.141337	4.398936	0.522714
H	0.132693	2.487831	0.522712

APPENDIX D

D. Cartesian Coordinates of Lowest Singlet Excited State Geometries of Studied Structures at CIS/6-31G* Level

All cartesian coordinates are in angstroms. All electronic energies are in Hartrees.

D.1 Cartesian Coordinates of Lowest Singlet Excited State Geometries of Thiophene Oligomers (**nT**) at CIS/6-31G* Level

Table D.1.1 Cartesian coordinates of **1T**(CIS)

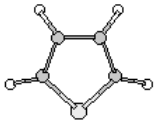

Electronic energy = -551.26948

Atom symbol	X	Y	Z
C	-1.335413	-0.682107	0.000000
C	-1.335439	0.682056	0.000000
C	-0.017088	1.230995	0.000000
C	-0.017042	-1.230996	0.000000
S	1.260728	0.000024	0.000000
H	-2.207523	1.305757	0.000000
H	0.236577	2.271228	0.000000
H	-2.207473	-1.305841	0.000000

Table D.1.2 Cartesian coordinates of **2T**(CIS)

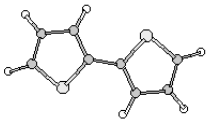

Electronic energy = -1101.41178

Atom symbol	X	Y	Z
S	-0.536503	-2.149740	0.000000
C	-2.260065	-2.214631	0.000000
C	-2.840774	-0.966217	0.000000
C	-0.580256	-0.373862	0.000000
C	-1.925856	0.078077	0.000000
H	-2.764107	-3.159595	0.000000
H	-3.905278	-0.826916	0.000000
C	0.580256	0.373862	0.000000
S	0.536503	2.149740	0.000000
C	2.260065	2.214631	0.000000
C	1.925856	-0.078077	0.000000
C	2.840774	0.966217	0.000000
H	2.764107	3.159595	0.000000
H	2.186028	-1.118935	0.000000
H	3.905278	0.826916	0.000000
H	-2.186028	1.118935	0.000000

Table D.1.3 Cartesian coordinates of **3T**(CIS)

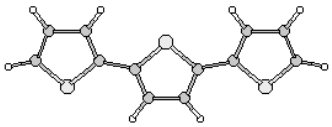

Electronic energy = -1651.55298

Atom symbol	X	Y	Z
S	-0.476446	-0.503880	-0.733397
C	0.733369	0.775596	-0.702530
C	1.056740	1.117587	0.630030
C	-0.522931	-0.553042	1.026458
C	0.373087	0.394569	1.570910
H	1.775742	1.877989	0.867261
C	-1.363659	-1.442178	1.710487
S	-1.420900	-1.502715	3.467560
C	-2.605039	-2.755036	3.429245
C	-2.245178	-2.374455	1.176922
C	-2.938339	-3.107527	2.160442
H	-2.989237	-3.161356	4.342604
H	-2.378564	-2.515521	0.121297
H	-3.659412	-3.870119	1.934089
H	0.495611	0.524149	2.629046
C	1.249613	1.321565	-1.886039
S	2.458122	2.599660	-1.870959
C	2.498061	2.641899	-3.593916
C	0.932899	0.986615	-3.196920
C	1.646334	1.741129	-4.149231
H	3.146088	3.327239	-4.101161
H	0.216227	0.228677	-3.449794
H	1.531387	1.619564	-5.209768

Table D.1.4 Cartesian coordinates of **4T**(CIS)

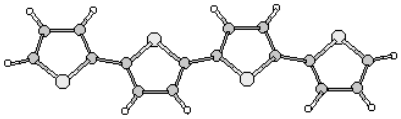

Electronic energy = -2201.69327

Atom symbol	X	Y	Z
S	-0.577369	-2.132216	0.000014
C	-0.588002	-0.371176	0.000012
C	-1.914340	0.099602	0.000013
C	-2.326209	-2.193273	0.000008
C	-2.858950	-0.906207	0.000012
H	-2.156066	1.145081	0.000012
C	-3.025937	-3.433096	-0.000001
S	-4.775985	-3.502897	-0.000005
C	-4.755617	-5.226985	-0.000017
C	-2.504452	-4.703447	-0.000002
C	-3.496924	-5.718376	-0.000013
H	-5.674893	-5.776335	-0.000025
H	-1.450405	-4.906643	0.000001
H	-3.271793	-6.768035	-0.000018
H	-3.916319	-0.721230	0.000008
S	0.577369	2.132216	0.000003
C	0.588002	0.371176	0.000008
C	1.914340	-0.099602	0.000010
C	2.326209	2.193273	-0.000001
C	2.858950	0.906207	0.000003
H	2.156066	-1.145081	0.000015
C	3.025937	3.433096	-0.000006
S	4.775985	3.502897	-0.000008
C	4.755617	5.226985	-0.000011
C	2.504452	4.703447	-0.000008
C	3.496924	5.718376	-0.000010
H	5.674893	5.776335	-0.000012
H	1.450405	4.906643	-0.000006
H	3.271793	6.768035	-0.000011
H	3.916319	0.721230	0.000004

Table D.1.5 Cartesian coordinates of **5T**(CIS)

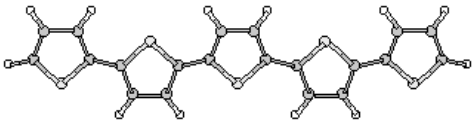

Electronic energy = -2751.83353

Atom symbol	X	Y	Z
S	-1.936308	-3.512858	-0.000004
C	-1.954837	-1.756975	0.000001
C	-3.269760	-1.299332	0.000000
C	-3.679324	-3.589805	-0.000003
C	-4.216968	-2.321430	-0.000003
H	-3.523632	-0.256636	0.000002
C	-4.372997	-4.849496	-0.000005
S	-6.118432	-4.930908	-0.000006
C	-6.087321	-6.655130	-0.000007
C	-3.842501	-6.106642	-0.000007
C	-4.828149	-7.136004	-0.000008
H	-7.003275	-7.209942	-0.000008
H	-2.786884	-6.301901	-0.000007
H	-4.592157	-8.183163	-0.000009
H	-5.274957	-2.139215	-0.000003
C	-0.773799	-1.002641	0.000004
S	-0.796997	0.753605	0.000007
C	0.957798	0.828659	0.000008
C	0.550796	-1.467379	0.000005
C	1.495885	-0.467873	0.000006
H	0.793720	-2.512690	0.000003
H	2.553145	-0.651959	0.000006
S	3.399075	2.129730	0.000007
C	1.644904	2.050034	0.000009
C	1.114442	3.337306	0.000010
C	3.378426	3.874321	0.000004
C	2.081969	4.340191	0.000008
H	0.059180	3.532469	0.000011
C	4.597353	4.637354	-0.000001
S	4.581026	6.384611	0.000003
C	6.304291	6.449974	-0.000010
C	5.882199	4.177993	-0.000009
C	6.854829	5.219665	-0.000014
H	6.807010	7.395521	-0.000013
H	6.136186	3.134948	-0.000012
H	7.913546	5.042602	-0.000021
H	1.840873	5.386334	0.000007

Table D.1.6 Cartesian coordinates of **6T**(CIS)

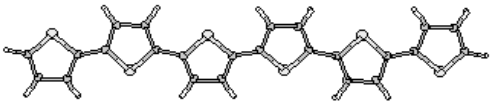

Electronic energy =-3301.97390

Atom symbol	X	Y	Z
C	-7.648335	-5.006346	-0.000001
C	-8.953455	-5.586733	-0.000002
C	-9.933568	-4.664020	-0.000003
C	-7.662747	-3.646830	-0.000001
S	-9.305281	-3.057785	-0.000003
H	-9.131991	-6.645129	-0.000002
H	-10.991832	-4.827806	-0.000004
H	-6.746217	-5.588363	0.000000
C	-5.274163	-0.785112	0.000000
C	-6.551241	-1.370460	-0.000001
C	-6.536581	-2.738017	-0.000001
C	-4.245438	-1.703429	0.000000
S	-4.897349	-3.328972	-0.000001
H	-7.457586	-0.795025	-0.000001
H	-5.112952	0.275968	0.000001
C	-0.550960	-1.831636	0.000002
C	-1.815037	-2.390245	0.000001
C	-2.850421	-1.459390	0.000001
C	-0.550109	-0.431487	0.000002
S	-2.201715	0.166608	0.000002
H	-1.990686	-3.449110	0.000001
H	0.352645	-2.410492	0.000002
C	1.815037	2.390245	0.000003
C	0.550960	1.831636	0.000003
C	0.550109	0.431486	0.000003
C	2.850421	1.459390	0.000002
S	2.201715	-0.166608	0.000002
H	-0.352645	2.410492	0.000004
H	1.990686	3.449110	0.000003
C	6.551241	1.370460	0.000000
C	5.274163	0.785112	0.000001
C	4.245438	1.703429	0.000002
S	4.897349	3.328972	0.000001
H	5.112952	-0.275968	0.000001
H	7.457586	0.795025	-0.000001
C	6.536581	2.738017	0.000000
C	8.953455	5.586733	-0.000003

Table D.1.6 (Continue) Cartesian coordinates of **6T**(CIS)

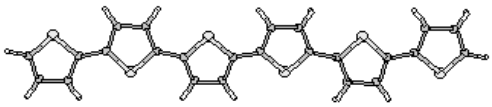

Electronic energy = -3301.97390

Atom symbol	X	Y	Z
C	7.648335	5.006346	-0.000002
C	7.662747	3.646830	-0.000001
C	9.933568	4.664020	-0.000003
S	9.305281	3.057786	-0.000002
H	6.746217	5.588363	-0.000001
H	9.131990	6.645129	-0.000003
H	10.991832	4.827806	-0.000003

D.2 Cartesian Coordinates of Lowest Singlet Excited State Geometries of Furan Oligomers (**nF**) at CIS/6-31G* Level

Table D.2.1 Cartesian coordinates of **1F**(CIS)

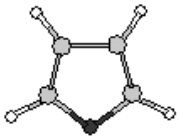

Electronic energy = -228.60309

Atom symbol	X	Y	Z
C	-1.004798	-0.683591	0.000000
C	-1.004868	0.683487	0.000000
C	0.361689	1.087171	0.000000
C	0.361803	-1.087133	0.000000
O	1.218584	0.000063	0.000000
H	-1.836652	1.355775	0.000000
H	0.820660	2.051523	0.000000
H	-1.836512	-1.355966	0.000000
H	0.820873	-2.051437	0.000000

Table D.2.2 Cartesian coordinates of **2F**(CIS)

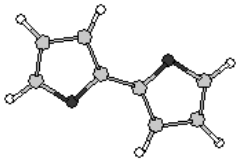

Electronic energy = -456.09116

Atom symbol	X	Y	Z
O	-0.611238	-1.695008	0.000000
C	-1.905951	-2.075864	0.000000
C	-2.741921	-0.994003	0.000000
C	-0.607319	-0.322091	0.000000
C	-1.941558	0.148268	0.000000
H	-2.088528	-3.128660	0.000000
H	-3.811921	-1.038029	0.000000
C	0.607319	0.322091	0.000000
O	0.611238	1.695008	0.000000
C	1.905951	2.075864	0.000000
C	1.941558	-0.148268	0.000000
C	2.741921	0.994003	0.000000
H	2.088528	3.128660	0.000000
H	2.235384	-1.176292	0.000000
H	3.811921	1.038029	0.000000
H	-2.235384	1.176292	0.000000

Table D.2.3 Cartesian coordinates of **3F**(CIS)

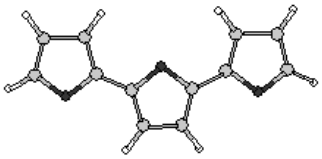

Electronic energy = -683.57566

Atom symbol	X	Y	Z
O	0.226677	-0.174293	0.000000
C	0.249808	1.190673	0.000000
C	-1.065197	1.685865	0.000000
C	-1.086533	-0.547312	0.000000
C	-1.902935	0.596341	0.000000
H	-1.327692	2.722642	0.000000
C	-1.372363	-1.908953	0.000000
O	-2.676168	-2.294212	0.000000
C	-2.692713	-3.639662	0.000000
C	-0.560087	-3.029330	0.000000
C	-1.436836	-4.139440	0.000000
H	-3.657323	-4.098736	0.000000
H	0.509400	-3.027239	0.000000
H	-1.171832	-5.176822	0.000000
H	-2.972351	0.583674	0.000000
C	1.492317	1.816719	0.000000
O	1.529694	3.175740	0.000000
C	2.825736	3.537380	0.000000
C	2.783768	1.319535	0.000000
C	3.631379	2.452049	0.000000
H	3.021590	4.587553	0.000000
H	3.056502	0.285406	0.000000
H	4.702024	2.462447	0.000000

Table D.2.4 Cartesian coordinates of **4F**(CIS)

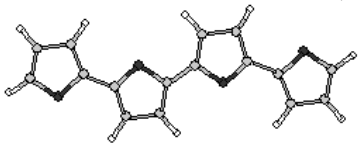

Electronic energy = -911.05950

Atom symbol	X	Y	Z
O	-0.661385	-1.671524	-0.000020
C	-0.617826	-0.308746	-0.000027
C	-1.925474	0.194621	-0.000025
C	-1.968848	-2.031697	-0.000010
C	-2.770117	-0.902527	-0.000014
H	-2.187083	1.231529	-0.000030
C	-2.267020	-3.410262	0.000007
O	-3.571158	-3.772958	0.000018
C	-3.612146	-5.116959	0.000030
C	-1.476154	-4.525225	0.000012
C	-2.369746	-5.634409	0.000026
H	-4.585065	-5.557700	0.000039
H	-0.406855	-4.538852	0.000004
H	-2.115365	-6.674191	0.000033
H	-3.839813	-0.908050	-0.000009
O	0.661385	1.671524	-0.000021
C	0.617826	0.308747	-0.000028
C	1.925474	-0.194621	-0.000025
C	1.968848	2.031697	-0.000011
C	2.770117	0.902527	-0.000015
H	2.187083	-1.231529	-0.000030
C	2.267020	3.410262	0.000005
O	3.571158	3.772958	0.000018
C	3.612147	5.116959	0.000030
C	1.476154	4.525225	0.000011
C	2.369746	5.634409	0.000026
H	4.585066	5.557700	0.000041
H	0.406855	4.538853	0.000004
H	2.115366	6.674191	0.000034
H	3.839813	0.908050	-0.000009

Table D.2.5 Cartesian coordinates of **5F**(CIS)

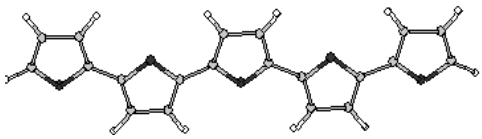

Electronic energy = -1138.54333

Atom symbol	X	Y	Z
O	-1.818361	-2.950351	-0.000003
C	-1.786771	-1.591608	-0.000005
C	-3.084708	-1.102835	-0.000002
C	-3.116594	-3.325028	0.000000
C	-3.926047	-2.219156	0.000000
H	-3.359687	-0.069419	-0.000002
C	-3.396232	-4.720937	0.000003
O	-4.694335	-5.093234	0.000008
C	-4.724759	-6.437409	0.000009
C	-2.596982	-5.818756	0.000002
C	-3.480416	-6.942772	0.000006
H	-5.694279	-6.885303	0.000013
H	-1.527661	-5.821810	-0.000002
H	-3.213898	-7.979346	0.000006
H	-4.995632	-2.233787	0.000003
C	-0.547246	-0.961226	-0.000007
O	-0.518512	0.398688	-0.000006
C	0.788380	0.775817	-0.000007
C	0.758753	-1.454040	-0.000008
C	1.600162	-0.359749	-0.000008
H	1.024978	-2.489861	-0.000008
H	2.669612	-0.350939	-0.000008
O	2.384202	2.515272	-0.000004
C	1.079175	2.135685	-0.000006
C	0.273370	3.264497	-0.000004
C	2.412791	3.866189	-0.000001
C	1.136087	4.364379	0.000000
H	-0.796005	3.264765	-0.000005
C	3.690014	4.495045	0.000002
O	3.716339	5.845224	0.000007
C	5.007586	6.219941	0.000010
C	4.956314	4.004644	0.000002
C	5.815655	5.147185	0.000007
H	5.191383	7.271985	0.000014
H	5.233970	2.971995	0.000000
H	6.885909	5.155903	0.000008
H	0.875453	5.401826	0.000002

Table D.2.6 Cartesian coordinates of **6F**(CIS)

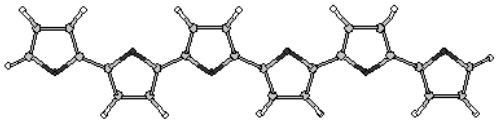

Electronic energy = -1366.02731

Atom symbol	X	Y	Z
C	-7.189721	-3.698010	-0.000001
C	-8.572584	-4.072475	-0.000002
C	-9.265857	-2.923965	-0.000003
C	-7.175541	-2.345244	-0.000001
O	-8.436064	-1.865925	-0.000002
H	-8.978192	-5.062827	-0.000003
H	-10.310323	-2.701413	-0.000004
H	-6.334642	-4.340083	-0.000001
C	-4.748833	0.366642	0.000001
C	-6.102497	-0.023641	0.000000
C	-6.112980	-1.385021	0.000000
C	-4.013804	-0.794358	0.000001
O	-4.850779	-1.860567	0.000000
H	-6.966188	0.607272	-0.000001
H	-4.350318	1.358943	0.000001
C	-0.556739	-1.847975	0.000001
C	-1.894188	-2.214209	0.000001
C	-2.632362	-1.042765	0.000001
C	-0.523910	-0.455379	0.000002
O	-1.796087	0.024361	0.000002
H	-2.304487	-3.201934	0.000000
H	0.301405	-2.486103	0.000001
C	1.894188	2.214209	0.000001
C	0.556739	1.847975	0.000001
C	0.523910	0.455380	0.000002
C	2.632362	1.042765	0.000001
O	1.796087	-0.024361	0.000001
H	-0.301405	2.486104	0.000002
H	2.304487	3.201935	0.000001
C	6.102497	0.023641	0.000000
C	4.748833	-0.366642	0.000000
C	4.013804	0.794358	0.000000
O	4.850779	1.860567	0.000000
H	4.350318	-1.358943	0.000001
H	6.966187	-0.607273	0.000000
C	6.112980	1.385020	0.000000
C	8.572585	4.072475	-0.000001

Table D.2.6 (Continue) Cartesian coordinates of **6F**(CIS)

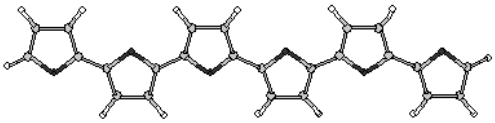

Electronic energy = -1366.02731

Atom symbol	X	Y	Z
C	7.189721	3.698009	0.000000
C	7.175542	2.345243	0.000000
C	9.265857	2.923964	-0.000001
O	8.436064	1.865925	-0.000001
H	6.334642	4.340083	0.000000
H	8.978193	5.062827	-0.000001
H	10.310323	2.701413	-0.000001

D.3 Cartesian Coordinates of Lowest Singlet Excited State Geometries of Pyrrole Oligomers (**nP**) at CIS/6-31G* Level

Table D.3.1 Cartesian coordinates of **1P**(CIS)

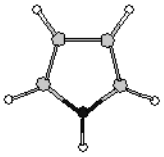

Electronic energy = -208.78960

Atom symbol	X	Y	Z
C	0.000000	0.682767	1.024942
C	0.000000	-0.682768	1.024942
C	0.000000	-1.128826	-0.344687
C	0.000000	1.128826	-0.344687
N	0.000000	0.000000	-1.178325
H	0.000000	-1.341068	1.868684
H	-0.000001	-2.121039	-0.742410
H	0.000000	1.341067	1.868685
H	0.000001	2.121039	-0.742409
H	0.000000	0.000001	-2.167337

Table D.3.2 Cartesian coordinates of **2P**(CIS)

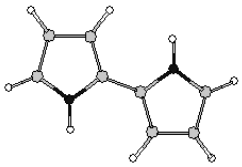

Electronic energy = -416.45363

Atom symbol	X	Y	Z
N	-0.577842	-1.775542	0.000000
C	-1.863118	-2.231140	0.000000
C	-2.719347	-1.146290	0.000000
C	-0.577478	-0.375465	0.000000
C	-1.959005	0.016072	0.000000
H	-2.081333	-3.278825	0.000000
H	-3.788997	-1.211219	0.000000
C	0.577478	0.375465	0.000000
N	0.577842	1.775542	0.000000
C	1.863118	2.231140	0.000000
C	1.959005	-0.016072	0.000000
C	2.719347	1.146290	0.000000
H	2.081333	3.278825	0.000000
H	2.319868	-1.024645	0.000000
H	3.788997	1.211219	0.000000
H	-2.319868	1.024645	0.000000
H	0.236084	-2.341999	0.000000
H	-0.236084	2.341999	0.000000

Table D.3.3 Cartesian coordinates of **3P**(CIS)

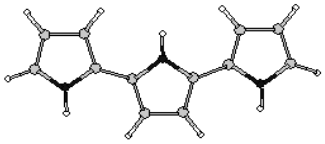

Electronic energy = -624.11824

Atom symbol	X	Y	Z
N	0.262572	-0.181732	0.000000
C	0.258080	1.205030	0.000000
C	-1.107265	1.599257	0.000000
C	-1.036896	-0.665995	0.000000
C	-1.886781	0.472985	0.000000
H	-1.457860	2.611842	0.000000
C	-1.338634	-2.031589	0.000000
N	-2.631096	-2.527302	0.000000
C	-2.605613	-3.889112	0.000000
C	-0.490537	-3.150686	0.000000
C	-1.299692	-4.298425	0.000000
H	-3.511214	-4.459187	0.000000
H	0.580664	-3.125565	0.000000
H	-0.966821	-5.316800	0.000000
H	-2.957963	0.444441	0.000000
C	1.429870	1.968442	0.000000
N	1.438562	3.352679	0.000000
C	2.722071	3.808510	0.000000
C	2.775977	1.568886	0.000000
C	3.565145	2.730458	0.000000
H	2.936624	4.856872	0.000000
H	3.129782	0.557488	0.000000
H	4.635502	2.777630	0.000000
H	1.076975	-0.745397	0.000000
H	-3.453610	-1.972729	0.000000
H	0.629811	3.927139	0.000000

Table D.3.4 Cartesian coordinates of **4P**(CIS)

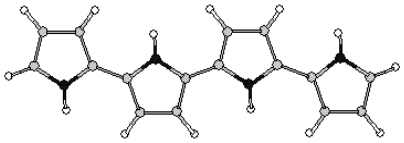

Electronic energy = -831.78148

Atom symbol	X	Y	Z
N	-0.587583	-1.769252	0.000003
C	-0.580092	-0.381614	0.000004
C	-1.941977	0.014346	0.000004
C	-1.879587	-2.243450	0.000002
C	-2.720781	-1.122977	0.000004
H	-2.296767	1.025337	0.000005
C	-2.184764	-3.629985	-0.000001
N	-3.474289	-4.110224	-0.000002
C	-3.463367	-5.471650	-0.000005
C	-1.349836	-4.737461	-0.000003
C	-2.165927	-5.890439	-0.000006
H	-4.375578	-6.030954	-0.000006
H	-0.278362	-4.719356	-0.000003
H	-1.835672	-6.909507	-0.000008
H	-3.792395	-1.150531	0.000004
N	0.587583	1.769252	0.000003
C	0.580092	0.381614	0.000004
C	1.941977	-0.014346	0.000004
C	1.879587	2.243450	0.000002
C	2.720781	1.122977	0.000003
H	2.296767	-1.025337	0.000005
C	2.184764	3.629985	-0.000001
N	3.474289	4.110224	-0.000002
C	3.463367	5.471650	-0.000005
C	1.349836	4.737461	-0.000003
C	2.165927	5.890439	-0.000005
H	4.375578	6.030954	-0.000006
H	0.278362	4.719355	-0.000004
H	1.835672	6.909507	-0.000007
H	3.792395	1.150531	0.000003
H	0.222909	-2.339741	0.000002
H	-4.291857	-3.547780	0.000000
H	-0.222909	2.339741	0.000001
H	4.291857	3.547780	0.000000

Table D.3.5 Cartesian coordinates of **5P**(CIS)

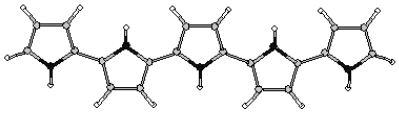

Electronic energy = -1039.44515

Atom symbol	X	Y	Z
N	-1.718250	-3.155687	-0.000005
C	-1.715638	-1.773744	-0.000009
C	-3.064316	-1.383076	-0.000005
C	-3.001494	-3.635428	0.000001
C	-3.845126	-2.533591	0.000000
H	-3.424276	-0.374016	-0.000007
C	-3.294020	-5.039256	0.000006
N	-4.577798	-5.521594	0.000012
C	-4.563524	-6.883163	0.000016
C	-2.456612	-6.133220	0.000007
C	-3.267050	-7.295499	0.000013
H	-5.474283	-7.444534	0.000021
H	-1.385274	-6.109557	0.000003
H	-2.929917	-8.312092	0.000015
H	-4.916511	-2.565634	0.000003
C	-0.546742	-1.003515	-0.000013
N	-0.547788	0.379135	-0.000013
C	0.746616	0.865177	-0.000013
C	0.809506	-1.396311	-0.000015
C	1.591960	-0.265791	-0.000016
H	1.162480	-2.408042	-0.000016
H	2.663181	-0.239775	-0.000016
N	2.348208	2.719681	-0.000005
C	1.055753	2.230464	-0.000010
C	0.215067	3.355097	-0.000008
C	2.345195	4.089666	-0.000001
C	1.016816	4.491121	-0.000002
H	-0.856114	3.336560	-0.000011
C	3.556014	4.857925	0.000005
N	3.555244	6.229324	0.000015
C	4.834579	6.695561	0.000018
C	4.874832	4.459522	0.000005
C	5.677155	5.627419	0.000011
H	5.039168	7.745686	0.000026
H	5.230051	3.448509	-0.000001
H	6.747346	5.669974	0.000012
H	0.669423	5.505129	0.000001
H	-0.905217	-3.723197	-0.000006
H	-5.396726	-4.961178	0.000012
H	-1.362475	0.942996	-0.000011
H	3.165728	2.158655	-0.000004
H	2.742287	6.798367	0.000018

Table D.3.6 Cartesian coordinates of **6P**(CIS)

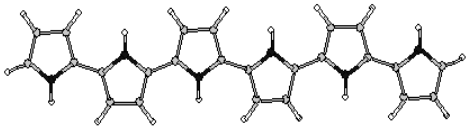

Electronic energy = -1247.10875

Atom symbol	X	Y	Z
C	-7.484045	-3.768602	0.000006
C	-8.850840	-4.151693	0.000009
C	-9.587363	-3.009563	0.000007
C	-7.436460	-2.396634	0.000004
N	-8.730686	-1.950854	0.000005
H	-9.236566	-5.150776	0.000012
H	-10.646911	-2.861727	0.000008
H	-6.642314	-4.431863	0.000006
C	-4.921818	0.277452	-0.000004
C	-6.266651	-0.111483	0.000000
C	-6.314286	-1.490016	0.000002
C	-4.143318	-0.875826	-0.000002
N	-5.021994	-1.935910	0.000001
H	-7.111485	0.548031	-0.000001
H	-4.555926	1.284396	-0.000007
C	-0.625460	-1.833320	-0.000007
C	-1.956388	-2.200390	-0.000006
C	-2.738686	-1.038404	-0.000004
C	-0.554310	-0.425627	-0.000007
N	-1.862038	0.023112	-0.000006
H	-2.332337	-3.203947	-0.000006
H	0.213562	-2.499617	-0.000009
C	1.956388	2.200389	-0.000004
C	0.625460	1.833319	-0.000005
C	0.554310	0.425627	-0.000007
C	2.738686	1.038404	-0.000004
N	1.862038	-0.023112	-0.000006
H	-0.213562	2.499617	-0.000005
H	2.332337	3.203947	-0.000003
C	6.266652	0.111483	0.000000
C	4.921819	-0.277452	-0.000003
C	4.143318	0.875826	-0.000002
N	5.021994	1.935910	0.000000
H	4.555926	-1.284396	-0.000006
H	7.111485	-0.548030	0.000000
C	6.314286	1.490016	0.000002
C	8.850840	4.151693	0.000007
C	7.484045	3.768602	0.000006
C	7.436460	2.396634	0.000004
C	9.587363	3.009563	0.000008
N	8.730686	1.950854	0.000005
H	6.642314	4.431863	0.000006

Table D.3.6 (Continue) Cartesian coordinates of **6P**(CIS)

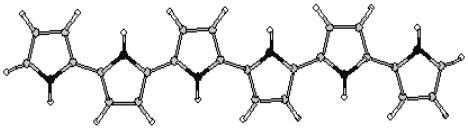

Electronic energy = -1247.10875

Atom symbol	X	Y	Z
H	9.236565	5.150776	0.000008
H	10.646911	2.861727	0.000009
H	-9.004337	-0.996939	0.000004
H	-4.756479	-2.891558	0.000002
H	-2.131659	0.976815	-0.000004
H	2.131659	-0.976816	-0.000007
H	4.756479	2.891558	0.000002
H	9.004337	0.996939	0.000005